CRANFIELD UNIVERSITY

CRANFIELD FORENSIC INSTITUTE

PhD THESIS

Academic Year 2013 - 2017

GEORGE JOHN ADAMS

Quality Factors at the Material and Structural Level that affect the Toughness of Human Cancellous Bone

Supervisor: Prof. P. Zioupos

September 2017

ABSTRACT

Cancellous bone tissue plays a vitally important role in the strength and mechanical competency of the bone throughout the body. It constitutes a large amount of the bone volume at the axial skeletal sites such as the proximal and distal ends of the femur. Cancellous bone is far less dense than the cortical shell within which it is encapsulated, and in the history of bone research it was first overlooked due in part to this dramatically increased porosity. Over the last few decades however there has been a push to understand the mechanical, structural and chemical properties of the tissue, as degenerative conditions affecting the cancellous tissue such as osteoporosis become more and more prevalent in an ever ageing society. This produces a need for a better clinical assessment of the bone health and strength of patients so that preventive measures can be taken earlier to reduce the risk of fractures, which can be extremely traumatic and sometimes fatal. To achieve a better clinical assessment of cancellous tissue we must first understand the material and structural properties that cause a reduction in the fracture toughness (FT) of the tissue.

In the present study there are three separate sections, the first is an investigation into the ability of micro-Computed Tomography (μCT) to assess the structural and density properties of bone tissue. This is achieved by imaging samples from the full spectrum of bone porosities, made possible by excision of an elephant femur, to assess the best methods for thresholding samples to produce data that most accurately matches laboratory measurements and to determine the density relationships that exist across this spectrum. It was found that the material density of bone is in fact non-linear across the full porosity of bone and that bone experiences its highest material density at the extremes of porosity (>99%, <1%), whilst the softest regions of bone exist in porosities of ~40%.

The second section is focused on the how the chemical and structural properties of cancellous bone tissue affect its FT. By using the protocols determined in the first section, cancellous bone tissue that had been previously FT tested were imaged, and the morphometric data obtained was analysed to determine what structural properties were impacting the FT. Multilinear regressions were then employed to produce statistical models to predict the FT, these models were able to predict FT with R^2 values as high as 0.798. The material level characteristics of the samples were then assessed by means of x-ray diffraction (XRD), infrared spectroscopy (FTIR), Raman Spectroscopy and nano-indentation. This assessment revealed that multiple chemical parameters were highly correlated with the fracture toughness; the parameters that correlated highly were added to the multiple regression models to produce R^2 values as high as 0.911 showing a marked improvement over the structural properties alone. These models were produced for samples loaded across and along the primary orientation of the trabecular struts, and for each direction the models contained different contributors marking clear adaptations in bone at the material and structural level to resist fracture in specific orientations.

The third and final stage of the study aimed to produce material models that could be utilised in micro-Finite Element (μFE) models to simulate a fracture like event. This was attempted by first μCT imaging bone from a wide array of different densities; the samples were subsequently indented to determine the material properties at the micron level. The indented areas were mapped in the image data to produce models to convert grey values to material level modulus. This modulus was applied to segmented μCT image data, collected from the fracture toughness samples, in μFE simulations. The simulations were then developed further to simulate the fracture by introducing an element softening protocol. This was carried out on five samples, due to limitations of computational time, three of which

closely matched the previously recorded data. With further development and validation these models may prove to be extremely valuable in the understanding of fracture risk.

To conclude, the fracture toughness of cancellous bone tissue is contributed to by a combination of the structural and chemical properties of the tissue. The quantity of bone was found to be the single largest contributor to toughness and with the addition of other structural or chemical properties of the tissue it may be possible to predict the fracture toughness of the tissue which with further work could be translated to an individual's fracture risk. Additionally the use of μFE simulations in conjunction with material models may with further work be able to predict the fracture risk of an individual. These two approaches will hopefully be able to help in the understanding of cancellous bone fractures to greater inform the fracture risk of those with conditions such as osteoporosis.

Keywords:

Cancellous bone, Biomechanics, micro-Computed Tomography, Raman spectroscopy, X-ray Diffraction, Infrared spectroscopy, Nano-Indentation, micro-Finite Element Analysis

ACKNOWLEDGEMENTS

This study has been hugely difficult and I would not have got this far if not for the support I have received along the way. First I must thank my supervisor and mentor Prof Peter Zioupos who threw me in at the deep end and has continued to provide guidance and support which has helped push me to complete my research. Further thanks must be extended to Prof Keith Rogers and Dr Charlene Greenwood who have helped guide me through the minefield of x-ray diffraction and physicochemical analysis. I must also thank the members of the Cranfield Forensic Institute in Shrivenham for their support; in particular Adrian Mustey for his maintenance of the laboratories and in guidance with health and safety procedures to allow the research to be carried out. I would also like to thank my fellow PhD candidates Constantinos Franceskides and Tobias-Akash Shanker who have supported my research and helped keep me sane during my study.

Special thanks must go to Dr Michael Gibson who tragically passed away shortly after the completion of these works. Mike was an amazing supervisor who guided me with patience as I grappled with micro-finite element analysis. Without his support this work would not have been possible.

Dr Richard Cook, who is arguably my predecessor on this research project, provided a foundation for my work as well as always being available to answer any questions I had. I would also like to thank Prof Nick Stone and Dr Benjamin Gardner from the University of Exeter for allowing me access to their Raman Spectroscopy equipment and for their support in the analysis of such data.

Throughout my research I have been a regular attendee of the annual congress of the European Society of Biomechanics (ESB) which has always provided me with the opportunity to present my findings, discover the latest in the field of biomechanics, and

discuss ideas with the leaders of the field. This could not have been possible if not for the funding of the Cranfield Students Association, the ESB travel grant, and funding from the Institute of Engineering and Physics in Medicine.

And I of course want to thank my family; my parents Dr Carl Adams & Melanie Adams for supporting me and always encouraging me to push myself. They helped in the much needed proof reading of all my work and sat down with me to challenge my work and ideas. I would also like to thank my sister Heather Adams for discussing chemistry techniques with me and my brother Wesley Adams for his fetching and carrying when I was recovering from my motorbike accident.

Lastly I would like to thank my girlfriend Amy Colbran for putting up with me and providing her constant support and advice throughout what I have found to be my largest challenge to date, which I could not have done without her. On top of all that she even read it cover to cover, twice!

CONFERENCE PRESENTATIONS

1. G. Adams‡ ^, R. Cook, J. Hutchinson, P. Zioupos (2014) Bone Surface Distribution from A Wide Porosity Range in Mammalian Bone Tissue

   World Congress of Biomechanics, July 6-11, 2014, Boston (USA)

2. G. Adams‡ ^, R. Cook, C. Greenwood, K. Rogers, P. Zioupos (2015) Fracture Toughness of Cancellous Bone: Predictions from micro-CT Values

   21st Congress of the European Society of Biomechanics, 5-8 July 2015, Prague, Czech Republic

3. G. Adams‡ ^, R. Cook, J. Hutchinson, P. Zioupos (2015) Micro-Ct Values Versus Material Properties Of Bone Over A Very Broad Range Of Mineralisation Levels.

   21st Congress of the European Society of Biomechanics, 5-8 July 2015, Prague, Czech Republic

4. G. Adams‡, R. Cook, J. Hutchinson, P. Zioupos ^ (2015) The Importance Of Thresholding In Micro-CT For The Histomorphometric Analysis Of Mammalian Bone Tissue.

   25th Congress of the International Society of Biomechanics, 12-16 July 2015, Glasgow, UK

5. G. Adams‡ ^, C. Greenwood, JG. Clement, AJ. Dicken, JPO. Evans, I.D. Lyburn, RM. Martin, KD. Rogers, N. Stone, P. Zioupos (2016) Fracture toughness of the cancellous bone of FNF femoral heads in relation to its micro-architecture

   22nd Congress of the European Society of Biomechanics, 10-13 July 2016, Lyon, France

6. G. Adams‡ ^, R. Cook, P. Zioupos (2016) Predictions for the fracture toughness of cancellous bone of fracture neck of femur patients

22nd Congress of the European Society of Biomechanics, 10-13 July 2016, Lyon, France

7. G. Adams‡, R. Cook, P. Zioupos ^ (2017) Fracture Toughness of Cancellous Bone as a Function of BV/TV and its Micro-architecture

   Bone Research Society Annual Meeting, 25-27 June 2017, Bristol, UK

8. G. Adams‡, R. Cook, C Franceskides ^, P. Zioupos (2017) Chemical and Structural Properties of Cancellous Bone and the Impact on Fracture Toughness

   23rd Congress of the European Society of Biomechanics, 2-5 July 2017, Seville, Spain

JOURNAL PUBLICATIONS

1. The micro-architecture of human cancellous bone from the fracture neck of femur patients in relation to the structural integrity and fracture toughness of the tissue. C. Greenwood*‡, J.G. Clement, A.J. Dicken, J.P.O. Evans, I.D. Lyburn, R.M. Martine, K.D. Rogers, N. Stone, G. Adams and P. Zioupos

   Bone Reports, Volume 3, December 2015, Pages 67-75

2. Localized tissue mineralization regulated by bone remodelling: a new computational illustrated paradigm. M. Berli‡, C. Borau, O. Decco, G.J. Adams, R.B. Cook, J.M. García Aznar, P. Zioupos*

   PLoS ONE, Volume 12, March 2017.

3. Bone apparent and material densities examined by cone beam computed tomography and the Archimedes technique: comparison of the two methods and their results", by G. J. Adams, R. B. Cook, J. Hutchinson and P. Zioupos

   Front. Mech. Eng., 05 February 2018

* - Submitting author

ǂ - Lead author

^ - Presenting author

TABLE OF CONTENTS

LIST OF FIGURES

LIST OF TABLES

LIST OF EQUATIONS

LIST OF ABBREVIATIONS

µ-CBCT	Micro Cone Beam Computed Tomography
µ-CT	Micro Computed Tomography
ATR-FTIR	Attenuated total reflection Fourier Transform Infrared Spectroscopy
BMD_a	Areal Bone Mineral Density
BMD_v	Volumetric Bone Mineral Density
BS/BV	Bone Surface/Bone Volume (mm^{-1})
BS/TV	Bone Surface/Total Volume (mm^{-1})
BV/TV	Bone Volume/ Tissue Volume
CBCT	Cone Beam Computed Tomography
Conn. D	Connectivity density
CT	Computed Tomography
DA	Degree of anisotropy
D_{app}	Apparent Density (g cm^{-3})
DEXA	dual-energy X-ray absorptiometry
D_{mat}	Material density (g cm^{-3})
DSC	Differential Scanning Calorimetry
FEA	Finite Element Analysis
FRAX	Fracture Risk Assessment
FTIR	Fourier Transform Infrared Spectroscopy Infrared Spectroscopy
K_C	Fracture Toughness (MPa $m^{-1/2}$)
OA	Osteoarthritis
OP	Osteoporosis
pXRD	Powdered X-Ray Diffraction
QUS	Quantitative ultra-sound

SMI	Structure Model Index
TbN	Trabecular Number
TbSp	Trabecular Spacing (mm)
TbTh	Trabecular Thickness (mm)
TMD	Tissue Mineral Density (g cm^{-3})
WHO	World Health Organisation
XRD	X-Ray Diffraction

1 Introduction

1.1 Bone disease

1.1.1 Osteoporosis

In an ever aging population the number of people suffering from osteoporosis is on the rise with the NHS estimating that 3 million people in the UK alone suffer from osteoporosis and that 250,000 fractures a year are due to fragility or low trauma fracture from osteoporosis (Johnell & Kanis 2006). Low trauma fractures are considered to be fractures caused by falling from a height of standing or less. Osteoporosis (OP) is a bone deterioration disease generally associated with postmenopausal women, however anyone can be at risk of OP and over 40 the risk of OP dramatically increases (Choices 2016). Low bone mass or low bone mineral density (BMD) is associated with changes in the bone remodelling.

OP sufferers are characterized by a reduction in the bone mass following peak bone mass which is achieved in the early 30's. This drop in bone mass is responsible for structure and material changes that results in the loss and thinning of trabecular struts and increases in the porosity of cortical tissue (Zioupos et al. 2008). Having reduced bone mass with age is normal after peak bone mass but in osteoporosis the bone mass has fallen below 2.5 standard deviations below the young adult reference mean (Summers 2001). This significant drop below the young adult reference mean has a dramatic effect on the mechanical competency of the skeleton. Having a reduced bone mass between 1 and 2.5 standard deviations below the reference mean is regarded as osteopenia (Summers 2001) and puts the suffer at an increased risk of fracture but to nowhere near the increased risk suffered by those with osteoporosis. Osteopenia is however considered a precursor to osteoporosis and in women suffering with primary type I osteoporosis (mentioned below) this highlights an opportunity to begin preventative treatment and life style changes to delay the onset of full osteoporosis.

There are two categories of osteoporosis, primary and secondary osteoporosis. Primary osteoporosis is the most prevalent form of osteoporosis and is that which occurs by either age or hormonal changes caused by menopause. Primary osteoporosis is more common in women than men. Secondary osteoporosis is osteoporosis caused by external factors outside of the normal processes associated with aging. Primary Osteoporosis can be subdivided into two types; type I and type II.

Osteoporosis link with substitution of PO_4^{3-} ions by CO_3^{2-} ion in the HA lattice (Barbani, et al. 2011)

1.1.1.1 Type I or Postmenopausal

Primary type I or postmenopausal osteoporosis affects women and can lead to losses as high as 5-6% of bone mass per year in the first 5 years after its initial onset. This marks a significant increase on the typical losses in women of ~0.5% per year which tend to occur after the peak bone mass has been reached (Bono & Einhorn 2003). These rates of bone loss stress a high importance on reaching a high peak bone mass before typical losses begin to occur, it has been suggested that this accumulation to bone can dramatically reduce as early as 16-20 years of age (Theintz et al. 1992).

1.1.1.2 Type II or senile:

Primary type II or senile osteoporosis is that which occurs naturally with the aging process and is not driven by any dramatic hormonal change as with type I. As already mentioned women suffer a loss rate of ~0.5% per year, men also suffer from an annual loss rate after peak bone mass has been reached of ~0.3% per year. This rate of bone loss typically starts between 35 and 50 years old (Summers 2001).

1.1.1.3 Secondary osteoporosis

Secondary osteoporosis is caused by a multitude of clinical and environmental factors which include; hypogonadism, medications, hyperthyroidism, vitamin D deficiency, primary hyperparathyroidism, solid organ transplantation, gastrointestinal diseases, hematologic diseases, Cushing's syndrome, idiopathic hypercalciuria, alcohol abuse and many others (Painter & Kleerekoper 2006; IOF 2017.).

Types I and II osteoporosis have different effects on how the net bone loss is experienced. Type I affects mostly the cancellous bone which, logically, will lead to a greater reduction in strength of the regions of bone that possess mostly cancellous tissue such at the spine and proximal end of the femur. Type II is typically affected evenly in both the cortical and cancellous regions of bone, this increased cortical bone loss will lead to an increased risk of fracture at the sites dominated by cortical bone such as the mid-shaft of the femur (Bono & Einhorn 2003). In men and women the changes due to osteoporosis are different and women tend to lose more trabecular struts where as men tend to suffer from a thinning of the struts.

Losing struts leads to a greater loss of mechanical strength put women with osteoporosis at a higher risk of fracture than men with osteoporosis.

The current 'gold standard' used in the diagnosis of osteoporosis is the assessment of areal bone mineral density (BMDa) using dual-energy X-ray absorptiometry (DEXA). The World Health Organisation (WHO) bases their recommended diagnosis around BMDa measurements taken from DEXA. DEXA measurements are typically taken at the hip which is a region of bone tissue that is predominantly spongey or cancellous bone. This cancellous bone tissue is a cellular solid formed of bony trabecular struts. The results of DEXA can be used in conjunction with the Fracture Risk Assessment Tool (FRAX), a 10 year tool developed by WHO. The tool is used to assess if a DEXA scan is appropriate and calculates the risk of fracture in the next 10 years. The use of DEXA in conjunction with the FRAX tool has had great success but the assessment of BMDa by DEXA confounds bone quality and micro-architecture, because the assessment of BMDa is the product of the quantity and density of the bone tissue and fails to consider the micro-architecture and materials properties of the tissue itself. It is therefore of great interest and importance to build a better understanding of these micro-architectural and material properties so that they could inform further on DEXA and the FRAX tool to help improve the reliability of the assessment of an individual's fracture risk. There is the possibility that there are also chemical markers within the bone tissue that might exist before low BMDa cannot be measured by DEXA which could enable an early identification of those at risk of developing OP.

1.1.2 **Osteoarthritis**

While osteoarthritis is normally considered only for its impact on the articular cartilage of the synovial joints the knock on effects of the compromised joints causes structural changes to occur in the subchondral bone. Osteoarthritis affects 8.75 million people in the UK and it is estimated that 33% of the population over the age of 45 have sought treatment for osteoarthritis. The joints most affected by the condition are the knee and hip affecting 4.7 and 2.46 million people respectively.

1.1.2.1 Primary

The primary form of osteoarthritis affects 50% of people in the over 65 age group and 85% over 75 years of age (Jordan et al., 1997). Within populations the ethnicity and gender does not appear to affect the prevalence of the condition, however there are differences in the prevalence of specific sites by gender (Jordan et al., 1997; Cimmino and Parodi, 2005). In

males the hip joint has been shown to be more susceptible to OA, whilst in women the knee joint has a greater occurrence of the condition (Jordan et al., 1997; Cimmino and Parodi, 2005).

1.1.2.2 Secondary

The secondary form of the condition is linked to the environmental factors and lifestyle of the individual. The additional stresses experienced by the synovial joints during high intensity exercise can cause damage to the cartilage at a rate that exceeds the rate at which the cartilage is able to self-repair. The rate of repair of the cartilage is limited by rate at which nourishment can be provided to the cells for repair by gleaming from the synovial fluid (Ghosh, 2003). Additionally factors such as poor dietary nutrition or obesity can lead to the deterioration of the cartilage by limiting nutrient supply or by cause continuous excessive load of the joint (Kee, 2000).

1.2 **Bone**

The skeletons primary role in the body is as a structural material. It provides support giving muscles sites to bind to and providing a mechanical advantage during motion. In addition to movement it provides protection for vital organs such as the brain, heart and lungs. As well as its structural role it acts as a mineral store accounting for 99% of the calcium, 85% of the phosphorus and 60% of the magnesium in the body (Currey, 2002). Bone is a multi-hierarchal composite material formed of individual units of collagen and mineral at the Nano level, to cortical and cancellous bone at the macro level.

Bone, the material, exists at the organ level as whole bones. Whilst bone may seem relatively inert compared to other structures in the bone it is in fact an adaptive material which responds to its environment, this aspect of bone provides an inconvenient obstacle for the engineer who is more used to dealing with manmade materials with controllable static properties. One of the first times the adaptive nature of bone was recognised was by Julius Wolff. Where stated that the bone of a healthy individual or animal will, over time, adapt to the loads under which it is placed. Therefore if the load on a bone were to increase or decrease the bone will remodel itself to react to its environment according. The fundamental results of Wolffs Laws hold true but his explanation and understanding of the underlying mechanisms were misunderstood (Currey, 2002). The natural of the biological and micro mechanical mechanisms that drive bone remodelling are still not fully understood (Currey, 2002). At its material level bone is a multiphase composite material formed of both organic

and inorganic constituents. It has a hierarchal structure that ranges from a sub-nano level of the collagen-mineral composite through to the macro structure of cortical and cancellous bone.

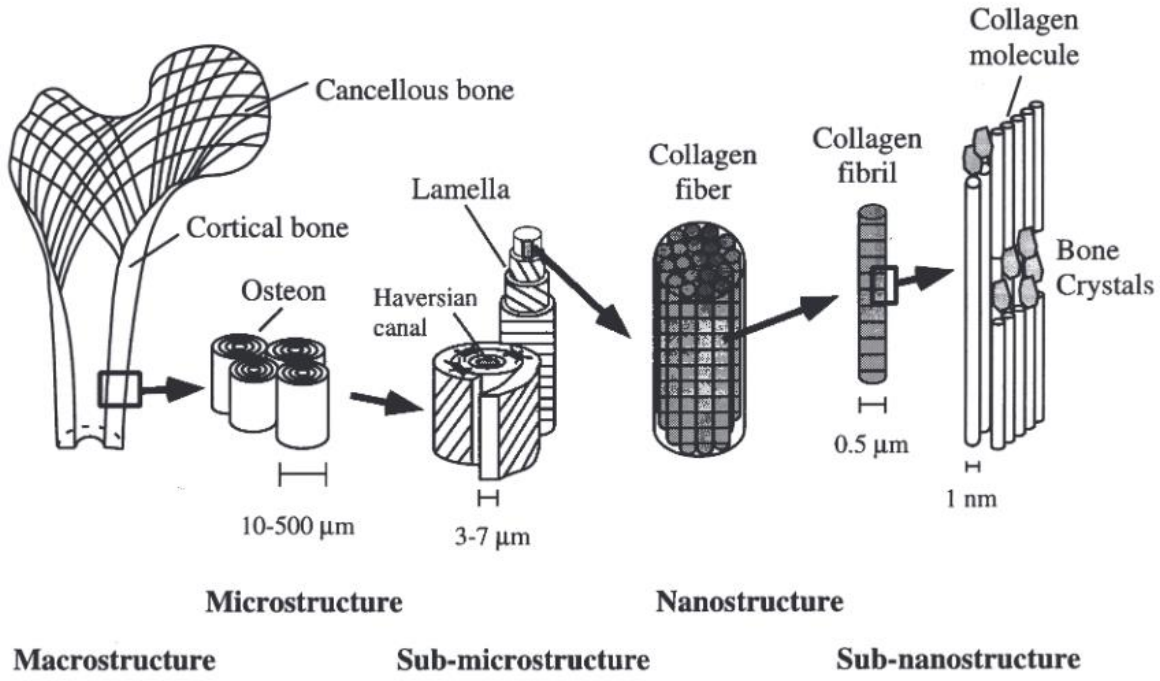

Figure 1-1 Hierarchical structural organisation of bone (J.-Y Rho et al. 1998).

1.2.1 **Bone: Macro-Structure**

The macro structure of bone can be, and normally is, considered in two discrete forms, Cancellous and Cortical. Cancellous bone is a porous 'spongey' material that tends to exist at the ends of long bone and fills the sandwich layers of flat bones. Cortical bone by comparison is far denser in structure and occupies the mid shaft of long bone and provides a shell at the ends of long bones and flat bones. Cortical and Cancellous bone exist on a spectrum ranging from near 0% porosity to >99%, throughout this work the porosity is refered to as that used by Martin (1984) which considers porosity as the void volume per unit volume of whole bone typical measured at the scale of microns (Zioupos et al., 2008).

Cortical bone is typically considered to be bone with a porosity of less than 15%, and as stated above, is relatively dense bone (Figure 1-1). Cortical bone normally displays densities of 1.7-2.1cm^{-3} at the material level, (Zioupos et al., 2000), and apparent densities of ~1.8gcm^{-3} (Zioupos et al., 2008). The voids in cortical bone are mostly associated with

vascular channels and Haversian systems used in bone remodelling. Cortical bone forms the largest structural units of the skeleton and encases all the bones with a cortical shell.

Cancellous bone in comparison is very porous with a low bone volume to total tissue volume ratio (BV/TV) with porosities exceeding 50%. Bone does however exist in porosities between what is normally considered cortical and cancellous and these regions occur normally in the ends of long bones where the bone transitions from cancellous to cortical bone. Cancellous bone is formed of small units called trabecular which can form in either rods or plates. This results in a cellular solid or foam (Brezny & Green, 1990; Gibson, 1985), depending on weather the structure is formed of rods or plates the structure is said to be either open or closed.

1.2.2 **Bone: Micro-Structure**

At the Micro-structure bone exists in two forms, primary and secondary, this bone is organized in 4 different ways; woven bone, lamellar bone, fibro-lamellar bone and secondary osteons.

Woven bone is primary bone that is found in young bone and is disorganized in structure; it displays more isotropic properties than that of more mature bone types. Lamellar bone is more organized in structure and can be both primary and secondary. Fibro-lamellar bone consists of both woven and lamellar bone and is primary. Secondary osteons or Haversian systems are highly organized secondary bone that is form as the result of remodeling (Currey, 2002; Martin, & Burr, 1989).

The remodeling of bone is driven by two types of cells osteoclasts and osteoblasts. During remodeling osteoclasts advance through bone in a, so called, cutting cone formation. In the advancement of osteoclasts bone is resorbed by the cells creating a void. Behind the advancing cutting cone osteoblasts lay down new bone in concentric rings (Figure 1-2).

The result of this remodeling is the previously mentioned Haversian system which consists of a central Haversian canal surrounded by concentric rings of lamellae. The central canal is used as a channel for blood vessels to exchange nutrients and waste (Currey, 2002). The remodeling of bone is considered to be a surface effect which shows the need to the presences of these systems in cortical bone, in cancellous bone however the exposed porous natural of the structure does not require such systems, therefore does not contain true Haversian systems (Currey, 2002).

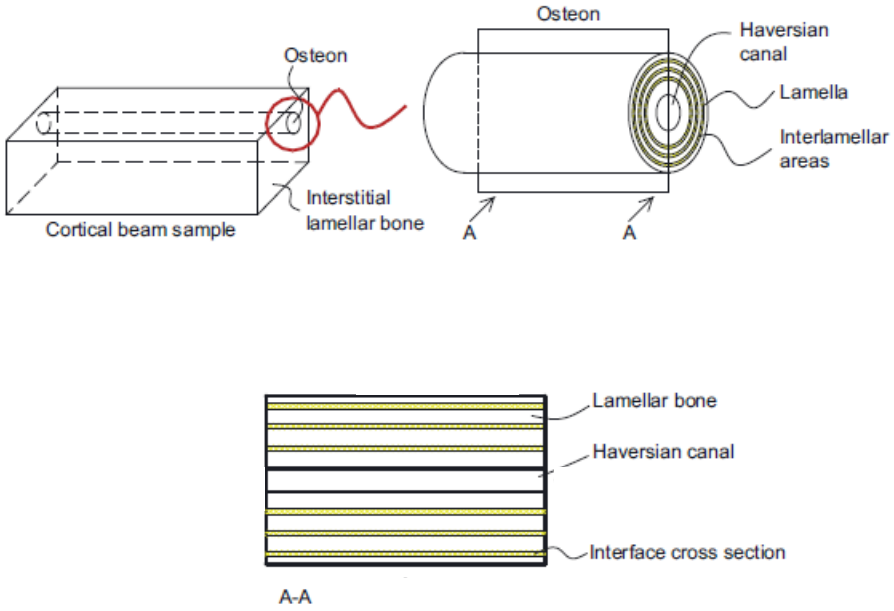

Figure 1-2 Diagram of an Osteon and Haversian system within cortical bone taken from Nobakhti et al. (2013)

1.2.3 **Bone: Nano-Structure**

The organic portion of bone can be further divided into collagenous and non-collagenous proteins, both of which play a vital role in the structure and strength of bone. The collagen in the bone matrix accounts for 85-90% of bone bound protein in the body, (Knott & Bailey 1998) the rest of the proteins are non-collagenous proteins (NCP's) and are mainly involved in the chemical and biological process involved in bone metabolism and formation. Multiple types of collagen are found in the bone, but like in most of the body, the predominant form is type I. There also exist small amounts of types III, V and VI (Bätge et al. 1992; Bailey et al. 1992; Bailey & Knott 1999; Viguet-Carrin et al. 2006). Collagen is formed on three polypeptide chains which form a triple helix (Viguet-Carrin et al., 2005). Collagen forms in helical structures called fibrils, collagen fibrils can be characterized by a 67nm periodicity and 40 nm gaps or holes between the ends of the molecules, and each molecule overlaps by 27 nm. (Weiner & Traub 1992; Rho et al. 1998; Viguet-Carrin et al.

2006). These spacing aligns the tails and heads of the molecules in a positon known as the quarter stagger.

The initial formation of the fibrils is governed by immature, bivalent cross-links located near the ends of new collagen fibres. Over time mature covalent cross-links form providing inter-fibrillar linkage of collagen molecules; this provides support and strength to the fibrils structure (Knott and Bailey, 1998). Different cross-links existed between the collagen fibrils. Pyridinium and Deoxy-Pyridinium are cross-links found in bone collagen, Deoxy-Pyridinium is only found in bone collagen. These bonds help to increase stiffness and enhance the dissipation of energy (Fantner et al. 2005). Changes in the collagen with age have been linked to deterioration in the mechanical properties displayed by bone tissue (Zioupos et al. 1999; Very et al. 1997).

Whilst they only make up ~10% of the organic matrix in bone the NPC's provide 'sacrificial' bonds that help provide stiffness and increase energy dissipation (Fantner et al. 2005). The proteoglycans and osteocalcin have previously been linked with the remodelling process (Butler, 1984; Bonucci, 2000).

As well as the organic component of bone there is an inorganic structure, calcium hydroxyapatite (HA). This crystallographic structure is the mineral in bone tissue; it is very stiff and provides rigidity to bone. It is brittle on its own and has very poor fracture toughness. This mineral is primarily responsible for the stiffness that bone provides (Zioupos et al. 1999). Bone mineral can be described as a poorly crystalline, nano-crystalline hydroxyapatite which contains contaminants and substitutions into the crystal lattice these include; HPO_4, Na, Mg, citrate, carbonate and K (Baxter et al. 1966; Rho et al. 1998; Shea & Miller 2005). A general chemical formula of HA of $Ca_{10}(PO_4)_6(OH)_2$, however this ideal formula is never actually found (Rey et al. 2006), due to substitutions within the crystal lattice which can dramatically affect the chemical composition of the mineral, an example of a proposed general chemical formula for bone is given in Equation 1-1:

$$\left[(Ca^{2+})_{10-a-b}\left(Sub^{Ca^{2+}}\right)_a\left(V^{Ca^{2+}}\right)_b\left|(PO_4{}^{3-})_{6-c-d}\left(Sub^{PO_4{}^{3-}}\right)_c\left(V^{PO_4{}^{3-}}\right)_d\right|(OH^-)_{2-3-f}(Sub^{OH^-})_e(V^{OH^-})_f\right]$$

$Sub^{Ca^{2+}} = calcium\ ion\ substitution\ (for\ example\ Mg2+, Na+, K+, Sr2+)$

$V^{Ca^{2+}} = calcium\ ion\ vacancy$

$Sub^{PO_4{}^{3-}} phosphate\ ion\ substitution\ (for\ example\ CO32-, HPO42-)$

$V^{PO_4{}^{3-}} =$ phosphate ion vacancy

$Sub^{OH^-} = hydroxyl\ ion\ substitution\ (for\ example\ CO32-, F-, Cl-)$

$V^{OH^-} =$ hydroxyl ion vacancy

$$\mathbf{10} > \boldsymbol{a} > \mathbf{0}\ \ \mathbf{10} > \boldsymbol{b} > \mathbf{0}\ \ \mathbf{10} > (\boldsymbol{a} + \boldsymbol{b})$$
$$\mathbf{6} > \boldsymbol{c} > \mathbf{0}\ \ \mathbf{6} > \boldsymbol{d} > \mathbf{0}\ \ \mathbf{6} > (\boldsymbol{c} + \boldsymbol{d})$$
$$\mathbf{2} > \boldsymbol{e} > \mathbf{0}\ \ \mathbf{2} > \boldsymbol{f} > \mathbf{0}\ \ \mathbf{2} > (\boldsymbol{e} + \boldsymbol{f})$$

Equation 1-1 *A proposed general chemical formula for bone mineral HA taken from* (Beckett 2009)

This formula considers the vacancy defects and lattice substitutions for calcium, phosphate and hydroxyl ions that can occur within HA, without making note of the quantity as this is variable depending on a multitude of environmental and biological factors affecting the bone (Beckett 2009).

The collagen has a helical structure formed into base units called fibrils and is very strong in tension but is structurally weak in compression and shear as it is non-rigid, similar to rope. The Crystals in contrast are brittle tough units; they are long and thin and provide compressive strength and rigidity.

The collagen and crystals align together in the principle direction of stress. This leads to an anisotropic material with a high compressive and tensile strength along the length of the bone. Interactions between the collagen matrix and collagen are highly important in determining the resultant strength of bone tissue. If during the mineralization process of the collagen matrix in young bone there abnormalities within the structure of the collagen matrix, for example in the cross linking profile leading to an irregular structure, this would inhibit the deposition of mineral in the regular sheets leading to compromised mechanical properties (Landis 1995).

1.2.4 **Bone fractures**

Bone fractures can occur in both the cortical and cancellous regions of the skeleton. Broadly speaking bone fractures can be put into 2 categories; simple and compound fractures. Simple fracture stay close and broken bone remain within the body whilst compound fractures occur when broken bones penetrate the skin. These categories can be further subdivided into; comminuted fracture, these involve the bone being broken in to several small pieces. Greenstick fractures the bone only fracturing on one side resulting in bending, this typical occurs only in children due to the soft bone tissue. Avlusion fractures, when a section of bone if torn off the main body of the bone (Innerbody, 2018).

Bone fracture can occur in different direction relative to the bone which are typically grouped into transverse, oblique and spiral. Transverse fractures occur at 90^{o} to the orientation of the bone, oblique fracture are slanted and occur closer at angles close then 90^{o} to the bone, and spiral fractures are caused by torsional forces (Innerbody, 2018).

1.3 **The current study**

The site of interest in this study is the proximal femur and in particular the fracture of the femoral neck which occurs when a crack propagates across the cancellous bone structure (Cook & Zioupos, 2009). The fracturing at the neck of the femur is typical most consistent with a simple transverse or oblique fracture (OrthoInfo, 2018). The plain strain fracture toughness of cancellous bone has been previously reported yet an understanding of how the micro-architecture and material quality impact the fracture toughness is needed (Cook & Zioupos, 2009). The previous measurements fracture toughness in this way gives understanding of the material properties that will impact transverse and oblique fractures. If the diagnosis of osteoporosis is to be improved assessment of the changes that occur due to the development of OP is needed alongside the well documented reduction in bone mass. Particular focus will be on the chemical and physiological variations that occur with reduced fracture toughness. It is hoped that this will lead to a better understanding of the material quality of osteoporotic bone. In addition to analysis of bone it is hoped that both a step-wise regression and micro finite element analysis will be able to predict the fracture toughness of the cancellous regions of bone, which will provide a basis for more accurate predictions of a patient's fracture risk.

1.4 **Aims and Objectives**

The overall aim of the research is to understand the fundamental structural and material properties of cancellous bone and their impact on the fracture toughness.

It was hypothesised that starting at the assessment of cancellous bone by micro-CT we would be able to develop models to predict fracture toughness and that at the second stage the physicochemical composition of the bone would be able to add to these models to predict fracture toughness. Additionally using this material and structural data it would be possible to simulate bone fracture toughness *in silico*. To test the hypothesis and deliver the overall research aim the following objectives were set:

Objective 1. Investigate the accuracy and suitability of assessing the structural characteristics of bone tissue and determine how the characteristics vary across the porosity of bone tissue.

Objective 2. Investigate how structural properties of human cancellous bone assessed by µ-CBCT affect the measured facture toughness of the tissue.

Objective 3. Investigate the Physicochemical properties of human cancellous bone and their impact on fracture toughness.

Objective 4. Develop statistical and Finite Element models to predict/simulate the fracture toughness of human cancellous bone.

1.5 **Thesis plan**

This thesis is presented as a series of chapters formatted as journal papers. All Papers, unless otherwise stated, were written by the primary author, George J. Adams and edited by Prof. Peter Zioupos, Dr Michael C. Gibson, and Prof. Keith Rogers, where appropriate. Initial human and elephant samples collection and segmentation was carried out by Dr Richard B. Cook formerly of Cranfield University (UK).

The first body of work presented in chapters 2 & 3 was undertaken to identify the suitability and accuracy of the assessment of bone tissue by micro-computed tomography (µ-CT) when compared with physical laboratory measurements. The primary goals were to investigate how to assess the density of tissue from micro-CT images and assess the impact of setting the threshold position on the results. This work was undertaken solely by George J. Adams, including the imaging, image processing and analysis of data. The samples were initially supplied to Cranfield University Biomechanics laboratories by Dr John Hutchinson

from Department of Veterinary Basic Sciences, RVC, University of London, Hatfield, UK and initial cut and analysed by Dr Richard B. Cook nCATS, School of Engineering Science, University of Southampton, Southampton, UK in work that was presented in Zioupos, Cook, & Hutchinson (2008).

The outcomes to chapters 2 & 3 were used to ensure that the methods used to assess the osteoporotic and osteoarthritic tissue by µ-CT were suitable. This work identified that the structural properties of bone contribute significantly to the ability of bone to resist fracture. Multiple Stepwise Regression analysis was able to combine multiple parameters to further assess the contribution of micro-architectural parameters to resistance to fracture. The result of the work produced predictive models with R2 values as high as ~0.8 which identified that the micro-structural and density properties of the tissue could not fully account for the fracture toughness of the tissue. This, therefore, identified that an assessment of the physicochemical properties of the tissue should further contribute to understanding and predicting fracture.

Findings from the previous chapter (4) suggested that non-density related chemical properties of the tissue contribute to fracture toughness such as the quality of the mineral and collagen rather than quantities of the components. This lead to the assessment of the tissue by various popular laboratory means which showed that the addition of some chemical parameters, most notably quantity assessed by Raman Spectroscopy, could improve the fracture predictive models developed in chapter 4 with R^2 values as high as ~0.88. The contribution of the quantity to the resistance to fracture throws into doubt the assessment of density by µ-CT which may be erroneous or lack in sensitivity compared to Raman Spectroscopy. The work also showed that Biomarkers exist within the Raman Spectra that can identify fracture from non-fracture samples. The quantity of mineral and collagen contributing to the fracture toughness should be reflected in the thermal decomposition of the tissue which may be able to more accurately assess the differences. This led to the work presented in chapter 6 in which differential scanning calorimetry (DSC) was used to assess if the thermal decomposition was able to identify the significant differences in the quantity of collagen with respect to fracture toughness. Some weak correlations were found, however nothing that improved over the already collected Raman and X-Ray diffraction (XRD) data.

Following the identification of the properties that contribute to fracture and the development of reasonably successful and significant predictive models based on architecture

and chemistry the next step was to determine if the fracture could be modelled using µ-CT data in conjunction with Finite Element Analysis (FEA) to contribute towards the development of patient specific models (chapter 8). This raised the need to develop grey scale based material models, presented in chapter 7. Here the widest possible range of bone densities were imaged using µ-CT and indented using nano-indentation to determine the sub-mm properties of the tissue with respect to the grey values to be used in µ-FEA model. This work showed that at the micron scale there existed a power relationship between the density and the indentation modulus.

The use of µ-FEA (chapter 8) showed that the stiffness of the samples could not be reasonably modelled without the introduction of element fracture so, in conjunction with Dr Michael C. Gibson, a new method of implementing fracture into bone µ-FEA was introduced. This improved the accuracy of the models but was unable to improve on the previously developed statistical models. The work does however provide a reasonable basis for fracture simulation by means of element softening that with fewer limitations than presented here might be more successful.

Chapter 9 discusses the overall implications of this work on the current body of literature and the benefits it provides to the understanding of bone fractures and diseases such as osteoporosis and osteoarthritis. Finally, chapter 10 summarises the key conclusions and recommends additional areas of works to further develop the understanding of cancellous bone fracture, and proposes possible steps that could be taken in the pursuit of a clinical application. Table 1-1 summarises the contribution of the individual chapters to the goals outlined in section 1.2, their intended journals, and current status.

The work carried out during this research was done so using two unique sets of samples. The first, a large number of samples from an elephant femur that spans the entire range of possible bone porosities, was used during chapters 2 & 3 to assess the suitability of µCBCT imaging to determine the micro-structure of bone to assess the surface volume characteristics that exist within mammalian bone tissue. Access to these samples has provided a unique opportunity to study these characteristics and relationships in great detail. The second sample set used is a collection of cancellous bone tissue excised from the femoral head of patients who had previously suffered a fracture of the femoral neck (FNF). The samples were initially acquired in a body of research carried out by Richard Cook (Cook 2009.). The initial research carried out on these samples provided the first ever assessment of

cancellous bone fracture toughness on such a large sample size of FNF samples. Having access to these samples following the initial research by Cook has provided the unique opportunity for the present study, in which great strides have been made towards determining the underlying factors that contribute to and determine the fracture characteristics of cancellous bone tissue at the proximal femur.

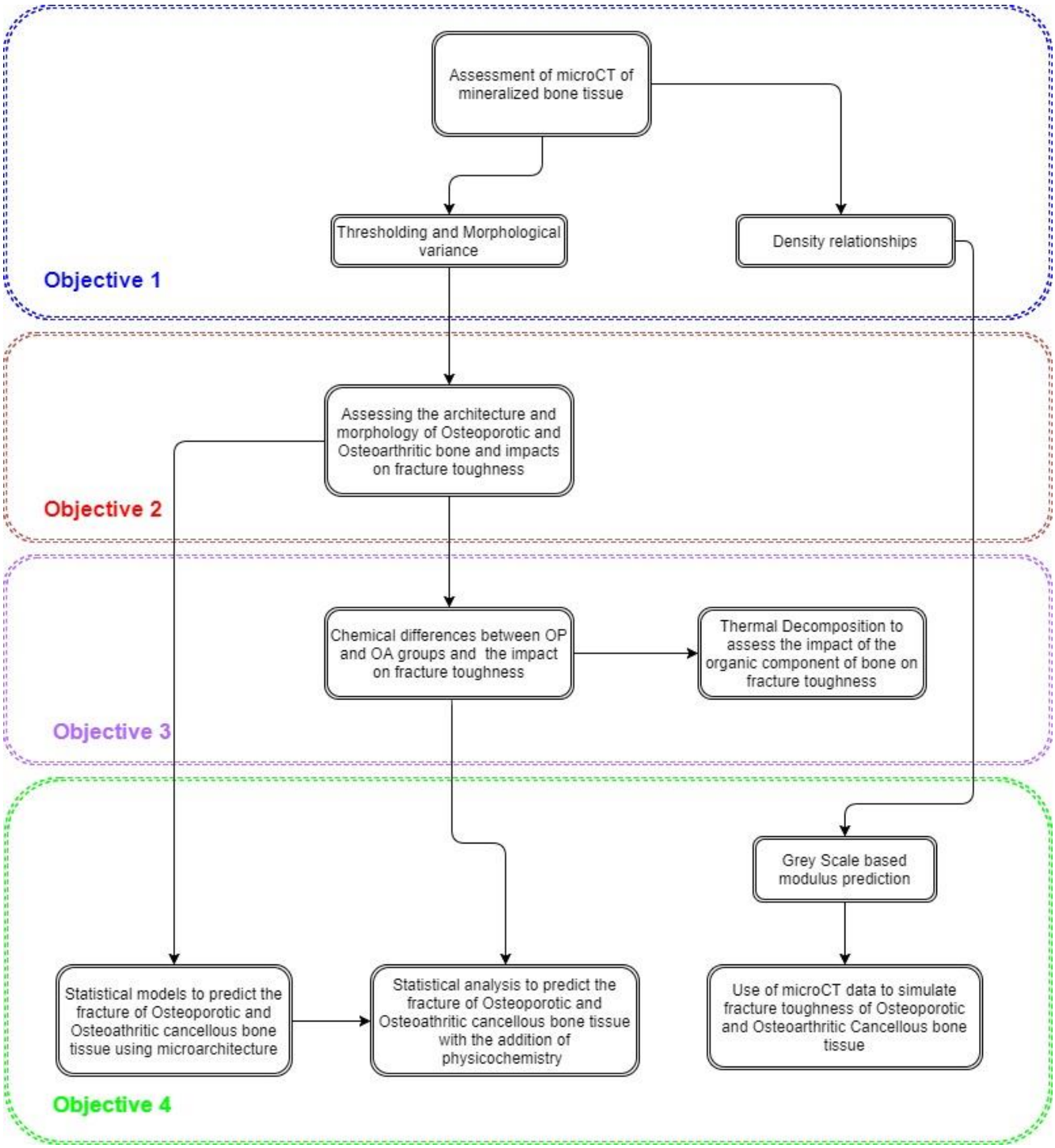

Figure 1-3 outline of how the individual chapters contribute to the subsequent chapters to achieve the primary objectives of the thesis outlined in 1.2. p. n = paper number, c. n = chapter number

Table 1-1 Status of suggested works included in the thesis, working title, proposed journals and the individual objectives they contribute to. The associated conference presentations are also included.

Chapter	Paper	Objective	Title	Journal	Conference
2	1	1	Comparison of Cone Beam Computed Tomography and the Archimedes Technique for the Measurement of Material and Morphological Properties of Bone	Frontiers in Mechanical Engineering / Computing tomography for biomechanics	WCB 2014 ESB2015
3	2	1	Assessment of the physical characteristics and morphology of mammalian bone tissue by Micro-Computed Tomography	Journal of Biomechanics	WCB 2014
4	4	2,4	Prediction the Fracture Toughness of Human Cancellous Bone from Fracture Neck of Femur Patients using its Micro-architecture	JBMR	ESB 2015 ESB 2016 BRS 2017
5	4	3,4	Assessment of the physiochemical properties of cancellous bone in relation to its fracture toughness	Osteoporosis International	ESB 2017
6	5	3	The Thermal Decomposition of Cancellous Bone Fails to identify the Mechanical Competency of the Tissue	Bone	
7	6	1, 4	Micro-CT Values versus Nano-Indentation for the Prediction of Micro Material Properties of Cortical Bone	CMBBM	ESB 2015
8	7	4	The use of micro-finite elements to predict the fracture toughness of human cancellous bone	CMBBM	
9	-	1, 2, 3, 4	Implications of the Work	-	-
10	-	-	Conclusions and Future Work	-	-

ǂ Accepted for publication

1.6 References

Bailey, A.J. et al., 1992. Post-translational modifications in the collagen of human osteoporotic femoral head. *Biochemical and biophysical research communications*, 185(3), pp.801–5.

Bailey, A.J. & Knott, L., 1999. Molecular changes in bone collagen in osteoporosis and osteoarthritis in the elderly. *Experimental gerontology*, 34(3), pp.337–51.

Barbani, N. et al, 2011. Hydroxyapatite-collagen composites. Part I: can the decrease of the interactions between the two components be a physicochemical component of osteoporosis in aged bone? *Journal of Materials Science:Materials in Medicine*, 22(3), pp.637–646.

Bätge, B. et al., 1992. Compositional analysis of the collagenous bone matrix. A study on adult normal and osteopenic bone tissue. *European Journal of Clinical Investigation*, 22(12), pp.805–812.

Baxter, J.D., Biltz, R.M. & Pellegrino, E.D., 1966. The physical state of bone carbonate. A comparative infra-red study in several mineralized tissues. *The Yale journal of biology and medicine*, 38(5), pp.456–70

Beckett, S., 2009. 'Inter-Species Variation in Bone Mineral Cranfield Defence and Security Cranfield Defence and Security Inter-Species Variation in Bone Mineral'. PhD, Cranfield University, Shrivenham

Bono, C.M. & Einhorn, T.A., 2003. Overview of osteoporosis: pathophysiology and determinants of bone strength. *European Spine Journal*, 12(2), pp.S90–S96.

Brezny, R. & Green, D.J., 1990. The effect of cell size on the mechanical behavior of cellular materials. *Acta Metallurgica et Materialia*, 38(12), pp.2517–2526.

Choices, N., 2016. Osteoporosis - Causes - NHS Choices. Available at: *http://www.nhs.uk/Conditions/Osteoporosis/Pages/causes.aspx* [Accessed July 8, 2017].

Cimmino M.A. and Parodi M. (2005) Risk Factors for Osteoarthritis. *Seminars in Arthritis and Rheumatism;* 35(1), pp 29-34

Cook, R.B. 2005. 'Non-invasively assessed skeletal bone status and its relationship to the biomechanical properties and condition of cancellous bone'. PhD, Cranfield University, Shrivenham

Cook, R.B. & Zioupos, P., 2009. The fracture toughness of cancellous bone. *Journal of biomechanics*, 42(13), pp.2054–60.

Currey, J.D., 2002. Bones: Structure and Mechanics, *Princeton University Press*.

Fantner, G.E. et al., 2005. Sacrificial bonds and hidden length dissipate energy as mineralized fibrils separate during bone fracture. *Nature materials*, 4(8), pp.612–6.

P. Ghosh (2003) Osteoarthritis: 2002 and Beyond. *Asia Pacific League of Associations for Rheumatology*; 6(1)**,** p.83-88

Gibson, L.J., 1985. The mechanical behaviour of cancellous bone. Journal of Biomechanics, 18(5), pp.317–328.

Greenwood, C. et al., 2015. The micro-architecture of human cancellous bone from fracture neck of femur patients in relation to the structural integrity and fracture toughness of the tissue. *Bone*, 3, pp.67–75.

Innerbody: types of Bone Fractures *http://www.innerbody.com/image/skel06.html* [Accessed January 18, 2017].

IOF, Facts and Statistics | International Osteoporosis Foundation. Available at: *https://www.iofbonehealth.org/facts-statistics* [Accessed January 18, 2017].

Johnell, O. & Kanis, J.A., 2006. An estimate of the worldwide prevalence and disability associated with osteoporotic fractures. *Osteoporosis International*, 17(12), pp.1726–1733.

Jordan, J.M.. Renner J.B, Luta G et al. (1997) Hip Osteoarthritis Is Not Rare In African-Americans And Is Different Than In Caucasians. *Arthritis and Rheumatism;* 40, pp.236

Kanis, J.A. et al., 1994. The diagnosis of osteoporosis. Journal of bone and mineral research : *the official journal of the American Society for Bone and Mineral Research*, 9(8), pp.1137–41.

Kanis, J.A. et al., 2008. FRAXTM and the assessment of fracture probability in men and women from the UK. *Osteoporosis International*, 19(4), pp.385–397.

Kee, C.K. (2000) Osteoarthritis: Manageable Scourge of Aging. *Rheumatology;* 35(1), pp.199-208

Knott, L. & Bailey, A.J., 1998. Collagen cross-links in mineralizing tissues: a review of their chemistry, function, and clinical relevance. *Bone*, 22(3), pp.181–7.

Landis, W.J., 1995. The strength of a calcified tissue depends in part on the molecular structure and organization of its constituent mineral crystals in their organic matrix. *Bone*, 16(5), pp.533–44.

Martin, R. B. & Burr, D.B., 1989. Structure function, and adaptation of compact bone. *American Journal of Physical Anthropology*, 82(1), pp.116–117.

Nobakhti S., Limbert G., Thurner P.J. 2013. Cement lines and interlamellar areas in compact bone as strain amplifiers - contributors to elasticity, fracture toughness and mechanotransduction. *Journal of the Mechanical Behavior of Biomedical Materials.* 29, pp.235-51

Orthoinfo Hip Fractures *https://orthoinfo.aaos.org/en/diseases--conditions/hip-fractures/* [Accessed January 18, 2017].

Rey, C. et al., 2007. Physico-chemical properties of nanocrystalline apatites: Implications for biominerals and biomaterials. *Materials Science and Engineering: C*, 27(2), pp. 198-205

Rho, J.-Y., Kuhn-Spearing, L. & Zioupos, P., 1998. Mechanical properties and the hierarchical structure of bone. *Medical Engineering & Physics*, 20(2), pp.92–102.

Shea, J.E. & Miller, S.C., 2005. Skeletal function and structure: implications for tissue-targeted therapeutics. *Advanced drug delivery reviews*, 57(7), pp.945–57

Painter S. E. Kleerekoper M. Camachio P. M., 2006. Secondary Osteoporosis: A review of the Recent Evidence. *Endocrine Practice*, 12(4), pp.436–445.

Summers, G.D., 2001. Osteoporosis in men. *Radiography*, 7(2), pp.119–123

Theintz, G. et al., 1992. Longitudinal monitoring of bone mass accumulation in healthy adolescents: evidence for a marked reduction after 16 years of age at the levels of lumbar spine and femoral neck in female subjects. *The Journal of Clinical Endocrinology & Metabolism*, 75(4), pp.1060–1065.

Very, J.M. et al., 1997. Effect of aging on the amide group of bone matrix, measured by FTIR spectrophotometry, in adult subjects deceased as a result of violent death. *Calcified tissue international*, 60(3), pp.271–5.

Viguet-Carrin, S., Garnero, P. & Delmas, P.D., 2006. The role of collagen in bone strength. *Osteoporosis international*, 17(3), pp.319–36.

Weiner, S. & Traub, W., 1992. Bone structure: from angstroms to microns. T*he Federation of American Societies for Experimental Biology*, 6(3), pp.879–85.

Zioupos, P., Currey, J.D. & Hamer, A.J., 1999. The role of collagen in the declining mechanical properties of aging human cortical bone. *Journal of biomedical materials research*, 45(2), pp.108–16.

Zioupos, P., Cook, R. & Coats, A.M., 2008. Bone quality issues and matrix properties in OP cancellous bone. *Studies in health technology and informatics*, 133, pp.238–45.

Zioupos, P., Cook, R.B. & Hutchinson, J.R., 2008. Some basic relationships between density values in cancellous and cortical bone. *Journal of Biomechanics*, 41(9), pp.1961–1968.

2 Comparison of Cone Beam Computed Tomography and the Archimedes Technique for the Measurement of Material and Morphological Properties of Bone

Adams G[1], Cook R[2], Hutchinson J[3], Zioupos P[1]

1 Cranfield Forensic Institute, Cranfield University, Defence Academy of the UK, Shrivenham, UK

2 nCATS, School of Engineering Science, University of Southampton, Southampton, UK

3 Department of Veterinary Basic Sciences, RVC, University of London, Hatfield, UK

2.1 Abstract

An understanding of bone densities and how they vary within bone at the organic level is of great interest in the understanding of degenerative bone conditions. The densities of bone tissue have been shown to impact significantly on the mechanical competency of bone tissue. In order to assess the density of bone in the body it is important to ensure that the parameters being measured are truly representative of the real world values that have been measured *in vivo*. To assess the densities of bone across the entire spectrum of available porosities 112 samples from an elephant femur were assessed using the Archimedes principle and by micro-computed tomography (μ-CT). Comparisons were drawn between the two methods to determine if the calculated densities from μ-CT were representative of physically measured densities. The results showed that the apparent density measured over the entire spectrum was very similar but varied in the intermediate regions of bone tissue due to closed cells in the cancellous matrix and a low density epithelial layer covering the surface of the tissue, and therefore it could be argued that the measurements taken from μ-CT are more representative of bone density. Further research is required into the structural properties of different bone tissue porosities which hopefully in turn will be able to provide a basis for the development of predictive remodelling models.

Keywords: *Bone; cancellous; cortical; density; Porosity; BV/TV; micro computed tomography (μ-CT)*

2.2 **Introduction**

The density and structure of bone are important characteristics that underpin its mechanical behaviour in everyday life. An understanding of these underpinning properties is crucial in the investigation of bone as a structural material. Density can be defined in a multitude of ways ranging from the micro to the macro or organ level. The two generally accepted ways of defining density are as the apparent and material. Apparent density (Dapp) is the mass of the mineralized tissue over the total volume occupied by the tissue with the inclusion of its voids (Equation 2-2), the most common representation of this used in respect to bone is bone mineral density (BMDa) which, when measured by dual energy x-ray diffraction (DEXA), is an areal assessment of this characteristic. Material density (Dmat) is the same mass as in the apparent divided by the volume the mineralised tissue occupies with the exclusion of the voids that may exist within the structure (Equation 2-3). The most popular use of this is often referred to as tissue mineral density (TMD). Following these outlined definitions the difference between these properties is the consideration of mass with respect to the micro-structure of the tissue, such as: voids, osteocyte lacunae, osteonal canals and analogous non-mineralised architectural features.

The assessment of densities with-in bone tissue is considered to be important as it will impact upon the resultant mechanical properties and remodelling characteristics of bone (Martin 1984; Zioupos et al. 2008; Fyhrie et al. 1993). Different methods for this assessment have however been met with a multitude of criticism (Schileo et al. 2008; Zioupos et al. 2008). The most conventional technique employed for this assessment relies on the Archimedes principle, but it has been criticised due to the importance of ensuring that pores must be fully flushed and refilled (Zou et al. 1997). This flushing and refilling is particularly difficult due to the presence of closed cells within the trabecular architecture (Rho et al. 1995). Comparisons of DEXA and the Archimedes technique have previously reported substantial differences (Keenan et al. 1997) whilst fractional quantitative and cone beam computed tomography have been shown to be in closer agreement with Archimedes (Lee et al. 2004; Ahlowalia et al. 2013). When investigating Dapp and Dmat consideration must be given to the volume of bone or BV/TV (dimensionless ratio of bone volume to the total volume of the sample). This can be calculated with the Archimedes principle using Equation 2-1. Calculating BV/TV with Archimedes carries the potential limitations previously mentioned. It has also been calculated/measured by using histological slices (Martin 1984). This technique can also carry an inherent error due to the limitation of physical slice

thickness which requires interpolation between each slice in the addition to sample destruction.

$$\frac{BV}{TV} = \frac{D_{app}}{D_{mat}} \qquad \textit{Equation 2-1}$$

$$D_{mat} = \frac{Bone\ mass}{Bone\ Volume\ (BV)} \qquad \textit{Equation 2-2}$$

$$D_{app} = \frac{Bone\ mass}{Total\ Volume\ (TV)} \qquad \textit{Equation 2-3}$$

The D_{app} is often considered to be one of the primary characteristics of bone that influence its mechanical properties and has been shown to influence not only the compressive properties but also the fracture toughness of bone tissue (Rice et al. 1988; Cook & Zioupos 2009). D_{mat} determines material behaviour at the trabecular level and later, due to the D_{app} being the product of D_{mat} and BV/TV, properties at the structural level. A previous study has shown that the relationship between D_{app} and D_{mat} are interdependent and that D_{mat} is at its highest (~2.3g cm^{-3}) value at the extremes of porosity, as BV/TV tends towards 1 and 0. It also showed that D_{mat} experiences a minimum at a D_{app} of ~1.3g cm^{-3} (Zioupos et al. 2008).

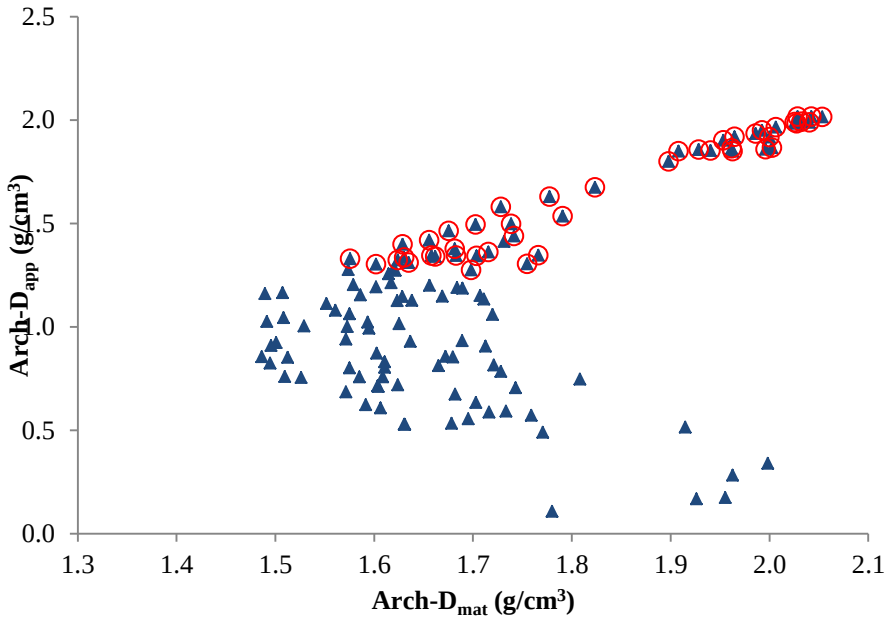

Figure 2-1 Apparent (D_{app}) vs. material density (D_{mat}) for all samples (triangles) produced from the same femur in both cortical and cancellous regions. The samples having D_{app}>1.3 are encircled and the same notation is used in the following figures to allow visual comparisons to be made (Zioupos et al. 2008).

This relationship has however been brought into question where it has been suggested that the relationship may be due to limitations of the Archimedes principle in the assessment of bone tissue (Schileo et al. 2009). To overcome this μ-CT can be used as it gives information on the internal structure, and marrow filled closed cells will not affect the results. Previous work has looked at the density relationship between the cortical and cancellous regions using μCT (Schileo et al. 2008). However this previous work has considered bone as either purely cortical or cancellous and not considered that bone exists over a spectrum (Zioupos et al. 2009). Therefore an understanding of the density relationships across the entire spectrum of bone porosities is warranted. This is the aim of the present study.

2.3 **Materials and Methods**

2.3.1 **Specimens**

In this study 112 samples were taken from the right femur of an adult Asian elephant (3432 kg, 24 year old). The specimen was collected shortly after the animal's euthanasia (for reasons unrelated to this study) at Whipsnade Zoo (Bedfordshire, UK) and frozen (-20oC) until sample testing. Whilst use of elephant tissue is not ideal is does have certain advantages as it is mammalian with the shape and properties at the bone matrix level (confirmed by nano-indentation tests in our laboratories) similar to those of a human femur, the only major difference, therefore, being one of size (Zioupos et al. 2008). This large size enabled extraction of extensive volumes of cortical and cancellous bone which allowed structural effects similar to human tissue to be observed on a scale in tens of millimetres additionally it enabled production of all cortical and cancellous samples from the same sections throughout the same bone (no intra- or inter-individual variability), and obtained from a sample from an animal known to have previously been healthy (Zioupos et al. 2008). The samples had been characterised in a previous study, Zioupos et al. (2008), where full details of sample extraction can be found.

2.3.2 **Imagining-μCT**

All samples were imaged using a cone beam μ-CT scanner, XTEK CT H 225. The samples were imaged in ABS plastic sample holders (~1mm thick) at 50 kV, 65 μA with a 500ms exposure time. The resultant voxel size was ~16 μm making them suitable to accurately determine the samples morphology (Yan et al. 2011). Each sample was imaged twice. First they were imaged fully submerged in deionised water. The samples were then

imaged again in air. All image data was manually reconstructed using CT Pro 3D. With CT Pro the beam hardening and noise reduction filters were applied to provide an optimal image, this image setting was then standardised across the data set to ensure the data collected was comparable.

2.3.3 **Image Analysis**

Image analysis was carried out using VG Studio Max 2.2. Regions of interest (ROI) were taken from the centre of each sample ~9 mm^3 to exclude any external surfaces from the calculations. A surface determination was performed using the grey level of an internal void as the background and the largest void-less section of bone as the sample grey value, as per the manufacturer's recommendations. After the surface determination an automatic morphometric report was exported which contained; BV/TV, specific surface, mean trabecular thickness, mean trabecular number, and mean trabecular spacing.

From the histogram the mean, modal, minimum and maximum grey level were recorded to be used in calculation of the material density. A QRM-MicroCT-HA calibration phantom was scanned and reconstructed under the same conditions in order to determine D_{mat}. Determination of material density is more favourable than deriving Hounsfield units (HU) in this context as HU provides a relative density based on the attenuation coefficients of the material that cannot be measured by traditional densitometry. However density as a mass per unit volume can easily be compared with physical densitometry techniques.

2.3.4 **Density Calibration**

Figure 2-2 shows the histogram of the QRM HA calibration phantom alongside the 3D image of the scan, both the histogram and image are obtained using VG studio. Within VG studio each density was isolated and the average grey scale was determined and plotted against the density provided by the supplier (Figure 2-2). This provided a calibration curve from which the density of the elephant samples could be determined. The average grey value of each sample was measured and using the calibration curve (Figure 2-3) D_{mat} was determined for each sample.

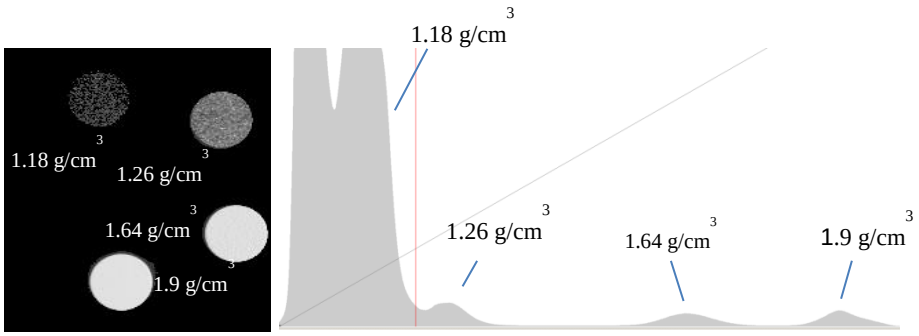

Figure 2-2 QRM Calibration phantom images and histogram the average density, grey and mineral % are given in

Table 2-1

Table 2-1 Properties of QRM calibration phantom

Sample	Mean grey level[i]	Density[ii] (g cm^{-3})	Mineral %[iii]
Standard 1	36.1 ± 6.4	1.13 ± 0.02	0
Standard 2	48.6 ± 9.4	1.18 ± 0.02	0.4
Standard 3	112.2 ± 12.6	1.26 ± 0.02	15.9
Standard 4	337.2 ± 33.7	1.64 ± 0.02	48.3
Standard 5	478.5 ± 42.0	1.90 ± 0.02	63.2

i measured in test

ii provided by calibration certificate for QRM standard

iii Calculated for resin D = 1.13 g cm^{-3} and Hap D = 3.3g cm^{-3}

The D_{app} was determined from the product of the BV/TV and D_{mat} by rearranging Equation 2-1. To distinguish between measurements taken from CT and measurements taken using the Archimedes technique the prefixes CT and Arch will be use respectively.

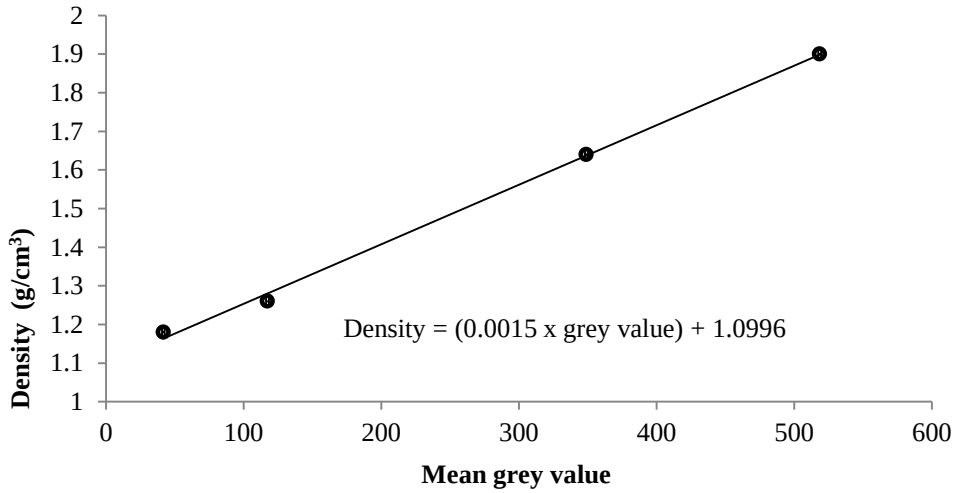

Figure 2-3 QRM Calibration phantom calibration curve

2.4 **Results**

Figure 2-6 shows a comparison of two possible methods for determination of density. Density can either be taken from the average grey value in the sample or from the centre of the peak on the histogram, which represents the modal grey value for the sample. Each method has advantages and disadvantages. Measuring the mean gives the average grey value however it inevitably includes voxel that are only partially filled with bone caused by the partial voxel effect, this can skew the mean to be less than the true mean. Taking the centre of the peak avoids this issue related to partial volumes but only takes the most common density in the scan and has the potential to ignore a non-uniform distribution of densities around the mode.

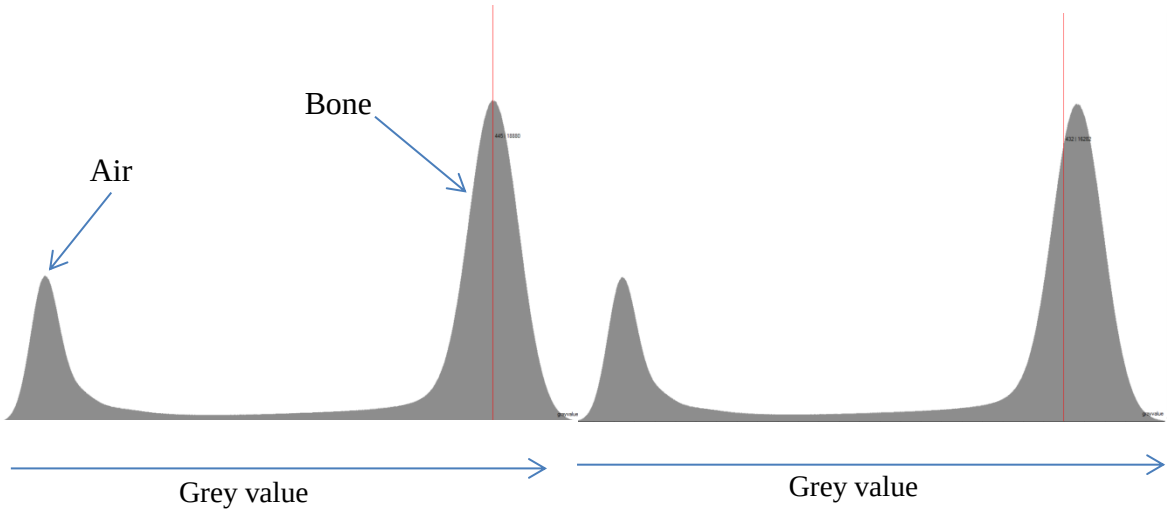

Figure 2-4 example of two possible ways to determining the material density from the histogram for a cortical bone sample, (a) taking a measurement of the peak value (modal), (b) taking the mean value above the determined threshold.

Figure 2-4 shows a comparison of the two methods that can be used to determine the density from the grey scale values from the µ-CT data. The modal value taken will always be higher than the mean value due to the non-zero region between the background, in this case water, and the bone peak. As such, taking the measurement from the modal value is unaffected by the background which would suggest that it is the best method to use. However in extremely porous cancellous bone (Figure 2-5) taking a measurement from the centre of the bone peak is extremely difficult, this is due to having a low quantity of bone tissue in the scan compared to the total volume of the image. It was therefore determined that taking the measurements from the mean value was the most suitable so that comparison of density could be drawn across the entire cohort.

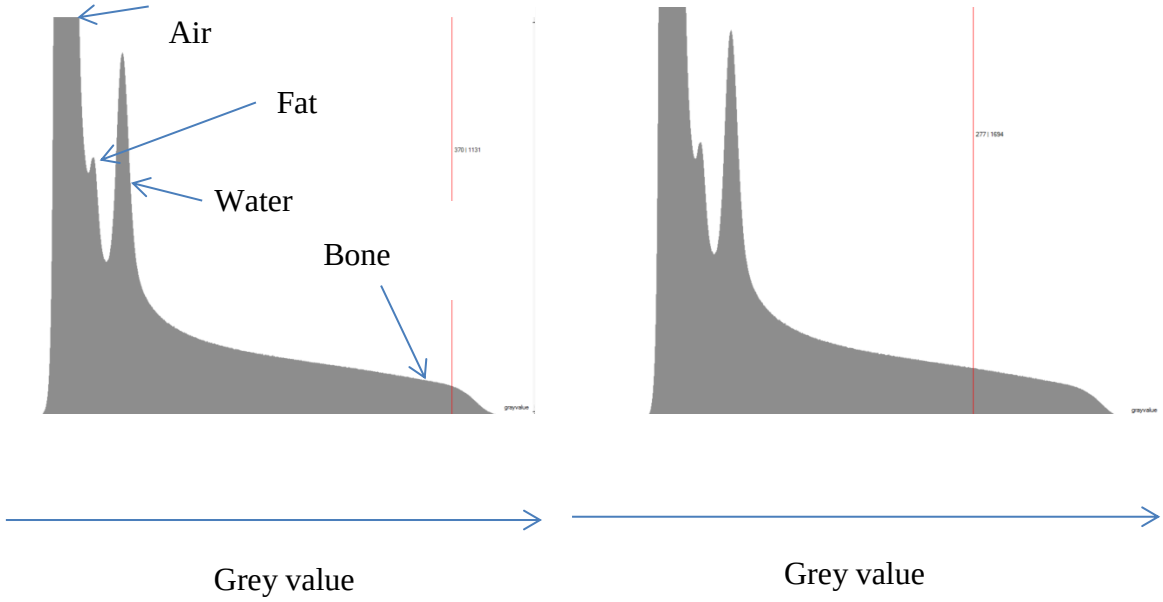

Figure 2-5 example of two possible ways to determining the material density from the histogram for a cancellous bone sample, (a) taking a measurement of the peak value, the location of the peak value is approximated due to the lack of a resolved peak in the low BV/TV samples, (b) taking the mean value above the determined threshold. The additional peaks on the left hand side of the histogram are due to the density of fats and other low density contaminants in the samples.

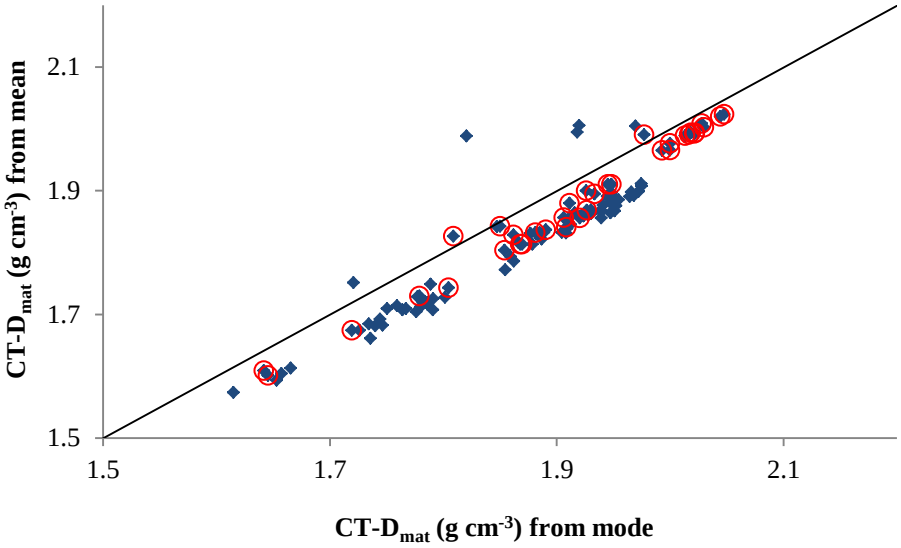

Figure 2-6 Comparison of measuring the material density by the mean and modal grey of the samples. Some outliers exist where there is little bone in the scan so the mode does not lie near the centre of the mean.

Figure 2-7 Comparison of Dapp Zioupos (2008) vs Dapp measured by CT

Figure 2-7 shows a comparison of the *CT-D_{app}* measured from the mean and *Arch-D_{app}* by Zioupos et al (2008). The plot has a slight inflection in the intermediate cancellous bone regions, which may be due to an underestimation of the densities in the CT data as the CT data only makes consideration of the mineralised tissue. Whereas in the data from Zioupos et al. (2008) the apparent density also includes the lower density non-mineralised portions of the bone samples such as less mineralised organic tissue.

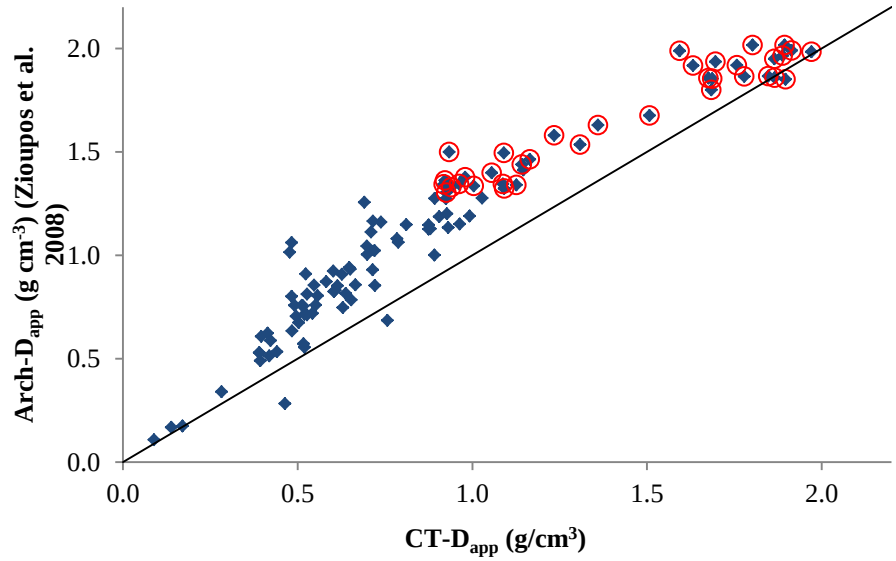

Figure 2-7 Comparison of D_{app} Zioupos (2008) vs D_{app} measured by CT

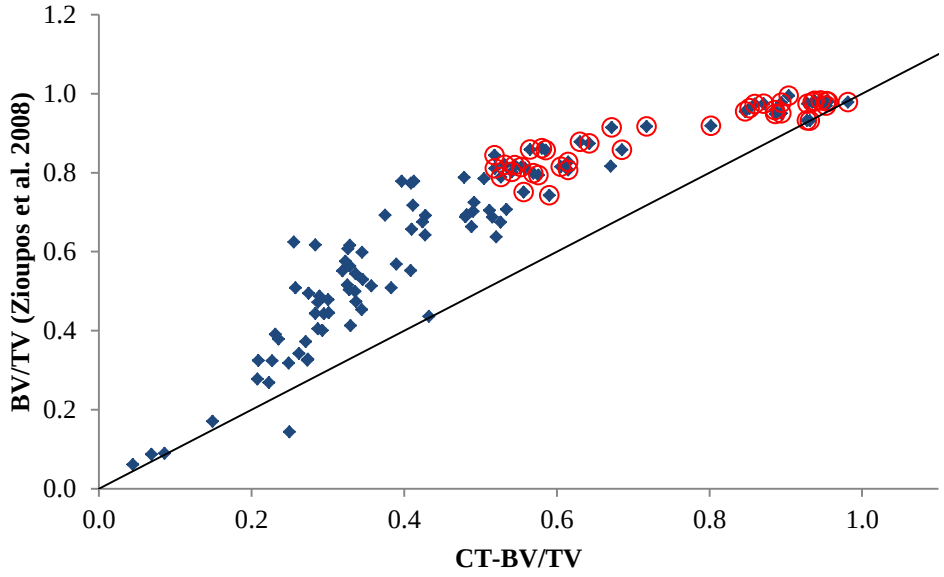

Figure 2-8 A comparison of the BV/TV measured by µCT with previous reported BV/TV values measured by Zioupos et al. (2008) for the same samples

The comparison of BV/TV measurements shown in Figure 2-8 shows that the BV/TV measured in the laboratory is higher in the intermediate regions most likely due to the fact that the Archimedes measurements consider all tissue including the un-mineralised layers on the surface of the tissue. It is most apparent in the intermediate region as it is a surface effect and in the intermediate regions there is the greatest amount of surface available (Martin 1984). The results of Figure 2-7 and Figure 2-8 are in agreement with each other as to what disparities exist between the methods. These low density regions on the surfaces of bone are due to the remodelling of bone where the younger regions are less mineralised. As such they have a lower density as shown in Figure 2-10. Microscope images displaying structural property of bone are shown in Figure 2-9.

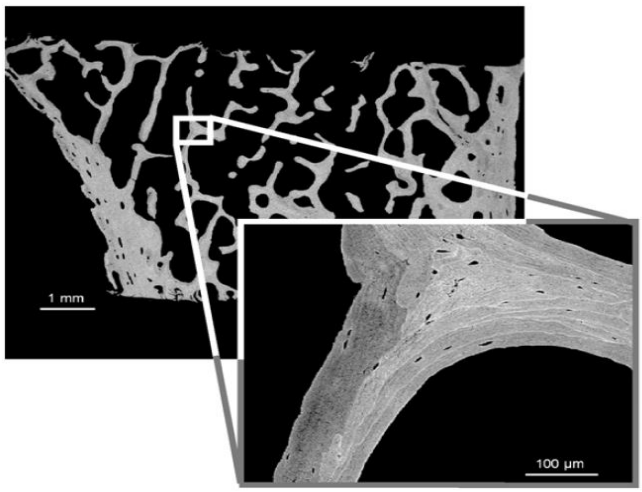

Figure 2-9 microscope images showing the layers of bone tissue taken from Ruffoni et al. (2007).

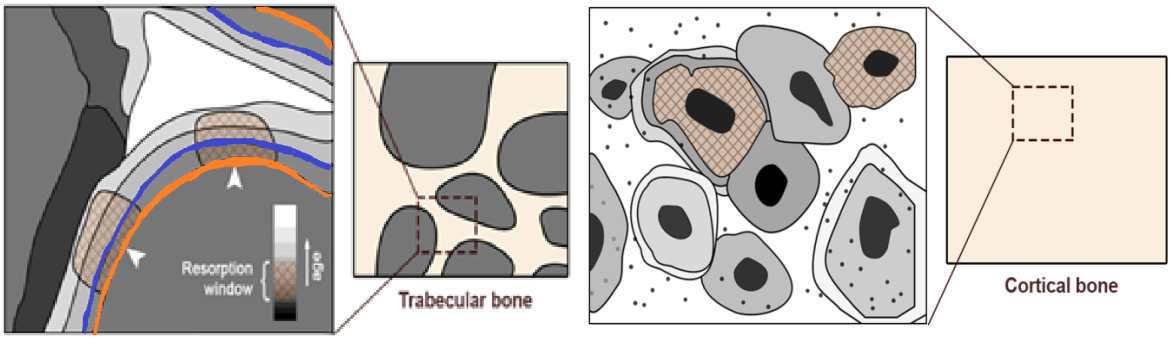

Figure 2-10 graphic displaying the remodelling regions of bone tissue adapted from Berli et al. (2017), proposed possible thresholds have been added to the trabecular bone image for the Archimedes and CT thresholds at ~1.1 (orange) and ~1.3 (blue) g/cm3 respectively

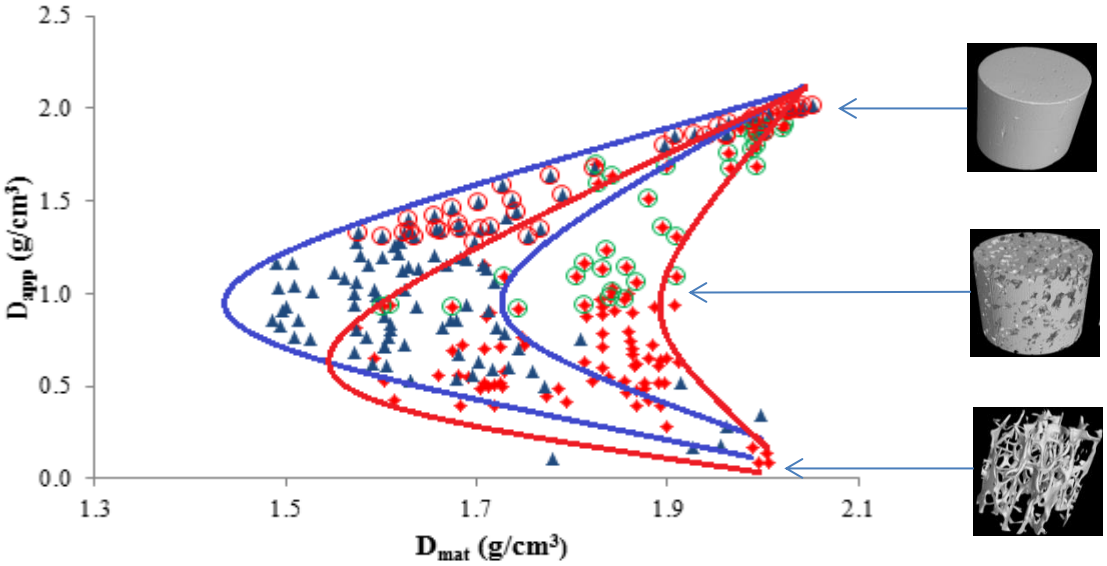

Figure 2-11 Apparent vs material density for all samples from both the cortical and cancellous regions. Blue triangles are produced from CT and red squares are from Zioupos (2008) the lines are hand drawn around the two data sets. 3D reconstructed images of samples are shown on the left at their respective densities

Figure 2-11 shows the 'boomerang'-like pattern previously shown by Zioupos et al. (2008) with a shallower inflection point at about ~1.1 g cm^{-3} and ~1.8 g cm^{-3} compared with ~1.3 g cm^{-3} and ~1.60 g cm^{-3}. The shallower inflection is due to higher measured D_{mat} in the intermediate bone porosities. These higher values for D_{mat} most likely exist for two possible reasons (i) the density measured by Archimedes is skewed by the presence of closed voids in the cancellous bone matrix which would overestimate the volume of bone. In the calculation of D_{mat}=*weight/volume* a higher volume will lead to a reduced D_{mat} whereas in µ-CT these closed voids do not impact on the data. (ii) the surface of cancellous bone in encapsulated by a low density layer that, of course, has a volume so will therefore displace water in the Archimedes test but not possess a density high enough to impact on the µ-CT measured density.

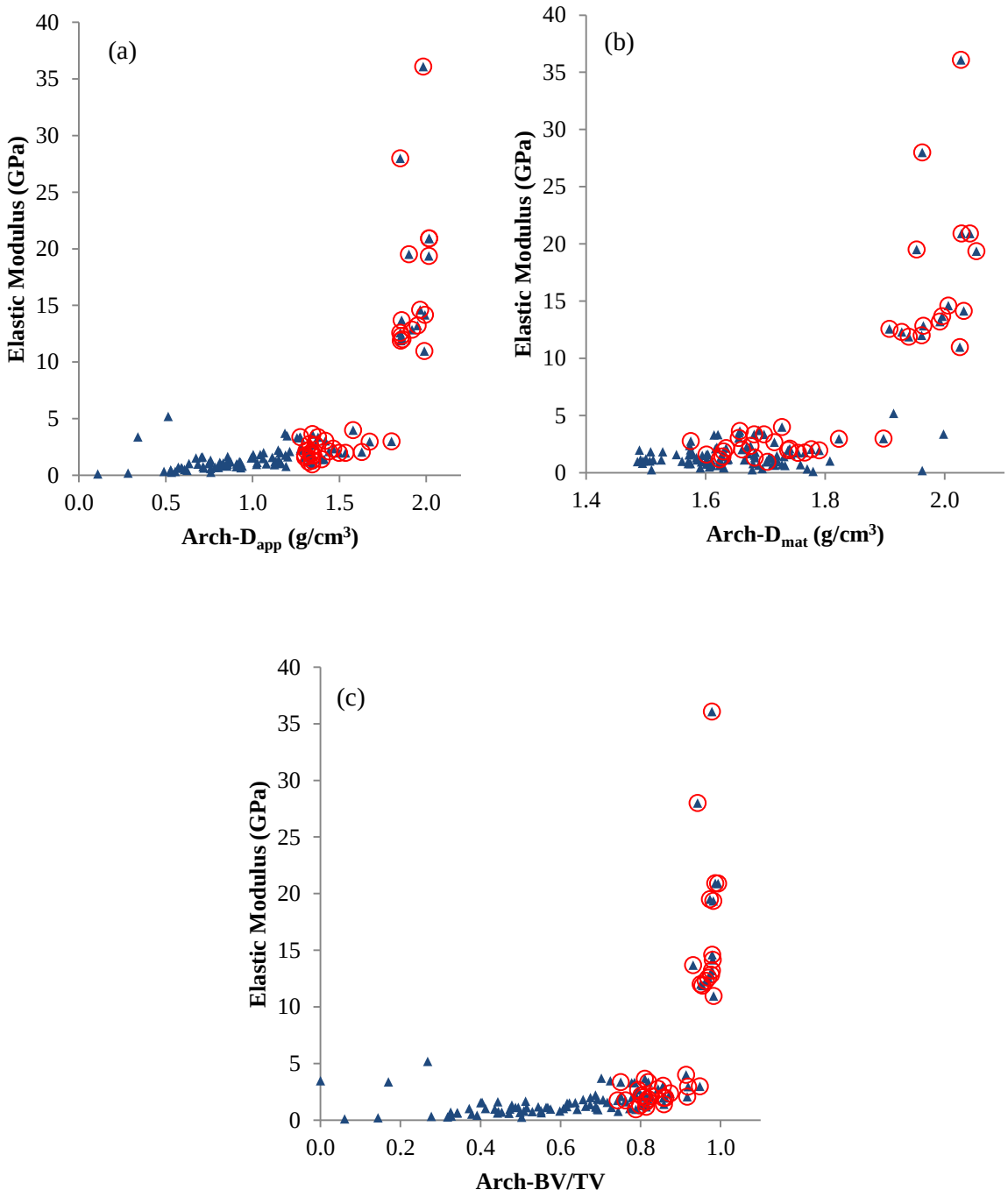

Figure 2-12 Plots of E vs (a) Dapp, (b) Dmat and (c) BV/TV measure using the Archimedes principle taken from (Zioupos et al. 2008).

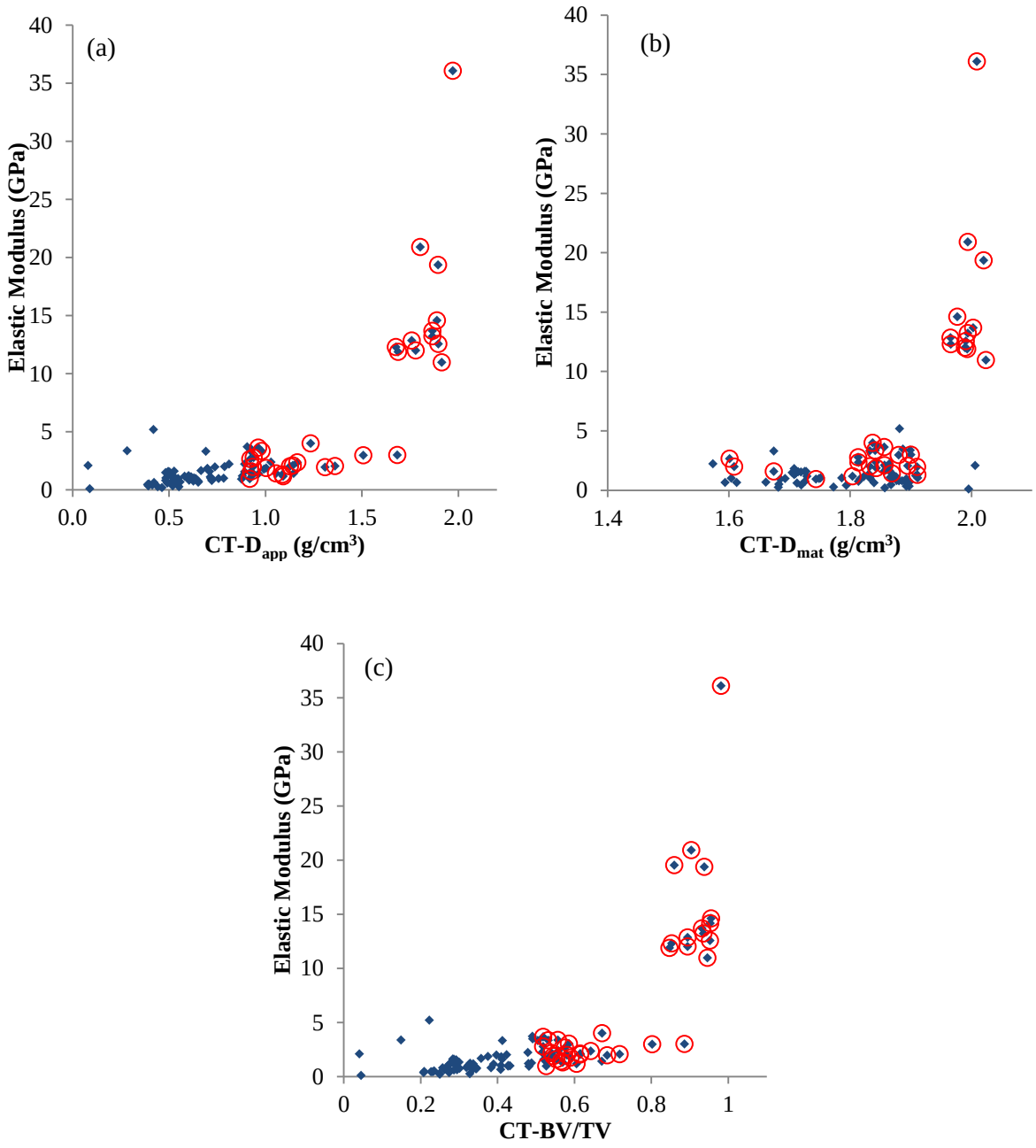

Figure 2-13 Plots of E vs (a) Dapp, (b) Dmat and (c) BV/TV CT

The difference between the measurements most likely exists due to a combination of these factors. The differences between the measurements are also apparent in Figure 2-8 which shows a clear inflection in the intermediate range of cancellous bone tissue. The relationships found between the structural parameters measured by µCT reported here are compared with elastic moduli previously reported by Zioupos et al. (2008). The curves shown in Figure 2-13 (a) & (c) shown plots very similar to those reported with inflections in similar positions as shown in Figure 2-12. Figure 2-13 (b) shows largely similar curves however as

previously stated the lowest values of material density are higher than those previously reported; however the inflection point between 1.9 and 2 g/cm^3 is similarly positioned. The curves show that the mechanical properties of the tissue are dependent on the structural properties of the tissue. The curves shown in Figure 2-13 could provide the potential basis for the development of material models that can be used in whole bone finite element simulations. A comparison of the material and millimetre scale modulus is not of great use to the development of μFE simulations as it does not account for the micro-structural nature of the material.

2.5 **Discussion**

Here we have furthered the investigation into the basic relationships that exist within bone between the cortical and cancellous regions. The densities of bone directly impact upon the mechanical competency of the tissue (Zioupos et al. 2008; J.-Y Rho et al. 1995). An understanding of bone density and porosity across the full range of bone from cancellous to cortical is vitally important and will help infer upon the remodelling rates at specific sites within the human body (Martin 1984; Fyhrie et al. 1993) and contribute to future development of patient specific finite element modelling which depends on accurate assessment of the material properties of the tissue and its structure (Schileo et al. 2008; Chevalier et al. 2007). Conflicting reports have been made on the nature of the density variations across the full porosity range (Zioupos et al. 2008; Zioupos et al. 2009; Schileo et al. 2008; Schileo et al. 2009). Assessing these properties of bone has typically been carried out by means of histological measurements and traditional densitometry techniques such as the Archimedes technique (Zou et al. 1997; J.-Y Rho et al. 1995; Martin 1984; Zioupos et al. 2008). These are either destructive or have been criticised for their limitations (Zou et al. 1997).

In μCT imaging it is important to ensure that image resolution is suitable for the size and structures being assessed. In this study the imaging resolution was sufficient for determination of cancellous micro-architecture but not for assessment of the vascular micro-architecture, which has been suggested should be <1 μm (Yan et al. 2011). This is important when looking at the specific surface of bone as when considering cellular sites for bone remodelling the cortical bone may be more porous than the results seen here would suggest, this is important for considering bone remodelling rates. Additionally the densities presented in this work were calculated in g/cm^3 for comparison with previous works however for

clinical relevance Hounsfield units would be of greater value which has been shown to be suitable using a cone beam micro-computed tomography (µ-CBCT) (Mah et al. 2010). Consideration must also be given to the methods of density determination be it by the mean or modal values as in highly porous samples determination of both can be problematic and as shown by Figure 2-6 there is some variation between both methods of density determination.

The results of this work have confirmed previous measurements on the same samples by Zioupos et al. (2008) that showed that the relationship between the D_{mat} of bone across porosities is non-linear and have an inflection in the intermediate regions of cancellous bone due to a lower density (Figure 2-7). The results however do not agree on the degree to which the inflection occurs and this may be due to limitations of µ-CBCT scanning to accurately assess the density of bone (Mah et al. 2010; Schileo et al. 2008) or may be due to limitations of the Archimedes principle due to the impact of residual fat and closed cells which in turn limits the full penetration of water in the sample. In spite of these differences both datasets are in agreement of the existence of the inflection which is in contradiction to previous work (Schileo et al. 2008; Schileo et al. 2009) that has suggested that the relationship across the range is largely constant with minor fluctuations.

This work has shown that the density across the full range of bone is non-linear which has implications regarding the remodelling rates of bone. Less dense regions of bone are typically considered to be younger bone suggesting that the intermediate regions of bone tissue remodel at a greater rate than the extreme cortical and cancellous regions. This is consistent with the fact that bone remodelling is a surface effect so where there is a greater surface area available it can be expected to remodel at a greater rate. Of course following this principle it could be expected for the most porous regions to also display a lower density than the largely cortical regions but due to bones adaptive nature it might be maintaining the bare minimum of tissue required at the highly porous regions in line with the assumptions of Wolff's law. The results have also confirmed that density measure by µCT directly impacts the mechanical strength of bone tissue. Figure 2-13 which provides a basis for the development of density dependant models to predict the modulus of bone in µ-CT images.

2.6 **Conclusion**

This research showed that the material density varies non-linearly across the spectrum of bone porosities, which further reinforces previous works. We have provided further evidence in favour of density dependant material models for the future development of

patient specific finite element models. Additionally care must be taken when setting thresholds and sampling the material density, it is recommended that further work be carried out into the impact of setting sampling thresholds on the material data. Further work should also be carried out into the source of the disparity between the Archimedes and μ-CT data.

2.7 **Acknowledgments**

The tests were carried out in the Biomechanics laboratories of the Cranfield Forensic Institute of Cranfield University in Shrivenham, UK. The Authors acknowledges the support of the EPSRC (GR/N33225; GR/N33102; GR/ M59167). And thanks the BBSRC (BB/C516844/1) and the Department of Veterinary Basic Sciences (RVC) for financial support, and Whipsnade Zoo for provision of the specimen.

2.8 **References**

Ahlowalia, M.S. et al., 2013. Accuracy of CBCT for volumetric measurement of simulated periapical lesions. *International Endodontic Journal*, 46(6), pp.538–546.

Berli, M. et al., 2017. Localized tissue mineralization regulated by bone remodelling: A computational approach R. K. Roeder, ed. *PLOS ONE*, 12(3), p.e0173228.

Cook, R.B. & Zioupos, P., 2009. The fracture toughness of cancellous bone. *Journal of biomechanics*, 42(13), pp.2054–60

Fyhrie, D.P. et al., 1993. Direct calculation of the surface-to-volume ratio for human cancellous bone. *Journal of biomechanics*, 26(8), pp.955–67.

Keenan, M.J. et al., 1997. Comparison of Bone Density Measurement Techniques: DXA and Archimedes' Principle. *Journal of Bone and Mineral Research*, 12(11), pp.1903–1907.

Lee, J., Shin, H.I. & Kim, S.Y., 2004. Fractional quantitative computed tomography for bone mineral density evaluation: accuracy, precision, and comparison to quantitative computed tomography. *Journal of computer assisted tomography*, 28(4), pp.566–71.

Mah, P., Reeves, T.E. & McDavid, W.D., 2010. Deriving Hounsfield units using grey levels in cone beam computed tomography. *Dento maxillo facial radiology*, 39(6), pp.323–35

Martin, R.B., 1984. Porosity and specific surface of bone. *Critical reviews in biomedical engineering*, 10(3), pp.179–222.

Rho, J.Y., Hobatho, M.C. & Ashman, R.B., 1995. Relations of mechanical properties to density and CT numbers in human bone. *Medical Engineering & Physics*, 17(5), pp.347–355.

Rice, J.C., Cowin, S.C. & Bowman, J.A., 1988. On the dependence of the elasticity and strength of cancellous bone on apparent density. *Journal of biomechanics*, 21(2), pp.155–68.

Ruffoni, D. et al., 2007. The bone mineralization density distribution as a fingerprint of the mineralization process. *Bone*, 40(5), pp.1308–1319.

Schileo, E. et al., 2008. An accurate estimation of bone density improves the accuracy of subject-specific finite element models. *Journal of Biomechanics*, 41(11), pp.2483–2491.

Schileo, E., Taddei, F. & Baleani, M., 2009. Letter to the Editor referring to the article "Some basic relationship between density values in cancellous bone and cortical bone" published on Journal of Biomechanics (volume 41, Issue 9, Pages 1961-8*). Journal of biomechanics*, 42(6), p.793.

Yan, Y.-B. et al., 2011. Relationship between architectural parameters and sample volume of human cancellous bone in micro-CT scanning. *Medical engineering & physics*, 33(6), pp.764–9.

Zioupos, P., Cook, R.B. & Hutchinson, J.R., 2008. Some basic relationships between density values in cancellous and cortical bone. *Journal of Biomechanics*, 41(9), pp.1961–1968.

Zou, L., Bloebaum, R.D. & Bachus, K.N., 1997. Reproducibility of techniques using Archimedes' principle in measuring cancellous bone volume. *Medical engineering & physics*, 19(1), pp.63–8.

3 Assessment of the physical characteristics and morphology of mammalian bone tissue by Micro-Computed Tomography

Adams G J[1], Cook R[2], Hutchinson J[3], Zioupos P[1]

1 Cranfield Forensic Institute, Cranfield University, Defence Academy of the UK, Shrivenham, UK

2 nCATS, School of Engineering Science, University of Southampton, Southampton, UK

3 Department of Veterinary Basic Sciences, RVC, University of London, Hatfield, UK

3.1 Abstract

The remodelling of bone is considered to be a surface effect. An understanding of the specific surface in relation to porosity is essential to understanding how bone remodelling and disease susceptibility of bone changes at different sites within bones; cancellous, cortical and the intermediate regions. In order to build valid models of the physical relationship between porosity and specific surface an understanding of their relationship needs to be determined by measuring them. 112 samples from an elephant femur were assessed by micro-computed tomography (μ-CT), 31 of which contained a demineralised slice (collagen). The scans were reconstructed and analysed using 3 different image backgrounds: air, water and collagen and the impacts of background thresholds on the physical characteristics of bone were determined. The results showed that using a collagen background had a profound effect on the morphology of bone when assessed by μCT. The differences between air and water are no significant and would suggest that comparable data can be produced in a laboratory environment under either wet or dry conditions, this is counter to common belief. Further understanding of the impact is required as in clinical CT the image background will be less dense than water but denser than air so determination of which is more suitable in laboratory μCT imaging is important to improve the quality and relevance of research.

***Keywords**: Bone; cancellous; Cortical; density; Porosity; BV/TV; Specific surface; μCT*

3.2 **Introduction**

Determination of the structural characteristics of bone is essential in understanding bone's mechanical properties, rates of remodelling or adaptation, and its susceptibility to disease. Three of the most important features of bone structure are the porosity, specific surface, and the density (Martin 1984; Zioupos et al. 2008; Fyhrie et al. 1993). Porosity is the void volume per unit volume of bone, which is often expressed as its inverse BV/TV (bone volume/total volume), which will be used throughout this article. Specific surface (BS/TV) is the total area of internal surfaces per unit volume of bone (Martin 1984). Density can be considered in two ways. Firstly as apparent density (D_{app}), this can be defined as the mass over the whole volume of the sample, and is often referred to as volume bone mineral density (BMD). Secondly as material density (D_{mat}), which can be defined as the mass of the bone over the volume occupied by the material within the sample, and is often referred to as tissue mineral density (TMD). BV/TV is a dimensionless ratio, BS/TV has the units cm^{-1}, and both densities have the same units g/cm^3. The BV/TV and D_{mat} are important as bone's primary role within the body is as a structural material and in many cases is treated as a cellular solid (Gibson 1985). An understanding of how BV/TV varies with D_{mat} is important in bone disease specifically when trying to understand the impacts of osteoporosis (P Zioupos et al. 2008). It is important to understand the relationship within 'normal' bone so irregularities in diseased bone can be identified.

Osteoclasts and osteoblasts are the two cells responsible for breaking down and rebuilding bone, respectively, during the remodelling process (Currey 2002). They are only active on the available surfaces of the bone tissue. The level of activity of these osteoclasts and osteoblasts is hormonally and metabolically driven. In addition to the chemically driven mechanisms determining the rate of remodelling the total area over which these cells can act will also have a profound effect, and as such the total BS/TV will impact the resultant rate of bone remodelling at specific sites (Rouhi 2004; Sharpe 1979). This BS/TV is determined by the micro-architecture of bone including osteocyte lacunae, osteonal canals and trabecular structure. Models of bone remodelling in the cortical regions of bone with variations in the specific surface bone have shown that with a higher specific surface the rate of remodelling is increased (Buenzli et al. 2012). More knowledge on the variations in the specific surfaces in both the cortical and

cancellous regions can help improve the quality and accuracy of the modelling of bone remodelling which in turn can help with the understanding of bone disease.

Understanding the structural and material properties of bone is vital in the understanding of bone diseases such as osteoporosis, as the current protocol in determining if a patient is osteoporotic relies on dual energy x-ray diffraction (DEXA). The DEXA system assesses the bone mineral density (BMD_a) of the area scanned (Greenwood et al. 2015). The BMD_a is an areal quantification of the apparent density of bone tissue which confounds the density and porosity of bone, as such understanding the individual parameters and their relationships to each other would prove to be advantageous in the assessment of an individual's fracture risk (Zioupos et al. 2008; Cook & Zioupos 2009).

The relationship between the porosity and specific surface of bone has been previously investigated by Martin (1984) in which histological slices were taken. However this method is time consuming and destructive so is not ideal in research and clearly impossible in clinical settings. The method also carries an inherent error as it is limited by slice thickness. By using μ-CT this relationship can be examined more easily with a potentially higher accuracy (Feldkamp et al. 1989). It is clearly important to accurately measure and understand the relationship using the most accurate method available so that models of bone remodelling can be built using the most accurate data. Zioupos et al. (2008) examined the relationship between the material density and the apparent density; these are often referred to as the tissue mineral density (TMD) and the bone mineral density (BMD) respectively (Zioupos et al. 2008). A 'boomerang' like curve was observed between these two parameters. This work however has been criticised by Schileo et al. (2009) as the technique used to measure the density and apparent density could be skewed due to the closed cell nature of cancellous bone and the fat removal method being insufficient (Schileo et al. 2009). To overcome this μ-CT can be used as it gives information on the internal structure, and marrow filled closed cells will not affect the results. Previous work has looked at the density relationship between the cortical and cancellous regions using μ-CT (Schileo et al. 2008). However this previous work has considered bone as either purely cortical or cancellous and not considered that bone exists over a spectrum (Zioupos et al. 2009). Here we consider

bone to exist across this spectrum and investigate the relationships between the porosity and structural characteristics of mineralised bone tissue.

3.3 **Materials and methods**

3.3.1 **Specimens**

In this study samples were taken from the right femur of an adult Asian elephant (3432 kg, 24 year old). The advantage of using the femur of such a large mammal is that a large number of samples (112) over a wide range of BV/TVs (0.04-0.98) can be taken. The suitability of this tissue was confirmed in a previous study (Zioupos et al. 2008). The specimen was collected shortly after the animal's euthanasia (for reasons unrelated to this study) at Whipsnade zoo (Bedfordshire, UK) and frozen (-20^{o}C) until testing. The samples were cut in either cylindrical cores or cubes approximately 10mm^{2}, larger than the minimum size recommended by (Yan et al. 2011). Full preparation details can be found in (Zioupos et al. 2008)

In a subsection of samples (31) a 2mm slice was taken from the bottom of each sample and submerged in EDTA for 168hrs (7 days) with daily changes to fully demineralise the slice. This demineralisation process left us with collagen which could then be used to provide an additional threshold density of approximately 1.1g cm^{-3} to be using during the analysis process. All the samples were stored frozen (-20^{o}C) until testing and were allowed to defrost for 2hrs prior to imaging.

3.3.2 **Imaging- μCT**

All samples were imaged using a cone beam μCT scanner, Nikon XTEK XT H 225. The samples were imaged in ABS plastic sample holders at 50 kV, 65 μA. The resultant voxel size was ~16 μm making them suitable to determine the samples' morphology (Yan et al. 2011). All samples were imaged whilst fully submerged in deionised water. The 31 samples were additionally imaged in air with their demineralised slices. All scans were manually reconstructed using CT Pro 3D. During reconstruction conditions were optimised to reduce beam hardening.

3.3.3 **Image Analysis**

Image analysis was carried out using VG Studio Max 2.2. Regions of interest (ROI) were taken from the centre of each sample ~9 mm^3 to exclude any external surfaces from the scan. These surfaces, which have been introduced during the sample preparation process, were excluded as the software would consider them in the BS/TV calculations and therefore give erroneous results. A surface determination was performed using the grey level of an internal void as the background and the largest void-less section of bone, as per the manufacturers' recommendations. This thresholding process introduces a surface threshold at an intermediate point between the average grey values of these two sections. For the samples imaged with a collagen slice the collagen was used as the background. After the surface determination an automatic morphometric report was exported. This contained: BV/TV, specific surface, mean trabecular thickness, mean trabecular number, and mean trabecular spacing.

From the histogram the mean, mode, minimum and maximum grey level were recorded to be used in calculation of the material density. A QRM-MicroCT-HA calibration phantom was imaged and reconstructed under the same conditions in order to determine D_{mat}. Determination of material density is more favourable than deriving Hounsfield (HU) units, which are typically used in medical CT imaging, as HU is an x-ray specific expression of a materials linear attenuation coefficient and does not have any consistent conversion to physical density measurements. Therefore using material density enables for comparison with physical density measurements that HU otherwise does not.

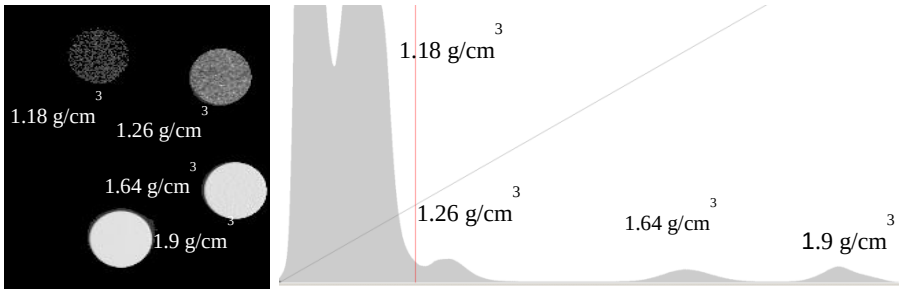

Figure 3-1 QRM Calibration phantom images and histogram the average density, grey and mineral % are given in Table 3-1

3.3.4 **Density Calibration**

Fig. 1 shows the histogram of the QRM HA calibration phantom alongside the 3D image of the scan, both obtained using VG studio. Within VG studio each density was isolated and the average grey scale was determined and plotted against the density provided by the supplier Figure 2-2. This provided a calibration curve from which the density of the elephant samples could be determined. The average grey value of each sample was measured and using the calibration curve (Figure 2-3) D_{mat} was determined.

Table 3-1 Properties of QRM calibration phantom

Sample	Mean grey	Density (g/cm^3)	Mineral %
Standard 1	36.10	1.13	0
Standard 2	48.60	1.18	0.42
Standard 3	112.20	1.26	15.89
Standard 4	337.20	1.64	48.29
Standard 5	478.45	1.90	63.17

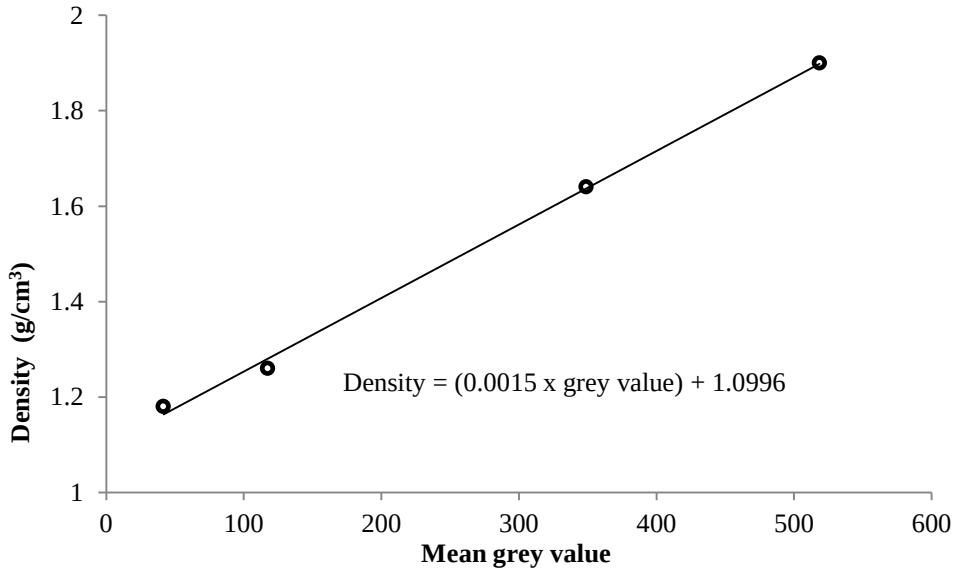

Figure 3-2 QRM Calibration phantom calibration curve, plotted without errors

The apparent density (D_{app}) was determined from the product of the BV/TV and D_{mat} by rearranging Equation 3-1. To distinguish between measurements taken from µ-

CT and measurements taken using the Archimedes technique, from previous work by Zioupos et al. (2008) the prefixes CT and Arch will be used respectively.

$$\frac{BV}{TV} = \frac{D_{app}}{D_{mat}} \qquad \textit{Equation 3-1}$$

3.4 **Results**

A statistical comparison of the 3 different thresholds is shown in Table 3-2. The results of the comparison showed that the air and water thresholds were not statistically different when comparing the two datasets. This suggests that imaging bone in air and in water using µ-CBCT produced no significant difference across the full range of bone porosities. A comparison of the three thresholds showed that increasing the value to the collagen threshold produced significantly different morphological parameters. This is most likely due to the layered nature of bone as shown in Figure 3-3. This significant change suggests that this small increase in threshold value crosses a significant point in the sample density, which is most likely related to a change in layer density

Table 3-2 p-values for the difference between the three data sets of the measured morphometric parameters, t-Test is for paired data sets using 2 tails

	BV/TV	BS/TV	TbN	TbSp
Collagen vs Air	**<0.001**	**<0.001**	**<0.001**	**<0.001**
Collagen vs Water	**<0.001**	**<0.001**	**<0.001**	**<0.001**
Air vs Water	**0.386**	**0.708**	**0.933**	**0.624**

Figure 3-4 shows the behaviour of specific surface vs BV/TV for all 118 samples. The curve shows a relationship similar to that shown by Martin (1984). However by overlaying this with his data (Figure 3-4) it shows that the maximums and minimums as well as the apex are located slightly differently. The data shows a minimum specific surface (~0.6 mm^{-1}) at the maximum and minimum BV/TVs, and a maximum (~4.0 mm^{-1}) at ~0.55 BV/TV.

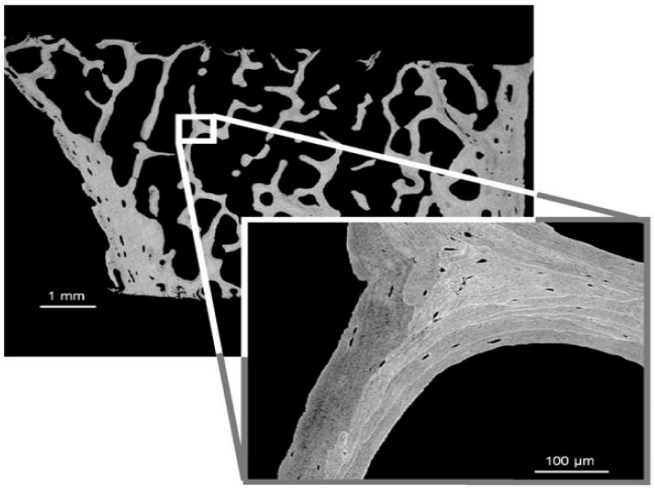

Figure 3-3 microscope images showing the layers of bone tissue taken from Ruffoni et al. (2007).

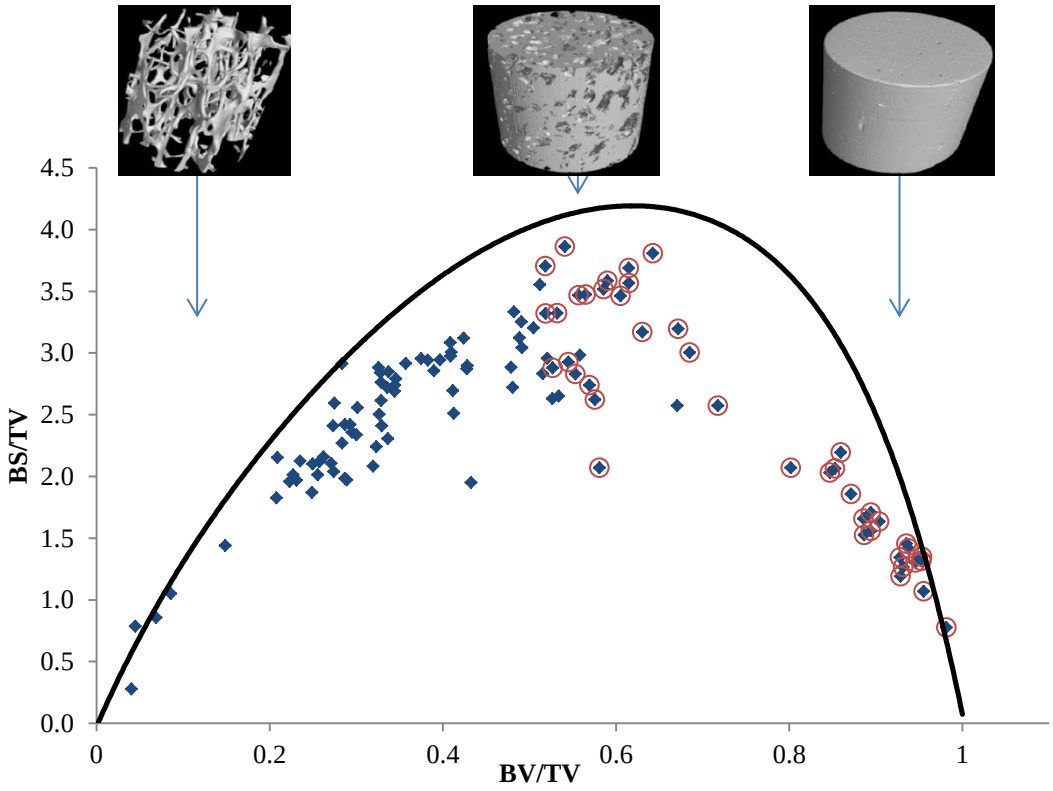

Figure 3-4 Specific surface vs BV/TV measured using µCT for all 118 samples from an elephant femur. The samples having Dapp>1.3 are encircled and the same notation is used in the following figures to allow visual comparisons to be made (Zioupos et al. 2008). Additional line plot is taken from Martin (1984) for comparison.

Using the three different backgrounds on the samples causes a shift in where the surfaces were determined, as the density of the background increases as the threshold grey values is increased. An example of this is shown in Figure 3-5. As can be seen from the histograms there is only a slight shift in the position of the threshold. This shift does however manifest itself as a noticeable difference in the micro-structural properties measured from the data, shown by Figure 3-6.

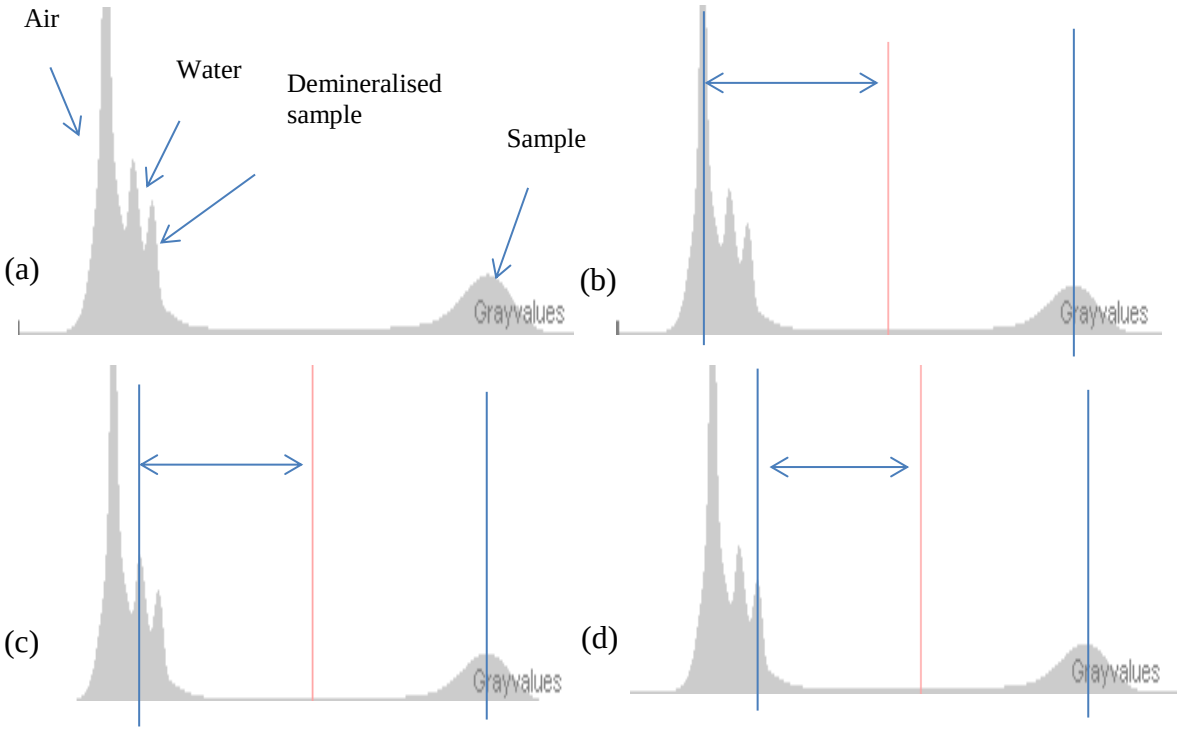

Figure 3-5 histogram showing the three thresholds used with the (a) peaks labelled for air, water, demineralised sample and sample. (b) shows where the threshold is placed when air is taken as the background, (c) shows where the threshold is placed when water is taken as the background, and (d) shows where the threshold is placed when the demineralised sample is taken as the background

Figure 3-6 shows the specific surface vs BV/TV relationship of the 31 samples imaged with demineralised bone tissue. The data shows differences in the maximums and minimums between air, water and collagen being taken as the background. When imaged in air and water the data points largely overlap suggesting this difference in thresholding does not have a significant impact on the measurements of BV/TV and BS/TV. However when collagen is taken as the background the curves show distinct differences to the other two curves suggesting that on the surface of the bone there is a

lower density layer of epithelial tissue. This lower density or less mineralised layer could be an important consideration in the modelling of bone remodelling.

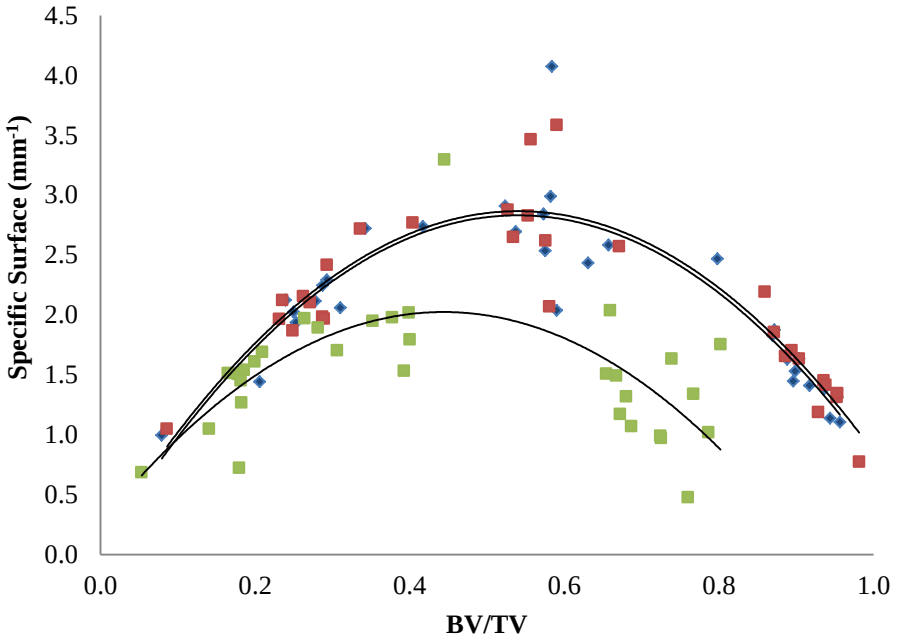

Figure 3-6 Specific surface vs BV/TV measured using µCT on 31 samples from an elephant femur. Red squares imaged in water, blue diamonds imaged in air, and green triangles with a collagen background

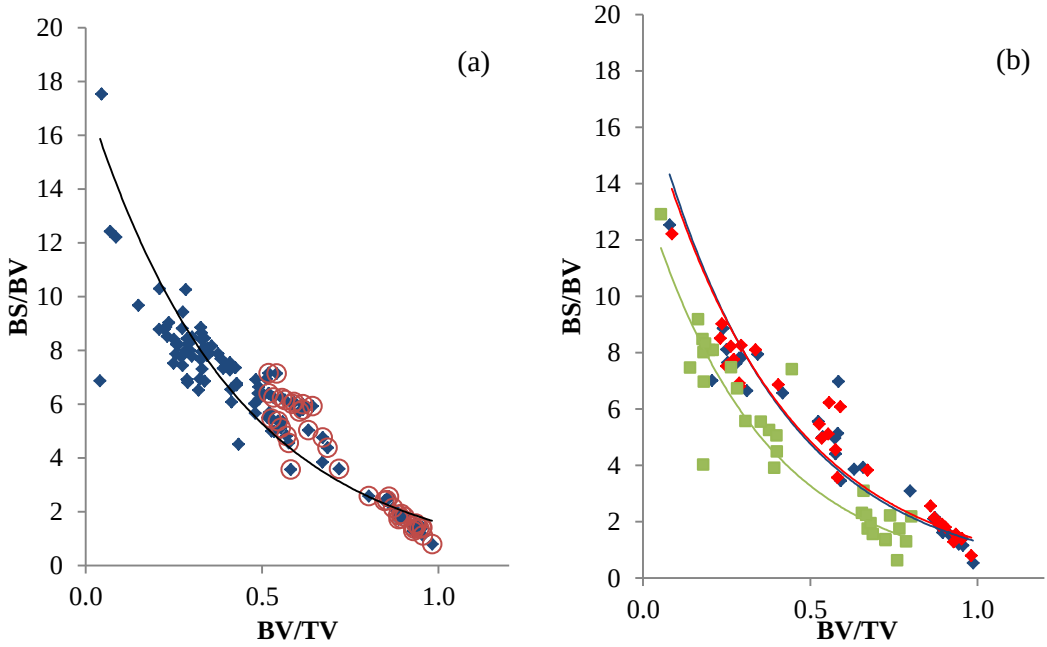

Figure 3-7 (a) bone volume to tissue volume ratio vs BV/TV for the full range of 112 samples and (b) the sub group of 31 samples measured with different backgrounds. Red diamonds imaged in water, blue diamonds imaged in air, and green squares with a collagen background

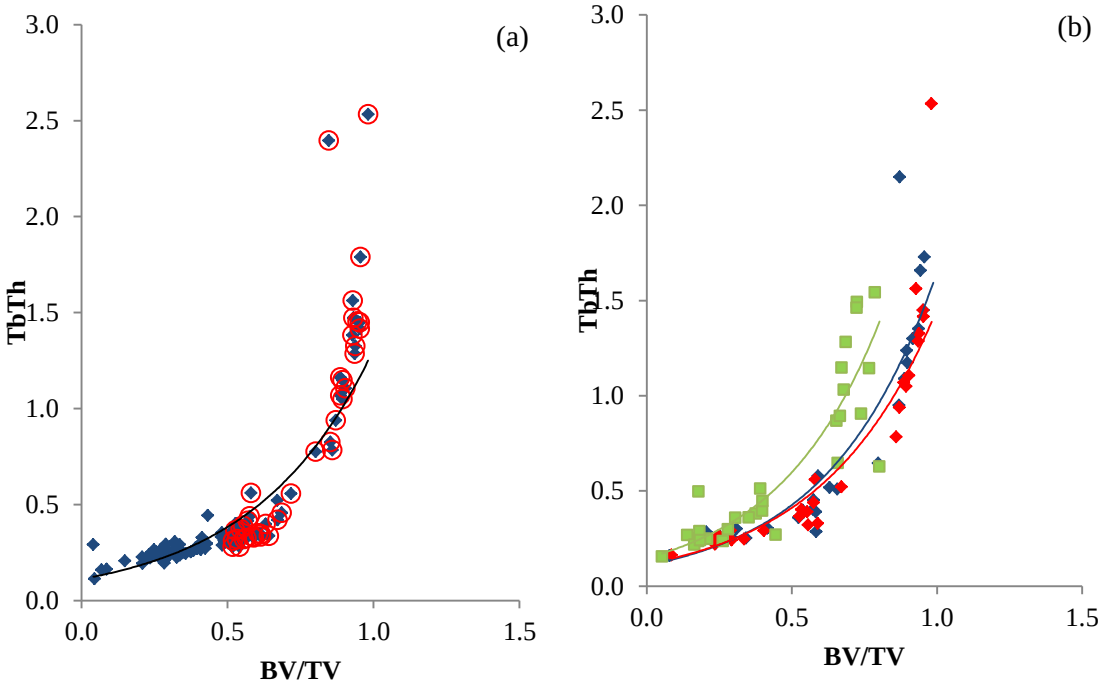

Figure 3-8 (a) Trabecular thickness vs BV/TV for the full range of 112 samples and (b) the sub group of 31 samples measured with different backgrounds. Red diamonds imaged in water, blue diamonds imaged in air, and green squares with a collagen background

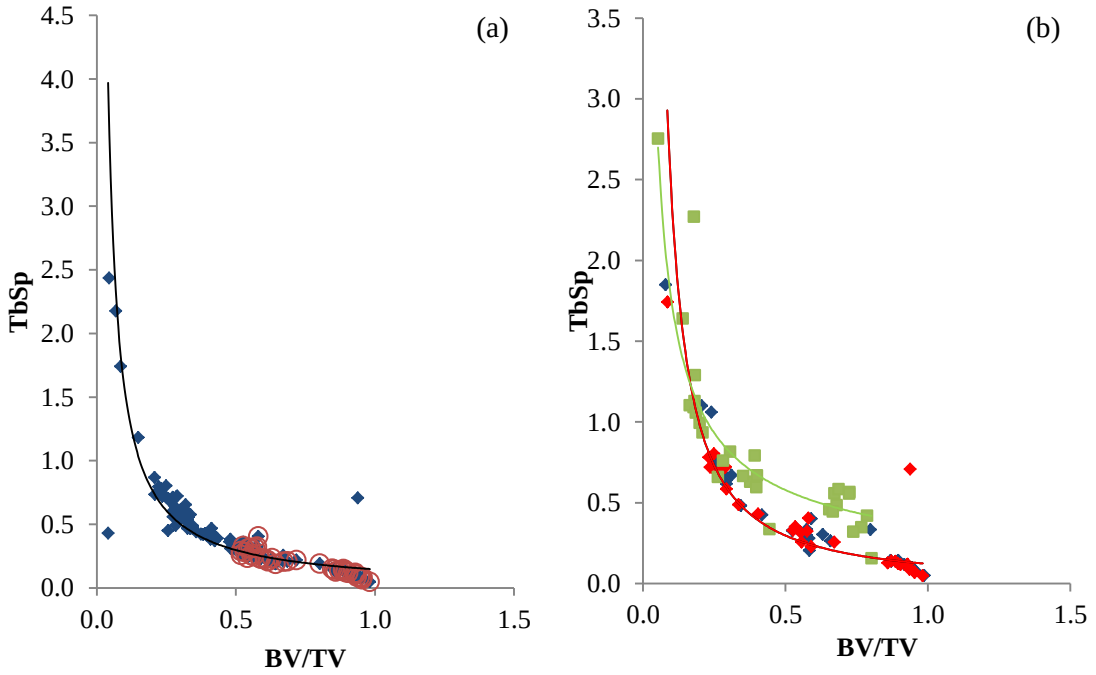

Figure 3-9 (a) the relationship between Trabecular spacing and porosity within the full spectrum of 112 samples and (b) the sub group of 31 samples measured with different backgrounds. Red diamonds imaged in water, blue diamonds imaged in air, and green squares with a collagen background

The relationship seen between BS/BV and BV/TV (Figure 3-7 (a)) is a self-evident relationship showing that as zero bone volume is approached the surface area to volume ratio tends towards infinity. The main point of interest here is that between 0.05-1 the relationship appears to be linear. Figure 3-7 (b) shows the bone surface to BV/TV ratio between air and water follow very similar trends. However when collagen is taken there is a systemic downward shift in the relationship.

The relationship between the trabecular thickness and porosity (Figure 3-8) behaves inversely to the relationship between the trabecular spacing and porosity (Figure 3-9) which seems to follow a power law. The collagen threshold does not show a large shift from the air and water backgrounds in trabecular thickness (Figure 3-8 (b)) however there does seem to be a shift when considering trabecular spacing (Figure 3-9 (b)).

3.5 **Discussion**

We have further investigated; the structural relationships that exist within mammalian bone tissue across the whole spectrum of bone porosity, carried out using cone beam μ-CT. Determination of these structural relationships is vital in understanding the mechanics of bone due to its cellular nature (Gibson 1985) and in understanding the remodelling rates at different sites within bone tissue (Buenzli et al. 2012). Establishing typical ranges of normal trabecular architectural parameters can provide a useful tool in determining if a patient's bones are mechanically compromised or at a greater risk of diseases such as osteoporosis. It has been shown that osteoporotic bone displays thinning or loss of trabecular which contributes to a reduced fracture toughness (Greenwood et al. 2015; P Zioupos et al. 2008).

A limitation of this research is that is uses elephant rather than human bone so the absolute number given may not be representative of human tissue. It has however been demonstrated that there is an offset in the structural properties of bone tissue micro-architecture based on the relative sizes of the animals (Ryan & Shaw 2013).

From this adjustments could be made to predict how the values might appear for humans. In an ideal scenario, this study would be repeated using whole human bones taken from various sites around the body, and using multiple individuals representative of both genders and a range of age groups. The clinical relevance of this work could be improved by deriving HU, which has been shown to be suitable using a cone beam μCT (Mah et al. 2010). The imaging resolution was insufficient to image vascular micro-architecture, which has been suggested should be <1 μm (Yan et al. 2011). This is an important consideration when looking at the specific surface of bone as when considering cellular sites for bone remodelling the cortical bone may be more porous than the results seen here would suggest. As shown by Figure 3-4, we have produced curves that are consistent with those previously reported by Martin (1984). However the peaks are in slightly different positions; this may be due to the use of elephant samples or the sampling method being used.

A comparison of the three backgrounds shows that using collagen has the greatest effect on the morphological results from μCT. This suggests that bone density varies with depth within the bone tissue and that the low density tissue exists on the available surfaces. It has also been shown that the imaging in either water or air does not produce significantly different results; this is an important discovery as it shows that, contrary to what is often recommended, imaging dry or wet does not have a statistically significant impact on the results. The differences seen between the collagen threshold versus the air and water may have implications regarding the structure of bone in that at its surface the tissue is less mineralised perhaps due to the remodelling process. This however could also be an artefact from the partial volume effect from μCT imaging, which occurs when the voxels in the scan at a boundary contain both the sample and the background which in turn reduces the density of the voxel.

3.6 **Conclusion**

This information about the relationship between BV/TV and BS/TV can be used in the development of models that predict bone remodelling. Developing such models is vitally important in understanding how the skeleton behaves and could lead to further understanding of the underlying mechanism that drives the remodelling process. It

could also enable earlier identification of abnormal or diseased bone or those that might be at greater risk. Additionally, there was not seen to be any significant difference between imaging in water or in air, suggesting that imaging in water is not a necessity for obtaining accurate micro-architectural data.

3.7 **Acknowledgments**

The tests were carried out in the Biomechanics laboratories of the Cranfield Forensic Institute of Cranfield University in Shrivenham, UK. The Authors acknowledges the support of the EPSRC (GR/N33225; GR/N33102; GR/ M59167). And thanks the BBSRC (BB/C516844/1) and the Department of Veterinary Basic Sciences (RVC) for financial support, and Whipsnade Zoo for provision of the specimen.

3.8 **References**

Buenzli, P.R. et al., 2012. Endocortical bone loss in osteoporosis: The role of bone surface availability. *Int J Numer Method Biomed Eng.*, 29(12)pp.1307-22.

Cook, R.B. & Zioupos, P., 2009. The fracture toughness of cancellous bone. *Journal of biomechanics*, 42(13), pp.2054–60.

Currey, J.D., 2002. *Bones: Structure and Mechanics*, Princeton University Press.

Feldkamp, L.A. et al., 1989. The direct examination of three-dimensional bone architecture in vitro by computed tomography. *Journal of bone and mineral research : the official journal of the American Society for Bone and Mineral Research*, 4(1), pp.3–11.

Fyhrie, D.P. et al., 1993. Direct calculation of the surface-to-volume ratio for human cancellous bone. *Journal of biomechanics*, 26(8), pp.955–67.

Gibson, L.J., 1985. The mechanical behaviour of cancellous bone. *Journal of Biomechanics*, 18(5), pp.317–328.

Greenwood, C. et al., 2015. The micro-architecture of human cancellous bone from fracture neck of femur patients in relation to the structural integrity and fracture toughness of the tissue. *Bone*, 3, pp.67–75.

Martin, R.B., 1984. Porosity and specific surface of bone. *Critical reviews in biomedical engineering*, 10(3), pp.179–222.

Rouhi G, et al., 2006. Free surface density instead of volume fraction in the bone remodeling equation: theoretical considerations. *International Journal of Engineering Science*, 44(7), pp.456-469

Ryan, T.M. & Shaw, C.N., 2013. Trabecular bone microstructure scales allometrically in the primate humerus and femur. *Proceedings of the Royal Society B: Biological Sciences*, 280(1758), pp.20130172–20130172.

Schileo, E. et al., 2008. An accurate estimation of bone density improves the accuracy of subject-specific finite element models. *Journal of Biomechanics*, 41(11), pp.2483–2491.

Schileo, E., Taddei, F. & Baleani, M., 2009. Letter to the Editor referring to the article "Some basic relationship between density values in cancellous bone and cortical bone" published on Journal of Biomechanics (volume 41, Issue 9, Pages 1961-8). *Journal of biomechanics*, 42(6), p.793.

Sharpe, W.D., 1979. Age changes in human bone: an overview. *Bulletin of the New York Academy of Medicine*, 55(8), pp.757–73.

Yan, Y.-B. et al., 2011. Relationship between architectural parameters and sample volume of human cancellous bone in micro-CT scanning. *Medical engineering & physics*, 33(6), pp.764–9.

Zioupos, P., Cook, R. & Coats, A.M., 2008. Bone quality issues and matrix properties in OP cancellous bone. *Studies in health technology and informatics*, 133, pp.238–45.

Zioupos, P., Cook, R.B. & Hutchinson, J.R., 2009. More thoughts on the relationship between apparent and material densities in bone. *Journal of Biomechanics*.

Zioupos, P., Cook, R.B. & Hutchinson, J.R., 2008. Some basic relationships between density values in cancellous and cortical bone. *Journal of Biomechanics*, 41(9), pp.1961–1968.

4 Prediction of the Fracture Toughness of Human Cancellous Bone from Fracture Neck of Femur Patients using Micro-architecture

G. J. Adams[1], R. B. Cook[2], M. Gibson[1,] P. Zioupos[1]

1 Cranfield Forensic Institute, Cranfield University, Defence Academy of the UK, Shrivenham, UK

2 nCATS, School of Engineering Science, University of Southampton, Southampton, UK

4.1 Abstract

The current protocol used to determine if an individual is osteoporotic relies on assessment of the individuals bone mineral density (BMD). The BMD is determined by used of dual energy x-ray absorptiometry (DEXA) which provide an areal assessment of the quantity and quality of the bone tissue. The BMD data obtained is used in the fracture risk assessment tool (FRAX) as recommended by the World Health Organisation. This provides valuable information on the individual by making consideration of their lifestyle. While this provides valuable data on a person's fracture risk, advancements in medical imagining technology such as CT imaging enables development of more robust and accurate risk assessment tools. As such there is a need to develop an understanding of how the morphological parameters impact the mechanical competency of the tissue. Using osteoporotic and osteoarthritic patients ranging from ages 59-96 years, samples were taken from the centre of the femoral head and used to determine the plane-strain fracture toughness. These samples have been imaged using μCT (XT H 225, X-Tek Systems Ltd) and from the 3D images various morphological parameters could be determined. Using these morphological parameters along with the measured fracture toughness multilinear regression analysis could be performed to determine a "model" for fracture toughness in cancellous bone. The use of multiple regression showed that the use of the BV/TV alongside additional morphological parameters can be used to predict the fracture toughness of the tissue in an across loading configuration (R^2=79.78), whilst in an along loading configuration (perpendicular to the across) no other parameters improve over the use of BV/TV alone (R^2=73.00). These findings show that cancellous bone remodels to resist fracture in a

specific direction and that architectural quality as well as quantity is important in the resistance to fracture.

Keywords: *micro-Computed Tomography, cancellous bone, linear regressions*

4.2 **Introduction**

Osteoporosis (OP) is a degenerative bone condition that is thought to be responsible for 8.9 million fractures per year (O. Johnell & J. A. Kanis 2006). It is estimated that 1 in 2 women and 1 in 5 men over the age of 50 will suffer a fragility fracture, which is defined as a fracture caused by a fall from standing height or less. These fractures are typically associated with or attributed to osteoporosis or osteopenia (International Osteoporosis Foundation 2015). In the UK these fragility fractures cost ~£3,496 million each year and that cost is estimated to increase to £ 5,465 million by 2025 (International Osteoporosis Foundation 2015). At present OP is defined as having a bone mass 2.5 standard deviations below the young adult reference mean (Summers 2001). Another prevalent condition that affects bone tissue is osteoarthritis. Osteoarthritis is normally considered only for its impact on the articular cartilage of the synovial joints; the knock on effects of the compromised joints causes structural changes to occur in the subchondral bone (Cook 2006). Osteoarthritis affects 8.75 million people in the UK and it is estimated that 33% of the population over the age of 45 have sought treatment for osteoarthritis. The joints most affected by the condition are the knee and hip affecting 4.7 and 2.46 million people respectively.

Current protocol in determining a patient's fracture risk and whether they are osteoporotic is based on dual energy X-ray absorptiometry (DEXA). This assessment using DEXA gives an indication of the patient's bone mineral density (BMD) which is the product of both the porosity and density of the mineralised bone tissue; this is usually taken at the hip (Greenwood et al. 2015). The DEXA results are assessed using the fracture risk assessment tool as recommended by the World Health Organization. While this provides valuable data on an individual's fracture risk, advancements in medical imaging technology allows development of more robust and accurate risk assessment tools. (van den Bergh et al. 2010)

The primary role of bone in the body is as a structural material and the cancellous regions can be considered as a cellular solid (Maiti et al. 1984; Gibson 1985; Brezny & Green 1990; Huang & Gibson 1991; Cook & Zioupos 2009). As such the mechanical properties of cancellous bone are impacted by the base material properties of the structure and the micro-architecture of the structure. All variations in the micro-

structural properties of the tissue from the quantity of bone tissue to the orientation of individual trabecular architecture will impact the resultant mechanical properties of the tissue. The current DEXA protocol however fails to consider the architecture of the individual trabeculae. The most common mechanical property that is investigated is the compressive strength of the bone tissue, which fails to consider the ability of the tissue to resist fracture, an extremely important consideration when assessing the ability of bone to carry out its daily tasks, specifically its ability not to fracture under load. This has been considered by a previous study by Cook & Zioupos (2009) in which the fracture toughness of discs and beams of cancellous bone were measured conforming to ASTM standards.

Multiple regression is a progression of conventional linear regression, which can be employed to predict the value of a variable based on the value of two or more predictors. The multiple regression explains the overall fit of multiple predictors to determine the outcome. It is a tool rarely used to predict the mechanical response of bone based on its architecture and has never before been used to predict the fracture toughness of bone. The authors recognise that in the application of multiple linear regression the resultant models are not prescriptive of the underlying mechanisms but a descriptive method to ascertain the relationships within the sample set.

In a previous study the impact of individual architectural and material properties have been considered in relation to the fracture toughness (Cook & Zioupos 2009; Greenwood et al. 2015), and this will provide a basis for the work we present here. In this study we have two primary objectives (a) investigate the use of predictive models to help in the prediction of fracture toughness and (b) investigate if there are any significant differences between the models produced from samples loaded in the along (A_L) and along (A_C) loading configurations.

4.3 **Materials and Methods**

4.3.1 **Bone specimens**

A sample set of femoral heads were collected from 37 osteoporotic (OP) and 8 osteoarthritic (OA) patients who had received a total hip replacement surgery due to suffering fragility fractures at the femoral neck or elective reasons. During the surgery,

specialist surgeons were able to remove the femoral heads intact. The femoral head was used in this study due the increased availability of tissue at the site compared to the femoral neck, where fracture typically occurs, whilst being physically close to the femoral neck. Population characteristics are provided in Table 4-1. Following removal all samples were kept at -20^{o}C prior to sample preparation. Ethical approval for the collection and use of these specimens was provided by Gloucestershire NHS trust REC (acknowledgments).

Table 4-1 Anthropometrical and demographic data of OP and OA groups

	OP	OA
Donors	37	8
Male/ Female	7 / 30	5/3
Number of specimens	60	19
Age range (yrs)	59 - 96	53-76
Age mean (yrs)	82.3 (SD=6.8)	66 (SD=7.3)
Weight range (kg)	41.3-82.6	68-108
Weight mean (kg)	64.2 (SD=10.5)	84.5 (SD=12.96)
Height range (m)	1.55-1.80	1.65-1.83
Height mean (m)	1.67 (SD=0.08)	1.76 (SD=0.074)

4.3.2 **Specimen preparation**

Specimen preparation (including sectioning from the femoral head and cleaning) has previously been described in detail (Cook and Zioupos, 2009; Cook et al., 2010). Single Edge Notched Disc Specimen (SEND) samples were prepared to conform to an adjusted ASTM standard E399-90 in order to assess the necessary stress conditions to instigate crack growth from a man-made notch. Samples were divided into two subsets; with samples orientated along (A_L) the primary direction of the trabecular and those orientated across (A_C) the primary orientation of the trabecular structure. This was due to the nature of cancellous bone being a cellular solid with a fibre like orientation. Where possible both A_L and A_C samples were taken from each specimen. All specimens were stored at −20°C following a defatting process detailed in (Cook and Zioupos,

2009; Cook et al., 2010). The sectioning was performed by using a metallurgical saw (Struers® Accutom-2). The samples were then sanded and polished by using progressively finer grades of carbide paper (400–2500 grit) to the dimensions required for material testing. Specimens were manufactured in the shape of discs, diameter 20mm and thickness 7.5mm, for mechanical material testing as SEND. Sample preparation was performed under constant water irrigation, to prevent the production of micro-cracks or other damage to the specimens.

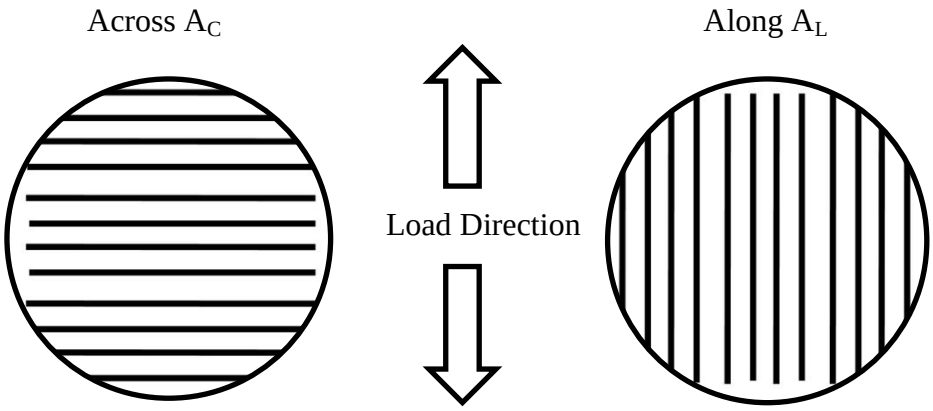

Figure 4-1 diagram of the primary orientation of the trabeculae in the A_C and A_L loading orientations (the lines represent the primary orientation of the individual trabeculae)

4.3.3 **Micro-computed tomography**

The samples' micro-architecture was imaged using micro-Computed Tomography (µ-CT). Each sample was imaged using a Nikon CT H225 (X-Tek Systems Ltd, Tring, Hertfordshire, UK) cone beam µ-CT (µ-CBCT) scanner. Samples were imaged at 50kV and 65µA with a 1000ms exposure. The resultant voxel size of the scan was ~24µm. All scans were manually reconstructed using CT Pro 3D. During reconstruction conditions were optimised to reduce beam hardening and noise, and the noise and beam hardening corrections were standardised across all the samples to ensure the results were comparable. Image analysis and visualisation were carried out using VG Studio Max 2.2 (Volume Graphics GmbH, Heidelberg, Germany). Firstly, the samples' structural properties were determined, and these parameters included; trabecular thickness (TbTh), spacing (TbSp) and number (TbN), surface area (BS), material volume (BV) and total volume (TV). The density of the samples was also determined using a QRM MicroCT-HA (QRM GmbH, 91,096 Möhrendorf, Germany)

calibration phantom. This uses hydroxyapatite of different known concentrations to produce a calibration curve of grey value versus density. Using this calibration the density of the samples can be determined, which is often referred to as tissue mineral density or material density (D_{mat}). Following the determination of the D_{mat} from the average grey value the apparent density (D_{app}) of each sample was determined using Equation 4-1. The D_{app} is often referred to as bone mineral density.

$$D_{app} = D_{mat} \times \frac{BV}{TV} \qquad \textit{Equation 4-1}$$

In this article the use of D_{mat} and D_{app} are used to indicate that they have been calculated on a volumetric basis using µ-CT data. This is important to distinguish as bone mineral density measured in DEXA is an areal representation of the characteristic. BoneJ© [http://bonej.org/; http://rsbweb.nih.gov/ij/] was employed at a second stage to calculate additional micro-architectural parameters such as structure model index (SMI), degree of anisotropy (DA), connectivity density (Conn. D) and Euler characteristic (Euler ch.) (Doube et al. 2010).

4.3.4 **Mechanical testing**

The SEND samples were mechanically characterised in previous papers for fracture toughness in linear elastic FM approach (Cook & Zioupos 2009). The Kc values were derived for the load at a point where the man-made notch started growing (following extensive yielding and bending of the trabeculae ahead of the notch) caused by snapping of one or more trabeculae in the first instance. The deformation was measured by a miniature extensometer (Model 3442-006M-050ST) attached at the mouth of the notch. The dimensions and other restrictions that were followed complied with the usual material testing standards such as ASTM E399-90 as reported in Cook and Zioupos (2009). The mechanical testing was undertaken using a Dartec Series HC25 materials testing machine (Zwick ltd., Leominster HR6 0QH, UK) driven by a 9610 series controller unit and operated using Workshop 96© software. Load was monitored using a 500 N load cell (RDP Electronics Ltd., Wolverhampton WV10 0PY, UK) whilst the gauge length of the crack mouth opening displacement measured by the extensometer was 6 mm. The loading rate during fracture toughness testing was 0.05 mm s−1 (3 mm min−1), with Data Acquisition at a capture rate of 1000 points per

minute. Unlike the more common compression studies which have tested cancellous bone in cylinders or cubes, these tests were the first ever to attempt a quantification of the necessary loading conditions that would allow a crack to start to grow from stability into an unstable fracture mode. In this respect the mechanical data offers a novel and invaluable way of assessing the structural integrity and loading ability of these samples in a way that resembles the conditions in FNF situations in a more biofidelic manner (Cook & Zioupos 2009).

4.3.5 **Statistical Analysis**

Statistical analysis was carried out in two steps. Firstly, comparisons of the multiple subgroups within the cohort such as: the A_L and A_C loading configurations, and the OP and OA groups. The relationships of these subgroups relative to the measured Kc were then carried out. Pearson's correlation coefficients were used throughout the study. In the second stage of statistical analysis multiple linear regressions were employed to develop models to predict the Kc using the morphological parameters. The multiple regression method chosen was a Stepwise selection as it is the most statistically robust of the multiple regression methods. The Stepwise selection combines forward selection and backward elimination where added variables are deleted if their contribution to the model is not determined to be significant. It must be considered that the trabecular thickness (TbTh) and trabecular number (TbN) are calculated interdependently therefore in the development of statistical models inclusion of both has been avoided. In this study Stepwise selection was performed using Minitab automated stepwise selection.

4.4 **Results**

A comparison of how the morphological data collected compares to previous studies is given in Table 4-3. Table 4-2 shows a comparison of the A_L and A_C separated groups as well as the average parameters collected for the entire cohort. Values measured between the groups were not statistically significantly different with the exception of DA, which may be an impact of the cutting and selection process. Even with this consideration in mind it shows that the differences between the subsequent correlations and regression analysis are due to the contribution of the parameters to the

loading in the specified direction. A comparison of the morphological data between males and females and with other studies was reported in a previous study (Greenwood et al. 2015).

As well as considering the different loading conditions, consideration is also made of differences between the OP and OA groups and the relationship they have with fracture toughness. Therefore the relationships between the architectural properties of OP and OA bone and their corresponding fracture toughness is presented (Table 4-3). Within the OP sample set, Kc had a higher correlation with trabecular spacing than observed in the OA group whereas BV/TV and TbN correlations in the OA groups were much higher than in the OP. There was a consistency in parameters that correlated significantly between the OP and OA groups with the exception of Conn. D, which was found to be significant ($p<0.05$) in the OA group but not in the OP group.

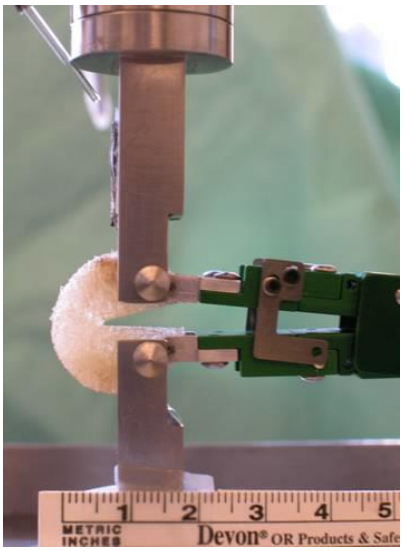

Figure 4-2 Sample being mechanically loaded and example of fracture toughness loading curve taken from Cook (2008)

4.4.1 **Micro-Architecture**

Table 4-2 Average micro-architecture properties for samples loaded A_L and A_C. Standard deviation and p-values denoting significant difference (P<0.05) between the two groups are included

	All Samples		A_L		A_C		
Parameter	Mean	Std. Dev.	Mean	Std. Dev.	Mean	Std. Dev.	P-values
BV/TV	0.21	0.079	0.23	0.09	0.202	0.073	0.14
BS/BV	14.53	2.62	13.99	2.43	15.00	2.72	0.09
BS/TV	2.94	0.57	3.03	0.62	2.86	0.51	0.18
TbTh	0.14	0.029	0.15	0.03	0.14	0.03	0.14
TbN	1.44	0.34	1.50	0.29	1.38	0.38	0.10
Tbsp	0.60	0.24	0.54	0.14	0.66	0.29	0.06
tDA	2.37	0.68	2.55	0.81	2.21	0.49	0.02
Conn. D	2.18	1.14	2.20	1.25	2.16	1.04	0.13
SMI	-5.87	4.65	-4.92	3.73	-6.70	5.24	0.10
D_{mat}	1.79	0.08	1.81	0.07	1.77	0.36	0.88
D_{app}	0.39	0.16	0.41	0.17	0.08	0.14	0.09

Table 4-3 Average micro-architecture properties for the OP and OA groups. Standard deviation and p-values denoting significant difference (P<0.05) between the two groups are included. Micro-architecture values from other studies are also provided for comparison (modified from Greenwood at al. 2015)

	OP		OA				
Parameter	Mean	Std. Dev.	Mean	Std. Dev.	P-Values	Ranges in literature	References
Kc	0.29	0.14	0.42	0.28	0.02	-	-
BV/TV	0.20	0.05	0.27	0.094	<0.01	0.07 – 0.30	(Link et al. 1998; Thomsen et al. 2015; Wu et al. n.d.; Perilli et al. 2008; Macdonald et al. 2011; Green et al. 2011; Mazurkiewicz & Topoliński 2009)
BS/BV (mm^{-1})	14.62	2.37	12.79	2.25	0.01	8.7 – 22.5	(Mazurkiewicz & Topoliński 2009; Zhang et al. 2010; Milovanovic et al. 2012)
BS/TV (mm^{-1})	2.86	0.47	3.33	0.75	<0.01	0.59-5	(Fyhrie et al. 1995; Martin 1984)
TbTh (mm^{-1})	0.14	0.02	0.16	0.03	<0.01	0.09 – 0.25	(Mazurkiewicz & Topoliński 2009; Green et al. 2011; Thomsen et al. 2015; Wu et al. n.d.; Ding & Hvid 2000; Perilli et al. 2008)
TbN (mm^{-1})	1.46	0.25	1.63	0.34	0.04	0.76 – 2.52	(Mazurkiewicz & Topoliński 2009; Yan et al. 2011; Ding & Hvid 2000; Green et al. 2011; Perilli et al. 2008)
Tbsp (mm^{-1})	0.57	0.13	0.50	0.16	0.15	0.30 – 1.22	(Mazurkiewicz & Topoliński 2009; Yan et al. 2011; Green et al. 2011; Wu et al. n.d.; Perilli et al. 2008)
tDA	2.41	0.62	2.25	0.81	0.16	1.73 – 2.0	(Green et al. 2011; Wu et al. n.d.)
Conn. D	1.83	0.88	3.36	0.94	<0.01	1.96-5.62	(Saers et al. 2016)
SMI	-6.15	3.48	-1.86	2.89	<0.01	0.50 – 2.61	(Wu et al. n.d.; Ding & Hvid 2000; Green et al. 2011; Milovanovic et al. 2012)
D_{mat} ($g\ cm^{-3}$)	1.80	0.09	1.80	0.05	0.74	1.4-2.0	(Galante et al. 1970; Gibson 1985; Zioupos et al. 2008; Cook & Zioupos 2009)
D_{app} ($g\ cm^{-3}$)	0.36	0.09	0.50	0.18	<0.01	0.12 – 0.37	(Mazurkiewicz & Topoliński 2009; Macdonald et al. 2011)

The data presented in Table 4-4 shows the correlations between the micro-architectural parameters and fracture toughness, with R^2 and p-values given, in the A_L and A_C groups as well as in the combined groups. The parameter with the highest R^2 value in the A_L and combined groups was BV/TV whilst in the A_C group it was the TbN and BS/TV. Most of the parameters measured were found to impact upon fracture toughness with the exception of DA across the entire cohort and Conn. D in the A_C loading group. In Table 4-5 the correlations within the OP and OA separate groups are shown. When considering the entire cohort the BV/TV had the highest R^2 value in both groups. The DA and Conn. D did not correlate significantly in either group. Additionally the D_{mat} was seen not to be significant with the OP OA separation.

Table 4-4 R^2 (bold) and P-values for correlations between architectural parameters and fracture toughness

	All		A_L		A_C	
Parameter	R^2	P-Value	R^2	P-Value	R^2	P-Value
BV/TV	**0.66**	<0.01	**0.74**	<0.01	**0.67**	<0.01
BS/BV	**0.25**	<0.01	**0.25**	<0.01	**0.35**	<0.01
BS/TV	**0.57**	<0.01	**0.51**	<0.01	**0.72**	<0.01
TbTh	**0.34**	<0.01	**0.37**	0.025	**0.39**	<0.01
TbN	**0.56**	<0.01	**0.51**	<0.01	**0.72**	<0.01
Tbsp	**0.40**	<0.01	**0.49**	<0.01	**0.41**	<0.01
DA	**0.00**	0.74	**0.01**	0.60	**0.10**	0.11
Conn. D	**0.16**	<0.01	**0.26**	<0.01	**0.09**	0.13
D_{mat}	**0.11**	0.01	**0.13**	0.04	**0.18**	0.025
D_{app}	**0.64**	<0.01	**0.73**	<0.01	**0.65**	<0.01

4.4.2 **Regression analysis**

For multiple regressions BV/TV was taken to be the base predictor as it was consistently the parameter that correlated highest with the fracture toughness. Additionally BV/TV is very closely linked to the metric currently used in the assessment of OP as results from DEXA are most influenced by the quantity of bone rather than the density of the material itself (Greenwood et al. 2015). By using multiple regressions for the entire cohort (Figure 4-5) and the A_C (Figure 4-3), the inclusion of

additional parameters helped produce a model that can, to some degree, predict the fracture toughness of cancellous bone. However as shown in Table 4-6 Stepwise regression was unable to identify any parameters that significantly improved the R^2 value for the A_L group beyond BV/TV alone because BV/TV and stepwise values are the same. The final fit for the A_C group is given in Table 4-7 with the subsequent plot of predicted vs measured in Figure 4-3 (b).

Table 4-5 R^2 (bold) and P-values for correlations between architectural parameters and fracture toughness with OP and OA groups separated

	OP		OA	
Parameter	R^2	P-value	R^2	P-value
BV/TV	**0.58**	<0.01	**0.69**	<0.01
BS/BV	**0.17**	<0.01	**0.37**	0.02
BS/TV	**0.52**	<0.01	**0.56**	<0.01
TbTh	**0.21**	<0.01	**0.40**	0.02
TbN	**0.44**	<0.01	**0.71**	<0.01
Tbsp	**0.48**	<0.01	**0.29**	0.05
DA	**0.01**	0.49	**0.01**	0.72
Conn. D	**0.03**	0.28	**0.28**	0.05
D_{mat}	**0.11**	0.22	**0.23**	0.08
D_{app}	**0.54**	<0.01	**0.68**	<0.01

Table 4-6 R^2, Adjusted R^2 (bold) and Significance-F multiple linear regressions for all samples as well as a separation of the A_L and A_C loading groups

	All			A_L			A_C		
	R^2	Adj-R^2	Signif-F	R^2	Adj-R^2	Signif-F	R^2	Adj-R^2	Signif -F
BV/TV	0.670	**0.656**	<0.001	0.738	**0.730**	<0.001	0.674	**0.661**	<0.001
Stepwise selection	0.759	**0.741**	<0.001	0.738	**0.730**	<0.001	79.78	**77.14**	<0.001

Table 4-7 stepwise regression steps for the A_C group using BV/TV as the base predictor with the addition of Degree of Anisotropy, TbTh, Connectivity Density, and Tbsp (Alpha to add 0.05), the final step with all predictors being significant (p<0.05) is given in bold

	Step				
	1	2	**3**	4	5
Constant	-0.133	-0.436	**-0.125**	$9.565x10^{-6}$	-0.262
BV/TV	2.31	2.26	**3.49**	3.97	4.74
T-Value	7.18	7.77	**6.21**	6.46	6.19
P-Value	<0.001	<0.001	**<0.001**	<0.001	<0.001
Degree of Anisotropy		0.60	**0.62**	0.50	0.53
T-Value		2.57	**2.93**	2.27	2.47
P-Value		0.017	**0.008**	0.033	0.022
TbTh			**-4.1**	-4.7	-5.4
T-Value			**-2.48**	-2.85	-3.26
P-Value			**0.021**	0.009	0.004
Connectivity Density				-0.040	-0.044
T-Value				-1.65	-1.85
P-Value				0.114	0.079
Tbsp					0.32
T-Value					1.59
P-Value					0.126
S	0.115	0.104	**0.0947**	0.0913	0.0883
R^2	67.33	74.38	**79.78**	82.00	83.94
R^2 (adjusted)	66.02	72.24	**77.14**	78.73	80.12

We have presented the results of multiple regression analysis for the sample sets loaded in the A_L and A_C configurations as well as for entire cohort (Table 4-6). Applying multiple regressions to the entire cohort adheres to the 'rule of ten' which suggests a minimum of ten samples for every predictor in the model, however in the A_L groups model this is not maintained. Whilst it has been suggested that this is not necessary, maintaining a high number of predictors to samples is advantageous and helps reduce the effects of over fitting (Austin & Steyerberg 2015).

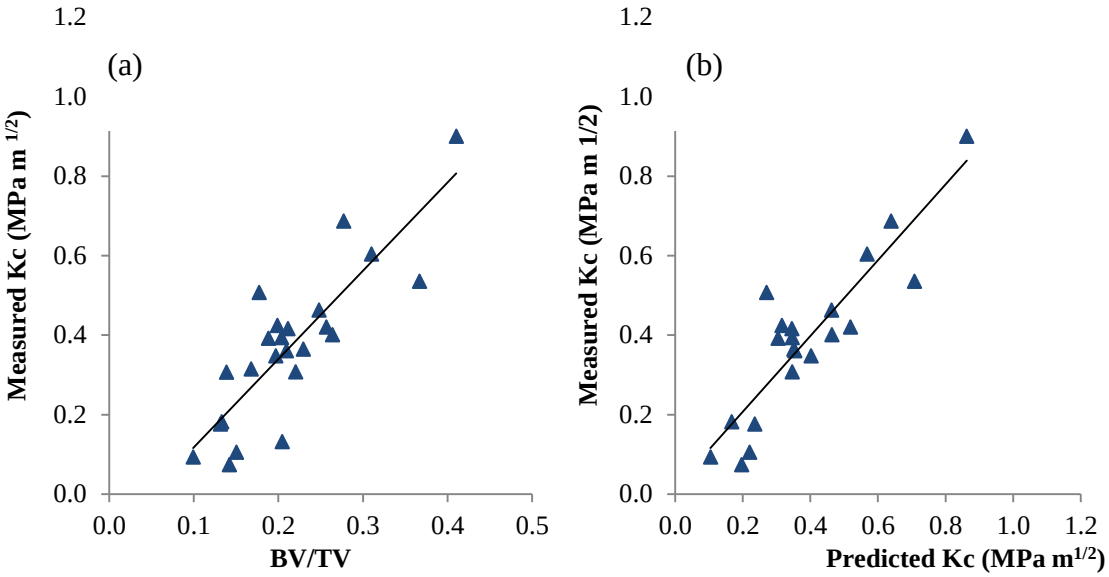

Figure 4-3 Plots for the A_C group of (a) BV/TV vs fracture toughness (K_C) (b) Stepwise selection method of predicted K_C vs measured K_C

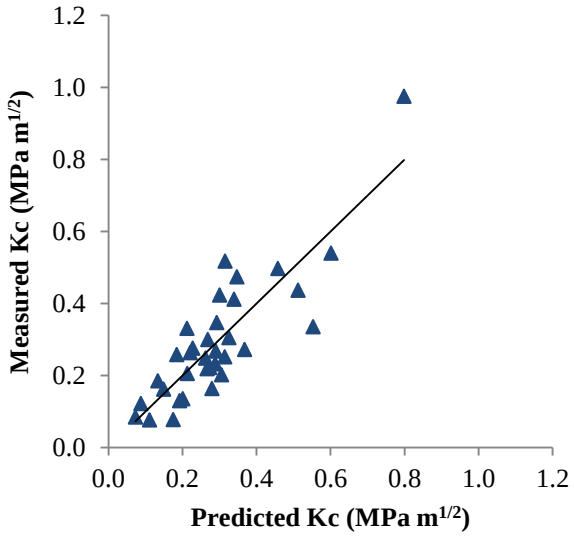

Figure 4-4 plot of the regression analysis applied to the A_L group of predicted K_C vs measured K_C

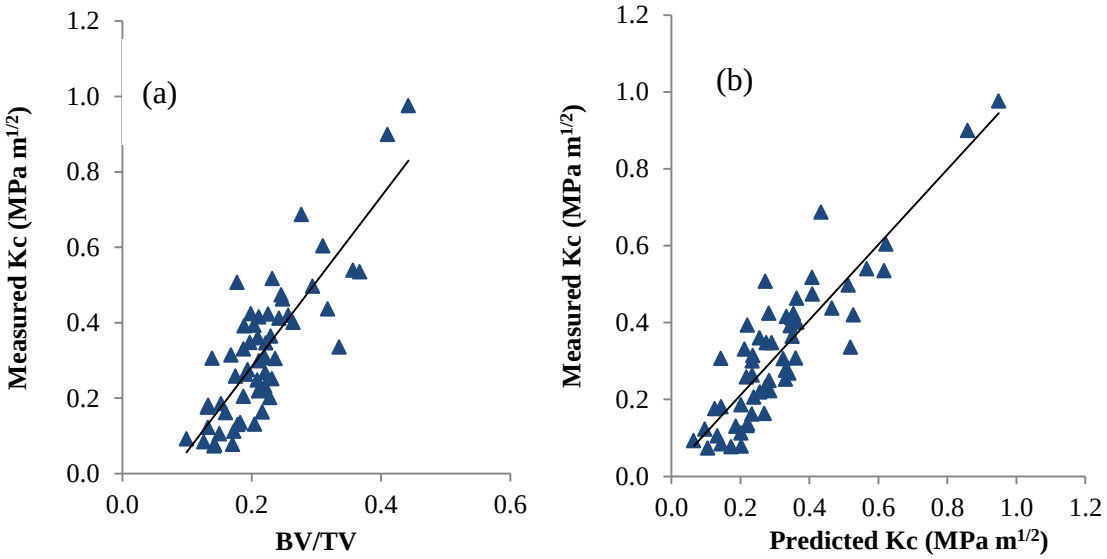

Figure 4-5 Plots both loading conditions of (a) BV/TV vs fracture toughness (K_C) (b) Stepwise selection method of predicted K_C vs measured K_C

To add a parameter to the model the maximum p-value to add to the model was set to 0.15. The final model selected with all p-values<0.05 for the entire cohort was from step 4 shown in Table 4-8 whilst step 3 from Table 4-7 was selected for the A_C group.

$$K_C = 2.29\left(\frac{BV}{TV}\right) - 0.217 \qquad \text{Equation 4-2}$$

Table 4-8 stepwise regression steps for the entire cohort using BV/TV as the base predictor with the addition TbN, Tbsp, BS/TV, and tDA (Alpha to add 0.15), the final step with all predictors being significant (p<0.05) is given in bold

	Step				
	1	2	3	**4**	5
Constant	-0.1712	-0.3650	-1.0018	**-1.0062**	-1.1267
BV/TV	2.27	1.37	1.60	**1.81**	1.74
T-Value	10.83	3.48	4.09	**4.71**	4.54
P-Value	<0.001	<0.001	<0.001	**<0.001**	<0.001
TbN		0.262	0.458	**0.983**	1.006
T-Value		2.64	3.65	**3.96**	4.10
P-Value		0.011	0.001	**<0.001**	<0.001
Tbsp			0.53	**0.54**	0.55
T-Value			2.40	**2.53**	2.62
P-Value			0.020	**0.014**	0.011
BS/TV				**-0.28**	-0.27
T-Value				**-2.42**	-2.36
P-Value				**0.019**	0.022
Degree of Anisotropy					0.028
T-Value					1.54
P-Value					0.129
S	0.109	0.104	0.0998	**0.0958**	0.0946
R^2	66.91	70.51	73.26	**75.83**	76.85
R^2 (adjusted)	66.34	69.48	71.83	**74.08**	74.71

4.5 **Discussion**

The research presented in this article outlines the fundamental relationships between the fracture toughness of cancellous bone and the material quality factors measured by µ-CT, and implements the use of statistical models to predict the mechanical properties of the samples. The collection of samples, which have been used in previous studies, are unique in that they are the only instance of measuring cancellous fracture toughness in this way (Cook & Zioupos 2009; Cook R. B. 2006). Previous µ-CT research on this cohort has investigated the micro-architecture and material quality whilst looking at differences between the male and female samples in the cohort, and treated the samples loaded in different configurations (A_L and A_C) indiscriminately (Greenwood et al. 2015). Here we have taken the opposite approach and treated the

male/female samples indiscriminately and separated the A_L and A_C loading configurations. This research also has the inclusion of OA samples which represent perhaps of the opposite of OP in that the effects of OA tend to lead to a thickening of the subchondral bone. The use of μ-CT imaging presents an opportunity to assess the skeleton not currently found across the array of medical machines available. Current OP diagnosis by DEXA assesses the BMD which is a representation of the density of cancellous architecture and the material density of the bone itself. Medical CT scanners can also be used to assess the structure of the skeleton; however the voxel size and image resolution currently obtainable from these systems is nowhere near as great as that which can be achieved in μ-CBCT. Therefore all data that has been presented here represents what could be assessed in the future, and is a precursor to the assessment of bone fracture toughness awaiting the ability to assess these characteristics *in vivo*.

As previously mentioned there is a real danger of over fitting data in a multiple regression analysis which would produce models that would claim to predict better than they would be capable of. Here we have taken every care to include the fewest number of predictors and to ensure that the predictors are independent of each other. In bone however this is very difficult due to the dependence of parameters on other physical characteristics including both the obvious links between BV/TV and apparent density and the less apparent links between the material density and the BV/TV (Zioupos et al. 2008). Multiple regression analysis was not carried out in the OP and OA sub groups due to a very small samples size of the OA group. The SMI values reported in this study were negative; this is due to the samples containing a significant number of concave surfaces. In the SMI calculation it is assumed that the number of concave surfaces are negligible (Salmon et al. 2015). Therefore SMI was excluded from the multiple regression models due to lack of suitability but was included to demonstrate that the number of concave surfaces in cancellous bone are significant.

The comparison of OP and OA subgroups has supported the notion that OP leads to the loss of bone, shown by the significant differences between the BV/TV of the two groups ($p<0.01$). The average BV/TV of the OA group is still within the range previously reported in the literature (Table 4-3) suggesting that in the OA condition there is no extreme deposition of new bone tissue within the cancellous regions. The

measured BS/BV and calculated BS/TV are within the literature ranges for both OP and OA groups. The differences between BS/BV for the OP and OA groups suggests that there are more surfaces available within the OP groups, which is consistent with the notion that remodelling is a surface effect (Currey 2002; Martin 1984). Therefore greater rates of remodelling could lead to a loss of bone which is typically associated with OP (Genant et al. 2008; Buenzli et al. 2012). The trabecular number and thickness are higher in the OA group which is typically consistent with the increased BV/TV and consistent with increases in mechanical strength (Currey 2002; Gibson 1985; Cook & Zioupos 2009; Kopperdahl & Keaveny 1998). There were not significant differences in the morphology measured between the A_L and A_C groups suggesting that any differences between correlations with the architectural parameters and any differences in the multiple regression models produced are due to the contributions of the individual parameters in the different loading directions.

When looking at the entire sample set the BV/TV was seen to have the highest correlation with fracture toughness, enforcing the assertion that the quantity of bone is the biggest contributor to bone strength. However in the division of the A_L and A_C subgroups this only held true for the A_L group, whilst in the A_C group the TbN was seen to have the highest correlation. This suggests that perhaps a denser trabecular packing may have a bigger impact on cancellous bones' resistance to fracture in the A_C loading configuration than in the A_L. The significant D_{mat} correlation across all the groups suggests that the chemical structure of the bone tissue plays an important role in the ability of the tissue to resist fracture, which supports previously found differences between the physio-chemistry of normal and OP bone tissue (Greenwood et al. 2016). However this effect is clearly not as important at the structural properties of the tissue evidenced in the much lower R_2 values. Between the OP and OA subgroups the parameters that impacted on fracture toughness followed the same trends, with the exception of connectivity density which was a significant contributor in the OA group but not the OP. This is perhaps due to the connectivity density being significantly higher in the OA group.

4.5.1 **Multiple Regressions**

Using multiple linear regressions we were able to demonstrate that multiple morphological parameters impact upon the fracture toughness of bone when loaded in the A_C direction or when loading direction is not considered and that by accounting for these parameters within the model it is possible to better predict the fracture toughness of bone than by consideration of multiple parameters. However in the A_L group the use of multiple regressions was unable to identify any parameter that would significantly improve the model. This has very profound implications on the understanding of bone fracture toughness and suggests that in the A_L loading direction the only parameter that resists fracture is the quantity of bone available, and that other parameters such as the average thickness of trabeculae do not develop in such a way to resist fracture in that specific direction. In the A_C direction however other parameters had a significant effect on the ability of material to resist fracture. This is consistent with basic underpinning mechanisms of bone remodelling suggested by Wolff, whereby bone is responsive and adapts to the loads applied to it. The samples in the A_C groups are orientated across the primary direction of loading in the hip, so the bone will have adapted to resist fracture in this direction and as such this adaptation has led to reorientation of the trabeculae to achieve this. The A_L group were orientated perpendicular to the primary loading of bone and as such the trabecular structure has not adapted in micro-orientation to resist fracture.

The two primary aims of this study have been addressed: (a) we have shown that across the entire cohort consideration of multiple morphological parameters can help produce models that can inform on bone quality and can perhaps be used to predict fracture toughness with further development. (b) Separation of the models produced between the A_L and A_C groups was found to be revealing in that for the A_L group no additional parameter was seen to improve the predictive ability over the use of BV/TV; this is incredibly surprising and has implications on how bone at the hip remodels to help resist fractures. To conclude, use of multiple regressions represents a real opportunity to develop models to predict the likelihood of a patient's fracture using the micro-architecture, and there is a clear case for investigation into the remodelling of bone at the hip.

4.6 **Conclusion**

This study has considered the impact of the micro-architecture of cancellous bone on the fracture toughness of the tissue. We have been able to use a relatively large cohort of samples collected from patients undergoing hip replacement surgery and determined to be either osteoporotic or osteoarthritic. The findings support the currently used DEXA model whereby a significantly reduced bone mass leads to a reduction in the mechanical competency of the tissue. It has additionally supported previous reports that multiple structural parameters such as TbTh, TbSp, TbN, and BS/BV also contribute significantly to the fracture toughness. We also employed the use of a statistical tool, multiple regression analysis, to demonstrate that the combination of multiple structural parameters can lead to an improved model of fracture toughness that may provide a basis to predict the fracture risk of a patient. The use of multiple regressions was also able to highlight that in the A_L loading condition the quantity of bone is the biggest contributor to fracture toughness and that the inclusion of additional parameters did not significantly improve the predictive power. The same cannot be said for the A_C group which showed a marked improvement with the addition of multiple parameters. This further concretes Wolff's law, or at least the principle, that bone truly remodels to its loading and in this case to resist fracture at the hip. The use of multiple regressions is not without its limitations; in this study from a statistical perspective the sample size is relatively small, however from a study on human bone samples it can be considered relatively large. Further work is required to investigate if these architectural parameters can be included alongside the currently collected BMD to improve the prediction of patients' fracture risk.

4.7 **Acknowledgments**

The tests were carried out in the Biomechanics and Analytical laboratories of the Cranfield Forensic Institute of Cranfield University in Shrivenham, UK. Additionally we would like to acknowledge the support provided by the UK Department of Transport under the BOSCOS (Bone Scanning for Occupant Safety) project for which the human material was obtained in the Gloucester and Cheltenham NHS Trust hospitals under ethical consent (BOSCOS—Mr. Curwen CI REC ref. 01/179G).

4.8 **References**

Austin, P.C. & Steyerberg, E.W., 2015. The number of subjects per variable required in linear regression analyses. *Journal of Clinical Epidemiology*, 68(6), pp.627–636.

van den Bergh, J.P.W. et al., 2010. Assessment of Individual Fracture Risk: FRAX and Beyond. *Current Osteoporosis Reports*, 8(3), pp.131–137

Brezny, R. & Green, D.J., 1990. The effect of cell size on the mechanical behavior of cellular materials. *Acta Metallurgica et Materialia*, 38(12), pp.2517–2526.

Buenzli, P.R. et al., 2012. Endocortical bone loss in osteoporosis: The role of bone surface availability. *International Journal for Numerical Methods in Biomedical Engineering*, 29(12) pp.1-13.

Cook, R.B. 2006. 'Non-invasively assessed skeletal bone status and its relationship to the biomechanical properties and condition of cancellous bone'. PhD, Cranfield University, Shrivenham

Cook, R.B. & Zioupos, P., 2009. The fracture toughness of cancellous bone. *Journal of biomechanics*, 42(13), pp.2054–60.

Currey, J.D., 2002. Bones: Structure and Mechanics, Princeton University Press.

Ding, M. & Hvid, I., 2000. Quantification of age-related changes in the structure model type and trabecular thickness of human tibial cancellous bone. *Bone*, 26(3), pp.291–295.

Fyhrie, D.P. et al., 1995. Human vertebral cancellous bone surface distribution. *Bone*, 17(3), pp.287–291.

Galante, J., Rostoker, W. & Ray, R.D., 1970. Physical properties of trabecular bone. *Calcified Tissue Research*, 5(1), pp.236–246.

Genant, H.K., Engelke, K. & Prevrhal, S., 2008. Advanced CT bone imaging in osteoporosis. *Rheumatology*, 47(4), pp.9-16.

Gibson, L.J., 1985. The mechanical behaviour of cancellous bone. *Journal of Biomechanics*, 18(5), pp.317–328.

Green, J.O. et al., 2011. Age-related changes in human trabecular bone: Relationship between microstructural stress and strain and damage morphology. *Journal of biomechanics*, 44(12), pp.2279–85.

Greenwood, C. et al., 2015. The micro-architecture of human cancellous bone from fracture neck of femur patients in relation to the structural integrity and fracture toughness of the tissue. *Bone*, 3, pp.67–75.

Greenwood, C. et al., 2016. Towards new material biomarkers for fracture risk. *Bone*, 93, pp.55–63.

Huang, J.S. & Gibson, L.J., 1991. Fracture toughness of brittle foams. *Acta Metallurgica et Materialia*, 39(7), pp.1627–1636.

International Osteoporosis Foundation, 2015 Facts and Statistics | International Osteoporosis Foundation. Available at: *https://www.iofbonehealth.org/facts-statistics* [Accessed January 18, 2017].

Johnell, O. & Kanis, J.A., 2006. An estimate of the worldwide prevalence and disability associated with osteoporotic fractures. *Osteoporosis International*, 17(12), pp.1726–1733.

Kopperdahl, D.L. & Keaveny, T.M., 1998. Yield strain behavior of trabecular bone. *Journal of Biomechanics*, 31(7), pp.601–608.

Link, T.M. et al., 1998. A Comparative Study of Trabecular Bone Properties in the Spine and Femur Using High Resolution MRI and CT. *Journal of Bone and Mineral Research*, 13(1), pp.122–132.

Macdonald, H.M. et al., 2011. Age-related patterns of trabecular and cortical bone loss differ between sexes and skeletal sites: A population-based HR-pQCT study. *Journal of Bone and Mineral Research*, 26(1), pp.50–62.

Maiti, S.K., Ashby, M.F. & Gibson, L.J., 1984. Fracture toughness of brittle cellular solids. *Scripta Metallurgica*, 18(3), pp.213–217.

Martin, R.B., 1984. Porosity and specific surface of bone. *Critical reviews in biomedical engineering*, 10(3), pp.179–222.

Mazurkiewicz, A. & Topoliński, T., 2009. Relationships between structure, density and strength of human trabecular bone. *Acta of Bioengineering and Biomechanics Original Paper*, 11(4).

Milovanovic, P. et al., 2012. Micro-structural basis for particular vulnerability of the superolateral neck trabecular bone in the postmenopausal women with hip fractures. *Bone*, 50(1), pp.63–68.

Perilli, E. et al., 2008. Dependence of mechanical compressive strength on local variations in microarchitecture in cancellous bone of proximal human femur. *Journal of Biomechanics*, 41(2), pp.438–446.

Saers, J.P.P. et al., 2016. Trabecular bone structural variation throughout the human lower limb. *Journal of Human Evolution*, 97, pp.97–108.

Salmon, P.L. et al., 2015. Structure Model Index Does Not Measure Rods and Plates in Trabecular Bone. *Frontiers in Endocrinology*, 6, p.162.

Summers, G.D., 2001. Osteoporosis in men. *Radiography*, 7(2), pp.119–123.

Thomsen, J.S. et al., 2015. Age-related changes in vertebral and iliac crest 3D bone microstructure—differences and similarities. *Osteoporosis International*, 26(1), pp.219–228.

Wu, Z., Laneve, A.J. & Niebur, G.L., In vivo microdamage is an indicator of susceptibility to initiation and propagation of microdamage in human femoral trabecular, *Bone*. 55(1), pp.208-15

Yan, Y.-B. et al., 2011. Relationship between architectural parameters and sample volume of human cancellous bone in micro-CT scanning. *Medical engineering & physics*, 33(6), pp.764–9

Zhang, Z.-M. et al., 2010. Micro-CT and mechanical evaluation of subchondral trabecular bone structure between postmenopausal women with osteoarthritis and osteoporosis. *Osteoporosis International*, 21(8), pp.1383–1390.

Zioupos, P., Cook, R.B. & Hutchinson, J.R., 2008. Some basic relationships between density

values in cancellous and cortical bone. *Journal of Biomechanics,* 41(9), pp.1961–1968.

5 Assessment of the physicochemical properties of cancellous bone in relation to its fracture toughness

G. J. Adams[1], R. B. Cook[2] C. Greenwood[1], B. Gardner[3], N. Stone[3], K.D. Rogers[1], P. Zioupos[1]

1 Cranfield Forensic Institute, Cranfield University, Defence Academy of the UK, Shrivenham, UK

2 nCATS, School of Engineering Science, University of Southampton, Southampton, UK3 Physics and Astronomy, Exeter University, Exeter, UK

5.1 Abstract

Osteoporosis and Osteoarthritis are prevalent bone conditions that affect millions of people globally. The current gold standard for identifying osteoporosis is an assessment and quantification of the bone mineral density (BMD) by means of dual x-ray absorption (DEXA). The results of DEXA are used in the fracture risk assessment tool to determine the patient's risk of fracture. This method of assessment of bone integrity does not account for the individual components of bone quality such as structure and chemistry. Samples were taken from osteoporotic and osteoarthritic patients ranging from ages 59-96 years. The samples were excised from the centre of the femoral head and cut into disks conforming to ASTM standard E399-90 to determine the plane-strain fracture toughness. These samples were imaged using μCT imaging (XT H 225, X-Tek Systems Ltd) to assess morphological parameters. XRD analysis was carried out using a PANalytical X'Pert PRO Multi-Purpose Diffractometer with Cu Kα radiation. FTIR analysis was carried out using an attenuated total reflectance (ATR)–FTIR. Raman spectroscopy was performed to compliment FTIR and to carryout Principal Component Analysis (PCA) which has never before been carried out on such a large cohort of fragility fracture samples alongside osteoarthritic and 'normal' samples. From the structural parameters obtained from μCT, BV/TV was determined to be the most significant impacter on the plane strain fracture toughness, to this multiple physicochemical parameters were added to multiple regression models to predict fracture toughness. The results showed that in an across loading configuration the addition of three parameters the fracture toughness could be predicted (R^2=91.09) and in an along loading configuration the addition of one parameter the fracture toughness could be predicted (R^2=87.17). An additional set of 'normal' sample were also analysed

using Raman spectroscopy in conjunction with PCA which showed a clear separation between the osteoporotic, osteoarthritic and normal samples. These findings can provide a potential basis for the development of an *in vivo* assessment of an individual's fracture risk.

5.2 **Introduction**

Osteoporosis is a bone condition that is characterised by degeneration of bone tissue and leads to an increased risk of fracture. Osteoporosis is a wide spread condition and according to the World Health Organisation is estimated to affect 200 million women worldwide and in the UK alone there are approximately 3.21 million people suffering with Osteoporosis (International Osteoporosis Foundation 2015; Society 2016). Osteoporosis is typically determined by and measured using a significant drop in bone mineral density (BMD) (Kanis et al. 1997). Having reduced bone mass with age, following peak bone mass, is normal but in osteoporosis the bone mass has fallen 2.5 standard deviations below the young adult reference mean. This significant drop below the young adult reference mean has a dramatic effect on the mechanical competency of the skeleton. Having a reduced bone mass between 1 and 2.5 standard deviations below the reference mean is regarded as osteopenia (Summers 2001) and puts the sufferer at an increased risk of fracture, but to nowhere near the increased risk suffered by those with osteoporosis. Osteopenia is however considered a precursor to osteoporosis and can present an opportunity to begin preventative treatment and lifestyle changes to delay the onset of full osteoporosis.

BMD is normally measured using dual-energy X-ray diffraction (DEXA). Measurements of BMD are a product of the quantity of bone and material quality of the bone tissue. As such it fails to account for the individual impact of bone chemistry and architecture and does not accurately predict a patient's fracture risk as there is significant overlap between the BMD of fracture and non-fracture groups (Gamsjaeger et al. 2014). The use of BMD alone is not suitable for the assessment of an individual's fracture risk as 82% of postmenopausal women with fracture were found to have normal BMD scores (Siris et al. 2004). The BMD results obtained from DEXA are often used in the Fracture Risk Assessment Tool (FRAX) as recommended by the World Health Organization (WHO) (FRAX 2017). The FRAX tool uses multiple risk factors such as age, sex, weight and life-style to inform on a patient's 10 year probability of a hip fracture or major osteoporotic fracture (Kanis et al. 2008). This presents and highlights an opportunity to potentially improve the diagnosis of osteoporosis and warrants investigation into the factors affecting bone strength. The development and implementation of tools that consider additional parameters or algorithms beyond those

currently utilised by FRAX will help in addressing the need to accurately estimate a patient's fracture risk (van den Bergh et al. 2010). Another wide-spread condition that affects the structure and properties of bone is osteoarthritis which isn't often considered for its impact on bone. The condition affects 8.75 million people in the UK and it is estimated that 33% of the population over the age of 45 have sought treatment for osteoarthritis. Whilst osteoarthritis is most often considered for its effects of the soft tissue of joints it does cause significant micro-structural and chemical changes to the subchondral bone tissue which are rarely considered (Cook & Zioupos 2009; Shea & Miller 2005; Zuo et al. 2016).

When investigating the strength of bone, research has typically focused on the elastic response of tissue (Reilly et al. 1974; Gibson 1985; Turner et al. 1999), which is of course important, but fails to consider the toughness which will ultimately determine if a bone will fail under loading (Yan et al. 2007; Cook & Zioupos 2009). The primary role of the skeleton in the body is to structurally support the body and protect vital organs. At the micro-structural level bone has a hierarchical structure (Rho et al. 1998), and the ability of the bone to act as a structural material is impacted by the hierarchical structures within it. At the macro level bone exists in two discrete forms, cortical and cancellous, whilst at the micro level bone exists in two main forms, primary and secondary, which can be further subdivided (Martin & Burr 1989; Currey 2002). Below the micro-structural level at the nano-scale there are organic and inorganic components; collagen and mineral respectively.

Due to the complexity of bone's hierarchal structure there is a wide array of parameters that need to be considered in order to assess the quality of bone as a material. The mechanical properties resulting from the chemical quality of bone can be assessed by means of micro- or nano-indentation, which have been used extensively to determine the micro-mechanical properties of bone tissue (Zysset et al. 1999; Hengsberger et al. 2002; Rho et al. 2002; Donnelly et al. 2006; Chevalier et al. 2007). A wide range of differences have been reported in the hardness and modulus measured by nano-indentation (Rho et al. 1997; Rho et al. 1998; Zysset et al. 1999; Hengsberger et al. 2002; Rho et al. 2002; Dall'ara et al. 2007; Boivin et al. 2008; Isaksson et al. 2010; Shepherd et al. 2011; Dall'Ara et al. 2013; Milovanovic et al. 2014;). In cortical bone

tisue, which has been shown to display similar properties to nearby cancellous bone (Rho et al. 1998), the modulus measured by indentation was seen to slightly decrease with age in the osteonal and interstitial regions, whilst the periosteal side showed an increase (Rho et al. 2002). It has been shown as a result of osteoporosis the Vickers hardness decreases with age in cancellous bone which is counter to what would be expected due to the increase in mineral content that has been reported with age (Zioupos et al. 2008). The mineral content in osteoporotic cancellous tissue has been shown to increase with Vickers hardness (Boivin et al. 2008; Zioupos et al. 2008).

Bone can be indented under either wet or dry conditions. Wet is typically seen to be the most representative of the properties of bone tissue in the body as this environment simulates physiological condition (Dall 'ara et al. 2007; Wolfram et al. 2010). Hardness measured under wet conditions have been shown to be as much as 30-40% lower when compared with dry conditions (Dall 'ara et al. 2007), whilst the modulus measured by instrumented nano-indentation has been shown to be ~29% lower in bone indented under the wet condition (Wolfram et al. 2010). It is not currently known what impact, if any, the hardness or modulus measured by nano-indentation has on the fracture toughness of osteoporotic cancellous bone. However the relationships between the mineral content and Vickers hardness (Boivin et al. 2008) would suggest that an increased Vickers hardness could correlate with a decreased fracture toughness.

Infrared spectroscopy has previously been used to assess osteoporotic bone and a reduction in mineral to organic ratios have been reported (Boskey et al. 2005; Gadeleta et al. 2000; Gamsjaeger et al. 2014) as well as an increase in the carbonate *v2*: phosphate *v1, v2* ratio. FTIR has been used to assess the crystallinity by means of the splitting factor (Surovell & Stiner 2001; Weiner ' & Bar-Yosefa 1990; Chadefaux et al. 2009) and has shown that in grade IV osteoarthritic groups there is an increase in splitting factor vs grade I groups. This increase in the splitting factor suggests there is an increase in the average crystallite size (Zuo et al. 2016). The use of FTIR to determine the crystal properties using the splitting factor however gives the average of the crystals in all directions, and as such does not show when crystals are more resolved in a single direction. Therefore the use of X-ray diffraction alongside FTIR may provide the necessary sensitivity to assess the crystallite size. It has been reported that mineral

content between fracture and non-fracture groups is 5-10% higher in the fracture samples (Buckley et al. 2015), however the study showed a large overlap between the two groups and had very low sample numbers. A study by Greenwood et al. (2016) showed significant difference between the carbonate:phosphate ratio of age matched fracture and non-fracture groups. This was consistent with findings by Gadeleta et al. (2000) who found high carbonate: phosphate ratios in osteoporotic vs normal groups in both human and osteoporotic induced monkeys. Assessment of osteoporotic rat models by Raman spectroscopy have reported significant reduction in the mineral: matrix ratio ($p<0.005$) as well as an increase in the carbonate: phosphate ratio ($p<0.005$) (Orkoula et al. 2012). The same study also reported a significant increase in the 1/FWHM at 959cm^{-1} ($p<0.005$); these are reported in a rat model and have yet to be confirmed in comparative human investigations. A Raman study on human tissue reported results contradicting this showing that fracture groups were 5-10% more mineralised than non-fracture controls, however the study was limited by a relatively low sample number (n=10) (Buckley et al. 2015)

As well as investigation of individual parameters of bone chemistry, principal component analysis (PCA) has also been shown to distinguish between fracture and non-fracture groups by analysing XRD diffractograms (Dicken et al. 2016). It has also been reported that the application of PCA to Raman spectra in combination with linear discrimination analysis may contribute to *in vivo* differentiation between fracture and non-fracture groups (Buckley et al. 2015).

The present study will aim to fulfil three primary goals: (i) to report the physicochemical properties of human cancellous OP and OA bone assessed using nano-indentation, pXRD, FTIR and Raman spectroscopy and the impact of these parameters on the fracture toughness of the tissue, which has previously been reported (Cook & Zioupos 2009); (ii) to determine what physicochemical properties, if any, can be used in conjunction with the micro-architecture to produce predictive models of fracture toughness; and (iii) to determine if principal component analysis can be applied to Raman spectra and whether this is capable of differentiating fracture from non-fracture groups.

5.3 **Materials and Methods**

5.3.1 **Samples**

A sample set of femoral heads were collected from 37 osteoporotic (OP) and 8 osteoarthritic (OA) patients who had received a total hip replacement surgery due to having suffered fragility fractures at the femoral neck or elective reasons. Specialist surgeons were able to remove the femoral heads intact during the surgery. Population characteristics are provided in Table 4-1. Following removal all samples were kept at -20^{o}C prior to sample preparation. Ethical approval for the collection and use of these specimens was provided by Gloucestershire NHS trust REC (acknowledgments).

Table 5-1 Anthropometrical and demographic data of OP and OA groups

	OP	OA
Donors	37	8
Male/ Female	7 / 30	5/3
Number of specimens	60	19
Age range (yrs)	59 - 96	53-76
Age mean (yrs)	82.3 (SD=6.8)	66 (SD=7.3)
Weight range (kg)	41.3-82.6	68-108
Weight mean (kg)	64.2 (SD=10.5)	84.5 (SD=12.96)
Height range (m)	1.55-1.80	1.65-1.83
Height mean (m)	1.67 (SD=0.080)	1.76 (SD=0.074)

Male/Female differences have previously been explored using samples from this cohort (Greenwood et al. 2016). Therefore herein we will be considering all samples indiscriminately of gender.

In addition to the samples taken from the OP and OA patients there is also a subgroup of ‘normal’ or non-fracture samples taken from the greater trochanter. Whilst this is a different site to the OP and OA samples the results can be compared due to the systemic nature of OP (Huston et al. 2013), however the results should of course be taken lightly due to this limitation. These samples were only analysed using Raman spectroscopy in order to carry out PCA to distinguish between the non-fracture, OP and OA groups.

5.3.2 **Fracture toughness**

In a previous study the fracture toughness (K_C) of excised cancellous bone samples and their apparent density were determined *in vitro* (Cook & Zioupos 2009) and compared with patient QUS measurements in-vivo (Cook et al. 2010). 62 samples were taken from 37 osteoporotic and 13 osteoarthritic patients ranging from ages 59-96 years. The samples were taken from the centre of the femoral head and cut into disks conforming to ASTM standard E399-90 to be used in determining the plane-strain fracture toughness.

5.3.3 **Specimen preparation**

Specimen preparation (including sectioning from the femoral head and cleaning) has previously been described in detail (Cook and Zioupos, 2009; Cook et al., 2010). Single Edge Notched Disc Specimen samples (SEND) were prepared to conform to an adjusted ASTM standard E399-90 in order to assess the necessary stress conditions to instigate crack growth from a man-made notch. Samples were divided into two subsets; those cut orientated along (A_L) the primary direction of the trabecular and those orientated across (A_C) the primary orientation of the trabecular structure. This was done due the nature of cancellous bone being a cellular solid with a fibre-like orientation. Where possible the A_L and A_C samples were taken from each specimen. All specimens were stored at −20 °C following a defatting process detailed in (Cook and Zioupos, 2009; Cook et al., 2010). The sectioning was performed by using a metallurgical saw (Struers® Accutom-2), and samples were then sanded and polished by using progressively finer grades of carbide paper (400–2500 grit) to the dimensions required for material testing. Specimens were manufactured in the shape of discs, diameter 20mm and thickness 7.5mm, for mechanical material testing as SEND. Sample preparation was performed under constant water irrigation, to prevent the production of micro-cracks or other damage to the specimens. During all sample preparation care was taken to avoid any heating of the sample and to minimise contact with any solutions to prevent any impact of the preparation on the physicochemistry of the tissue.

Analysis by pXRD and IR required the samples to be powdered. The samples were powdered using zirconium crucibles in a Mill MM 200. The particulates produced from the milling process were sieved to <106µm. The powering process is carried out

over short intervals (1 min periods) to prevent any heating of samples to attempt to maintain the chemical and nano-structural nature of the bone.

5.3.4 **Micro-CT**

The samples' micro-architecture was imaged using micro-Computed Tomography (µ-CT). Each sample was imaged using a Nikon CT H225 (X-Tek Systems Ltd, Tring, Hertfordshire, UK) cone beam µ-CT (µ-CBCT) scanner. Samples were imaged at 50kV and 65µA with a 1000ms exposure. The resultant voxel size of the scan was ~25µm. All scans were manually reconstructed using CT Pro 3D. During reconstruction conditions were optimised to reduce beam hardening, and the noise and beam hardening corrections were standardised across all the samples to ensure the results were comparable. Image analysis and visualisation were carried out using VG Studio Max 2.2 (Volume Graphics GmbH, Heidelberg, Germany). Firstly the samples structural properties were determined, and these parameters included; trabecular thickness (TbTh), spacing (TbSp) and number (TbN), surface area (BS), material volume (BV) and total volume (TV). The imaging and analysis process was informed by chapters 2-4.

5.3.5 **Nano-indentation**

Nano-indentations were performed on both the SEND and cortical samples. In the case of the SEND samples 40-80 indentations were carried out per sample with half the indentations being carried out transversely on the trabeculae and half in the longitudinal on the trabeculae. The cortical samples were indented at the previously determined locations measured in the results from µ-CT, with 20 indentations per 100x100µm site. All indentations were carried out using a CSM-Nano Hardness tester. Testing was load controlled to 10mN with a linear loading rate and unloading rate of 30s and a 30 second pause.

5.3.6 **X-Ray Diffraction**

The powdered cancellous bone specimens were individually loaded into a pXRD sample holder with a glass spacer. pXRD analysis was carried out using a PANalytical X'Pert PRO Multi-Purpose Diffractometer with Cu Kα radiation. Data was collected across an angular range of 15–80 2θ (°) (5.90–1.20 Å) using a PIXcel strip detector at a

coutn rate of /~1s. (Greenwood et al. 2016). Data was also collected for two further stepped scans under the sample conditions but across an angular range of 23–27 2θ (°) (3.86–3.30 Å d-spacing) and 50–55 2θ (°) (1.82–1.67 Å d-spacing), and with a count time at each step equivalent to ~3 s. The two additional stepped scans were collected to provide greater quality data for the 002 and 004 Bragg maxima respectively, from this data the full width at half maximum (FWHM) of the 002 and 004 Bragg maxima(Greenwood et al. 2016). The FWHM values were then used to calculate coherence length using the Scherrer equation (Equation 5-1). Bruker Topas software (Version 4.1, 2008) was employed to undertake profile fitting of each diffraction profile. This provided quantitative crystallite size and morphology parameters through calculation of the coherence length and structural parameters of the crystal lattice through the lattice parameters. Coherence length was calculated for three orthogonal crystallographic directions, ⟨00ℓ⟩, ⟨hk0⟩ and ⟨0k0⟩ using the Scherrer equation, which uses the instrument corrected, full width at half maximum of the desired peak (Greenwood et al. 2016). The lattice parameters were calculated from whole pattern fitting refinement of diffraction profiles to obtain the 2θ peak positions (Greenwood et al. 2016).

$$\boldsymbol{\tau = \frac{K\lambda}{\beta cos\theta}} \qquad \text{Equation 5-1}$$

The Scherrer equation is shown in Equation 5-1 where τ is the mean coherence length often referenced to as crystallite size, K is a dimensionless shape factor, λ is the x-ray wave length, β is the line broadening at half the maximum intensity of the selected peak (FWHM), and θ is the Bragg angle.

5.3.7 **Infrared Spectroscopy**

FTIR analysis was carried out using an attenuated total reflectance (ATR)–FTIR which reduces the potential for contamination by removing the need to extensive sample preparation. Approximately 3 mg of homogenised bone powder (~106 μm particle size) was used for analysis. FTIR spectra were collected using a Bruker Alpha Platinum ATR and analysis carried out using PerkinElmer Spectrum software. A scan resolution of 4 cm^{-1} was used and 16 scans were employed for data collection, within a range of 2500– 400 cm^{-1}. FTIR analysis was employed to provide semi-quantitative

data on the organic and carbonate content in the specimens. The mineral: organic ratio was assessed through measuring the area of the v3 phosphate (1200–900 cm^{-1}) and the amide I (1750–1600 cm^{-1}) bands (Greenwood et al. 2016). The carbonate: phosphate ratio was assessed through measuring the area of the v2 carbonate (890–850 cm^{-1}) and v3 phosphate band (1200–900 cm^{-1}). Carbonate type A (1450)/type B (1409) ratio was assessed using the base line method (Baxter et al. 1966; Collares et al. 2014). The splitting factor was measured using the 567 and 605 peaks (Weiner ’ & Bar-Yosefa 1990; Surovell & Stiner 2001; Beckett 2009; Chadefaux et al. 2009).

5.3.8 **Raman Spectroscopy**

Raman spectra were measured on a previously described bespoke transmission Raman (TRS) instrument (Vardaki et al. 2015), where the Raman illumination zone and collection zone are on the opposite sides of the sample. Transmission Raman measurements provide a signal which comprises of all constituents present within the sample. A laser with an 830 nm excitation wavelength was used (Innovative Photonic Solutions: I0830MM0350MF-EM), and the laser beam was filtered using two 830 nm laser line filters (Semrock) to provide a spectrally clean laser profile. The resulting laser power at the sample surface was around ~400 mW. All Raman spectra were collected using an Andor iDus 420 deep depletion CCD, which was coupled to a Kaiser spectrometer (Holospec 1.8i) with an f-number of 1.8. Each sample was measured for 12× 5s acquisitions in three separate positions. All Raman spectra were processed using Matlab 2014a, and for ratio metric analysis spectra were averaged to each positional measurement, thereby providing three Raman spectra per sample. Data was also baseline corrected using a previously described method (Eilers 2003; Eilers & Boelens 2005) and intensity normalised.

For the construction of the principal component analysis linear discriminant analysis (PCA-LDA) classification model, the only pre-processing step was data normalisation. PCA-LDA is a dimensionality reduction technique that aims to find patterns in a dataset with minimal loss of information. Only principal component scores above a critical value of 0.01, which were determined by Analysis of Variance (ANOVA) (Otto 2007), were used in the linear discrimination model for pathology

classification. The classification model was validated using leave one sample out cross validation.

5.3.9 **Statistical analysis**

Statistical analysis was carried out in two steps. Firstly the relationships between the various subgroups that exist within the sample group were determined through a comparison of the properties between the groups loaded in the A_L and A_C configurations previously mentioned, and a comparison of the OP and OA groups. The relationships of these subgroups in relation to the measured Kc were then carried out. Pearson's correlation coefficients were used throughout the study. In addition to investigating the correlations present within the dataset, multiple linear regression was also employed in order to further the statistical models developed in previous works that have considered the structural properties of osteoporotic and osteoarthritic bone and the impact of various micro-structural parameters on fracture toughness (Chapter 4)

5.4 **Results**

5.4.1 **Parameterised**

Table 5-2 Mean values (bold) and standard deviations for the material parameters obtained from nano-indentation, ATR-FTIR, pXRD, and Raman spectroscopy for the entire cohort and A_L and A_C separation.

.	Both		A_L		A_C		Technique
Parameter	Mean	Std. Dev.	Mean	Std. Dev.	Mean	Std. Dev.	
Vickers Hardness	**50.10**	7.29	**50.90**	8.05	**49.47**	6.71	Nano-indentation
Modulus	**14.50**	1.82	**15.04**	2.09	**13.89**	1.32	
Splitting Factor	**3.26**	0.049	**3.26**	0.042	**3.27**	0.038	ATR-FTIR
Phosphate: Amide I	**7.41**	0.599	**7.37**	0.52	**7.46**	0.64	
Carbonate v2: Phosphate	**0.028**	0.002	**0.028**	0.002	**0.028**	0.002	
Carbonate A v3:Phosphate	**0.00038**	0.00017	**0.00039**	0.00015	**0.00037**	0.00021	
Carbonate B	**0.048**	0.004	**0.048**	0.004	**0.048**	0.003	

v3:Phosphate							
Carbonate A:B	**2.46**	0.33	**2.44**	0.31	**2.51**	0.37	
CL_{002}(nm)	**23.00**	1.08	**22.85**	1.07	**23.27**	1.08	XRD
CL_{030}(nm)	**8.22**	0.39	**8.12**	0.38	**8.35**	0.38	
CL_{210}(nm)	**10.25**	0.96	**10.22**	0.92	**10.33**	1.03	
LP 'a' axis (Å)	**9.408**	0.004	**9.408**	0.004	**9.408**	0.004	
LP 'c' axis (Å)	**6.902**	0.003	**6.902**	0.003	**6.902**	0.003	
Carbonate: Phosphate	**0.198**	0.012	**0.197**	0.014	**0.200**	0.010	Raman Spectroscopy
Hydroxy Apatite: Protein	**11.02**	1.50	**11.11**	1.41	**10.80**	1.64	
1/Width	**0.051**	0.001	**0.051**	0.001	**0.051**	0.001	

This study reports on how the material quality of osteoporotic and osteoarthritic cancellous bone impacts upon its measured plane strain fracture toughness. In a previous study correlations between micro-architecture have been investigated which will help to further provide an understanding of how structural parameters correlate with bone quality (Chapter 4). Additionally in this work statistical models were developed to provide a basis for the prediction of bone fracture toughness, and the inclusion of bone quality in these micro-architectural models will help develop them further. The average parameterised values of the material properties determined by nano-indentation, ATR-FTIR, pXRD and Raman spectroscopy are presented in Table 5-2.

Table 5-3 R^2 (Bold) p-values for Nano-indentation vs Fracture Toughness for both groups and an A_L and A_C separation

	All		A_L		A_C	
Parameter	R^2_{adj}	P-Value	R^2_{adj}	P-Value	R^2_{adj}	P-Value
Hardness	**0.192**	0.001	**0.207**	0.011	**0.227**	0.019
Modulus	**0.065**	0.056	**0.078**	0.135	**0.030**	0.418

Table 5-3 shows the results from nano-indentation, the hardness across the entire cohort and with the A_L and A_C separation all had weak but significant correlations with Kc (p=0.001, p=0.011, p=0.019), whereas, surprisingly, the indentation modulus did not

(p>0.05). Table 5-4 shows the results of ATR-FTIR, the splitting factor as well as Amide I: Phosphate (organic: mineral) ratio, which were not found to correlate significantly with fracture toughness in either of the groups. All measures of carbonate: phosphate ratios (v2, type A v2, and type B v2) were found to correlate significantly with fracture toughness across all groups. The highest correlation in the data collected from ATR-FTIR was found in the carbonate v2 type A: B ratio (R2=0.386, p<0.001). A comparison of ATR-FTIR with previously reported micro-architecture (Chapter 4) showed that with an increase in carbonate v2: phosphate ratio BV/TV increased significantly (R2= 0.180, p=0.001) whilst the Carbonate v3 type A/type B ratio was found to decrease with BV/TV (R2=0.368, p<0.001). The material density was also found to increase with Carbonate v2: Phosphate ratio (R2=0.079, p=0.034).

Table 5-4 R^2 (Bold) and p-values for ATR-FTIR vs Fracture Toughness for both groups and an A_L and A_C separation

	All		A_L		A_C	
Parameter	R^2_{adj}	P-Value	R^2_{adj}	P-Value	R^2_{adj}	P-Value
Splitting Factor	**0.000**	0.89	**0.007**	0.655	**0.030**	0.439
Amide I: Phosphate	**0.062**	0.059	**0.080**	0.131	**0.091**	0.151
Carbonate v2: Phosphate	**0.118**	0.008	**0.150**	0.034	**0.258**	0.011
Carbonate A v3: Phosphate	**0.339**	<0.001	**0.420**	<0.001	**0.350**	0.003
Carbonate B v3: Phosphate	**0.092**	0.023	**0.231**	0.007	**0.001**	0.879
Carbonate v3 A:B	**0.386**	<0.001	**0.450**	<0.001	**0.506**	<0.001

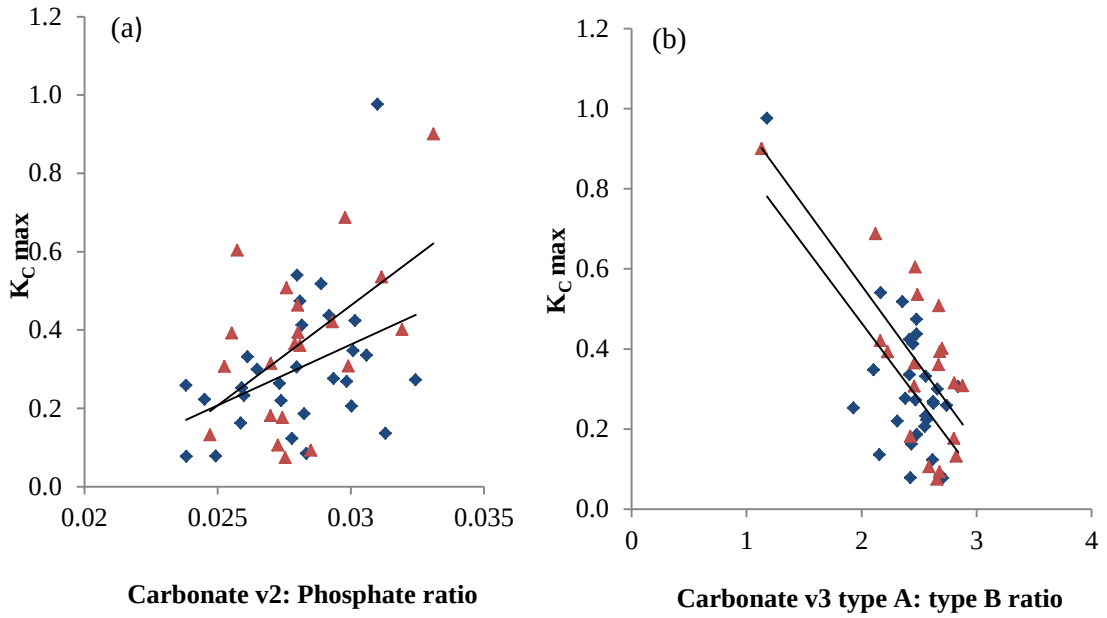

Figure 5-1 Relationships between ATR-FTIR parameters and facture toughness (a): Carbonate v2: Phosphate ratio vs K_C max, (b): Carbonate v3 type A/ type B ratio vs K_c max with the A_L (diamonds) and A_C (triangle) groups separated

Table 5-5 R^2 (Bold) and p-values for pXRD vs Fracture Toughness for both groups and an A_L and A_C separation

	All		A_L		A_C	
Parameter	R^2_{adj}	P-Value	R^2_{adj}	P-Value	R^2_{adj}	P-Value
CL_{002}	**0.107**	0.011	**0.088**	0.106	**0.097**	0.138
CL_{030}	**0.048**	0.097	**0.007**	0.653	**0.097**	0.139
CL_{210}	**0.077**	0.565	**0.001**	0.887	**0.059**	0.253
LP 'a'	**0.073**	0.049	**0.000**	0.973	**0.011**	0.658
LP 'c'	**0.001**	0.804	**0.270**	<0.004	**0.005**	0.762

Measurements taken in the $CL_{00\ell}$ were found to correlate poorly yet significantly across the entire cohort (R^2=0.107, p=0.011), however the correlations were not seen to be significant in the A_L, A_C separation (Table 5-5). No other correlations were found

between pXRD data and fracture toughness. Table 5-5 shows the parameterised data collected using Raman spectroscopy. Significant correlations were found between the carbonate:phosphate ratio and fracture toughness which was consistent with the results from ATR-FTIR (Table 5-4). The hydroxyl apatite: protein ratio was also found to correlate significantly with fracture toughness (Table 5-6).

Table 5-6 Raman Spectroscopy vs Fracture Toughness for both groups and an AL and AC separation

	All		A_L		A_C	
Parameter	R^2	P-Value	R^2	P-Value	R^2	P-Value
Carbonate: Phosphate	**0.260**	<0.001	**0.263**	0.003	**0.345**	0.003
Hydroxy Apatite: Protein	**0.381**	<0.001	**0.313**	0.001	**0.419**	0.001
1/Width	**0.070**	0.600	**0.052**	0.216	**0.082**	0.176

5.4.2 **Parameterised Stepwise Selection**

In addition to observing the correlations between the parameters reported here and the previously reported fracture toughness and architectural parameters (Cook & Zioupos 2009, Chapter 4), the parameters were also included in statistical models to further the prediction of fracture. Multiple stepwise regressions were carried out using an alpha of 0.05, and the resultant correlations are reported in Table 5-7. Implementing multiple regression across the entire cohort found the highest R^2 (with all predictors being significant) included BV/TV and Hydroxyl Apatite: Protein Ratio (measured by Raman). In the A_L group, contrary to previous models where no architectural parameter improved the R^2 over BV/TV alone (chapter 4), the inclusion of Hydroxyl Apatite: Protein Ratio (measured by Raman), <004> CL and 'a' axis LP measured by XRD resulted in a significant improvement over BV/TV alone. In the A_C group it was found that the addition of 'c' axis LP produced the best fit.

Table 5-7 stepwise regression steps for the entire cohort using BV/TV as the base predictor with the addition of Hydroxy apatite: protein ratio measured by Raman spectroscopy (Alpha to add 0.05), the addition of Raman Spectroscopy increases the adjusted R^2 value from 75.51 to 81.72Figure 5-4

	Step	
	1	**2**
Constant	-0.1984	**0.3060**
BV/TV	2.36	**1.98**
T-Value	12.20	**10.32**
P-Value	<0.001	**<0.001**
Hydroxy-Apatite: Protein		**-0.0380**
T-Value		**-4.12**
P-Value		**<0.001**
S	0.0981	**0.848**
R^2	76.02	**82.48**
R^2 (adjusted)	75.51	**81.72**

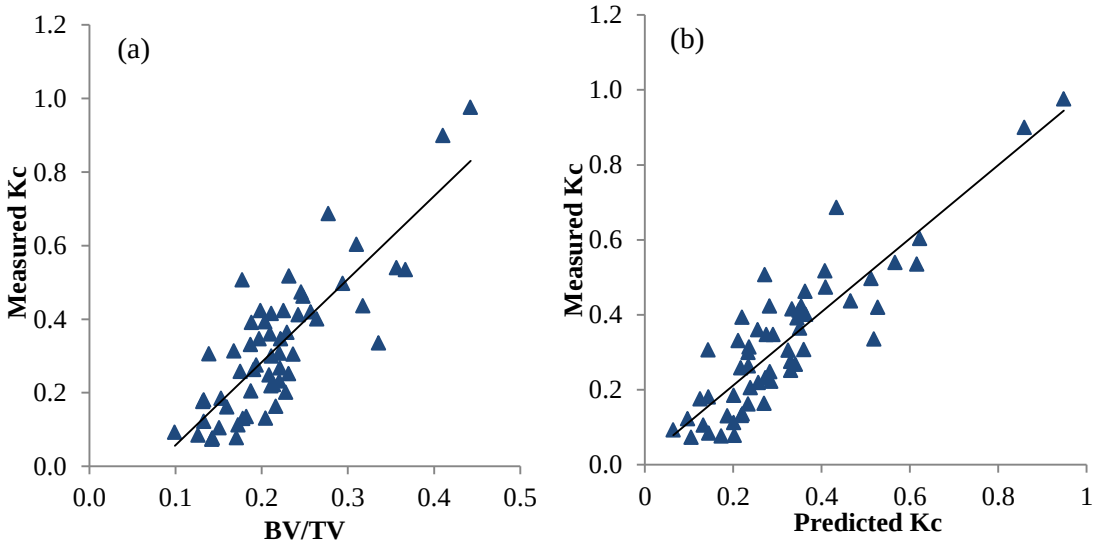

Figure 5-2 (a) BV/TV vs measure Kc for the entire cohort, (b)Predicted vs measured Kc for the entire cohort using BV/TV as the base predictor with the addition of Hydroxy apatite: protein ratio measured by Raman spectroscopy

Table 5-8 stepwise regression steps for the A_L group using BV/TV as the base predictor with the addition of Hydroxy apatite: protein ratio measured by Raman spectroscopy, coherence length <004> and LP 'a' measure by XRD (Alpha to add 0.05), the inclusion of additional parameters increases the adjusted R^2 value from 75.46 to 89.54

	Step			
	1	2	3	4
Constant	-0.2063	0.3995	-0.4486	**-81.7675**
BV/TV	2.29	1.94	1.98	**1.94**
T-Value	9.17	9.07	10.16	**10.80**
P-Value	<0.001	<0.001	<0.001	**<0.001**
Hydroxy-Apatite: Protein		-0.0472	-0.0467	**-0.0436**
T-Value		-4.18	-4.55	**-4.58**
P-Value		<0.001	<0.001	**<0.001**
CL_{00l}			0.044	**0.054**
T-Value			2.50	**3.22**
P-Value			0.020	**0.004**
LP 'a'				**8.6**
T-Value				**2.35**
P-Value				**0.028**
S	0.0938	0.0734	0.0668	**0.0613**
R^2	76.37	86.08	88.96	**91.09**
R^2 (adjusted)	75.46	84.97	87.57	**89.54**

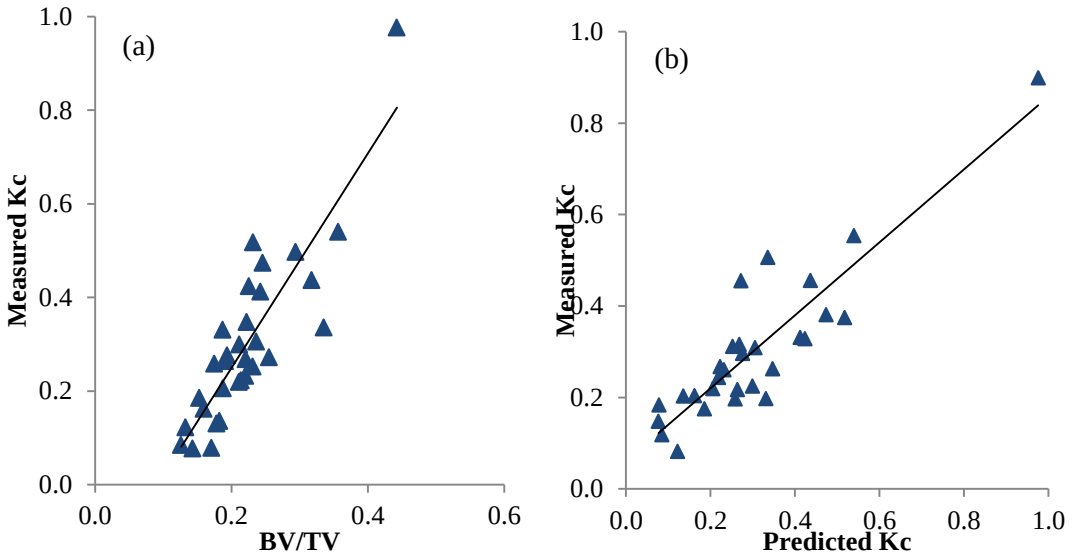

Figure 5-3 (a) BV/TV vs measure Kc for the A_L group, (b) Predicted vs measured Kc for the A_L subgroup using BV/TV as the base predictor with the addition of Hydroxy apatite: protein ratio measured by Raman spectroscopy, <004> CL and 'a' axis LP as measured by XRD

Table 5-9 stepwise regression steps for the A_C group using BV/TV as the base predictor with the addition of LP 'c' measure by XRD (Alpha to add 0.05), the inclusion of additional parameters increases the adjusted R2 value from 81.97 to 85.46

	Step	
	1	**2**
Constant	-0.1492	**-97.4657**
BV/TV	2.37	**2.42**
T-Value	8.85	**10.03**
P-Value	<0.001	**<0.001**
LP 'c'		**14.1**
T-Value		**2.20**
P-Value		**0.044**
S	0.0911	**0.0818**
R^2	83.03	**87.17**
R^2 (adjusted)	81.97	**85.46**

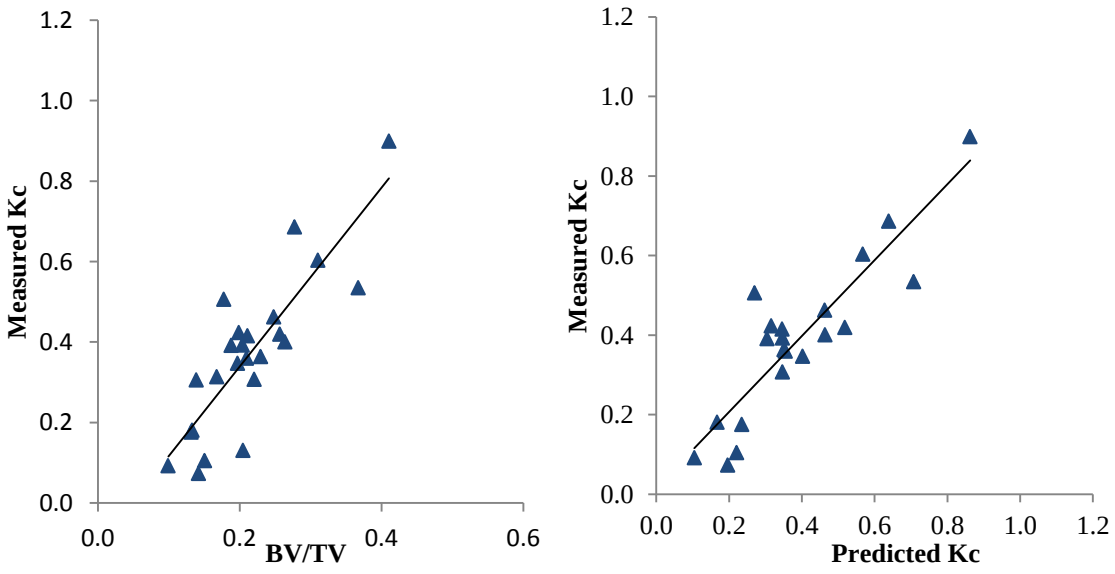

Figure 5-4 (a) BV/TV vs measure Kc for the A_C group, (b) Predicted vs measured Kc for the A_C subgroup using BV/TV as the base predictor with the addition of 'c' axis LP as measured by XRD

By employing PCA on the Raman spectra it was possible to distinguish between the osteoporotic, osteoarthritic and normal samples by considering the LD1 and LD2 separation (Figure 5-5). This shows a clear grouping of all three different groups suggesting that it may be possible to distinguish patients at risks of osteoporotic and osteoarthritic fracture from typically 'normal' or non-fracture groups.

5.4.3 **Principal Component Analysis**

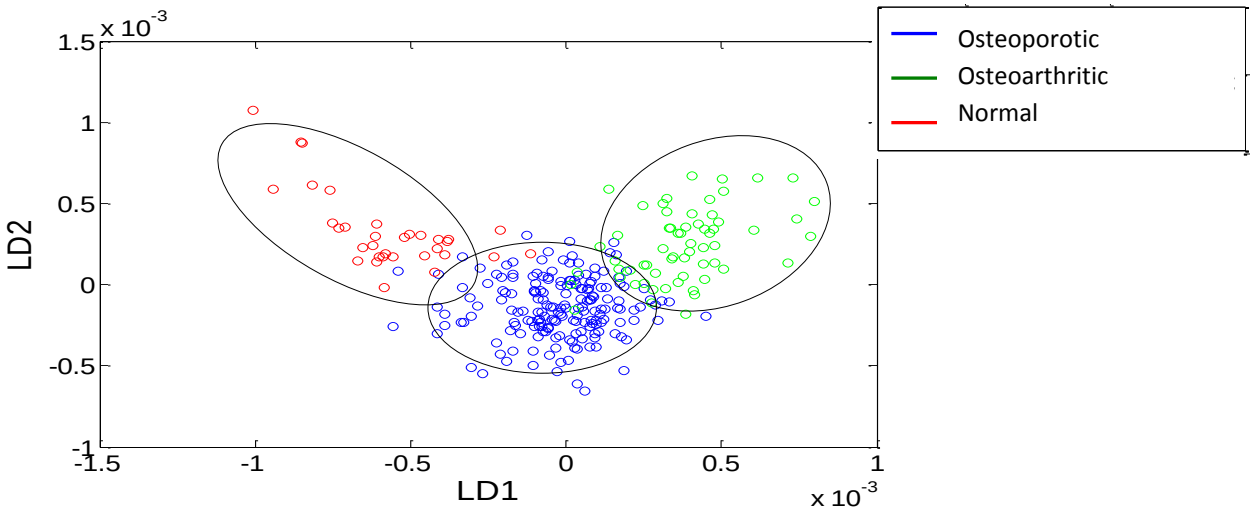

Figure 5-5 results of principal component analysis using data obtained from Raman spectroscopy showing grouping of the 3 groups included in the study

5.5 **Discussion**

The assessment of bone quality as well as quantity is important in the understanding and subsequent diagnosis of disease. Therefore *ex vivo* investigations into the chemistry of the tissue and their impact on the mechanical competency of the tissue are invaluable. Unlike many previous studies we have chosen to investigate primarily the impact of the chemical composition on the measured fracture toughness (Cook & Zioupos 2009) rather than biomarker differences between fracture and non-fracture groups (Buckley et al. 2015; Dicken et al. 2016; Greenwood et al. 2016). Developing this understanding of the different measurable contributors to the fracture toughness of the tissue could be more beneficial to predicting a patient's fracture risk and treatment as it can provide a better understanding of the tissue. It is important to note that the relationships and models developed here have been investigated within OP and OA bone and may not be applicable to normal bone, which can be exceptionally difficult to obtain. The non-fracture samples used in this study were not of suitable size to be accurately fracture toughness tested and as such a comparison of fracture toughness was not possible.

The hydroxyapatite:protein ratio, measured by Raman spectroscopy, showed a negative correlation with fracture toughness suggesting that an increase in the amount of

organic component of the tissue leads to an increase in the fracture toughness, which supports previous hypothesis by Zioupos et al. (1999). This is however not supported by the results from ATR-FTIR, which was unable to detect significant changes in the respective ratios. This highlights the importance of assessing the individual parameters with multiple techniques as they may produce access the same properties differently. In this case without further information we cannot determine which method is providing the correct result. The differences seen between the techniques may have also been caused by the different preparation of the samples for each analysis; for Raman spectroscopy the samples were analysis unmolested following the fracture toughness testing, whilst the use of ATR-FTIR required that the samples be powdered for analysis.
.

The results of the PCA must be considered with reasonable scepticism for comparison of the OA and OP with the normal tissue due to the different location from which the samples were obtained; greater trochanter versus the femoral head. The comparison of the OA and OP groups are however site matched and displayed a clear difference between the two groups. Due to the possibility of intra patient variations this may be the source of the apparent differences, however given the generally accepted systemic nature of osteoporosis the authors would expect the result to hold true for site matched samples, as was shown in the comparison of OA and OP groups (Huston et al. 2013).

5.5.1 **Nano-Indentation**

No correlations were found in the assessment of the modulus of the tissue by nano-indentations, which was unexpected as the fracture toughness of the tissue would depend to some extent on the elastic response of the tissue. However as highlighted the commonly assessed elastic response of the tissue (Reilly et al. 1974; Gibson 1985; Turner et al. 1999), is inferior to the assessment of the fracture toughness (Yan et al. 2007; Cook & Zioupos 2009). Additionally nano-indentation only considers a relatively small region of the sample and as such any potential relationships might not be observed as the other techniques used consider a significantly larger amount of the sample. The significant ($p<0.001$) negative correlation that was found between the

hardness and the fracture toughness is indicative of an increase in tissue stiffness leading to a greater vulnerability to fracture.

5.5.2 **XRD**

Coherence length values for the $CL_{00\ell}$ were found to be lower than in a previous study (Greenwood et al. 2016). The lattice parameters reported for the 'a' axis were consistent with those previously reported, whilst the 'c' axis values are notably higher (Meneghini et al. 2003; Greenwood et al. 2016). This difference could be due to the use of silicon being used as an internal standard in the study by Greenwood et al. (2016). A weak positive correlation was found in the $CL_{00\ell}$ when both the A_L and A_C groups were combined, which would suggest an increase in $CL_{00\ell}$ leads to an increase in fracture toughness. However when the groups were separated the correlations were weaker and no longer significant. This is surprising as typically in the A_L/A_C separated groups any correlations have been shown to become stronger as the two groups are in different loading orientations (chapter 4), which indicates that the micro-architectural properties of the tissue are having a far greater impact on the tissue than the coherence length. The same can be said of the 'a' axis LP which showed a significant correlation in the entire cohort that was not present in the A_L/A_C subgroups. Despite this not being apparent in the sub groups it is consistent with a previous study that showed a difference in the 'a' axis LP between fracture and non-fracture groups (Greenwood et al. 2016). The 'c' axis LP showed a significant negative correlation in the A_L sub group. No other correlations were found between measurements of $CL_{<hkl>}$ and fracture toughness. The lack of correlations found in the sub groups between the fracture toughness and the coherence lengths and lattice parameters measured by XRD suggests that the micro-architecture and other chemical properties of the bone have a greater impact on the fracture toughness than the mineral quality.

5.5.3 **FTIR**

Assessment of the material characteristics of the tissue by FTIR showed that an increase in the carbonate v2: phosphate ratio had a significant positive correlation with fracture toughness. This suggests that an increase in the number of substitutions in the lattice and subsequently an increase in disorder leads to higher fracture toughness. This is contrary to previous work that showed an increase in carbonate *v2*: phosphate ratio in

a fracture vs non-fracture groups analysis (Greenwood et al. 2016). The strong negative correlation found in the carbonate *v3* type A: type B ratio has not previously been reported and suggests that the reduction in fracture toughness is coupled with a shift from more type A substitutions to more type B. The quantity of type A has previously been found to correlate positively with crystal thickness (Camacho et al. 1999) suggesting that the fracture toughness may be decreasing with crystal size. No correlations with amide I: phosphate (mineral content) were observed; this is surprising because of changes typically reported between fracture and non-fracture groups (Buckley et al. 2015). The collagen is assumed to be responsible for resistance to fracture whilst mineral is assumed to be responsible for stiffness (Zioupos et al. 1999) therefore it would be expected that differences in collagen/mineral ratio would be seen to impact fracture toughness. This might not have been observed because in the ATR-FTIR data collection only a small amount of sample was analysed so the relationship might be apparent if the entire sample were to be analysed. However this is not possible because the sample would not be recoverable following the analysis.

5.5.4 **Raman Spectroscopy**

In the parameterised results from Raman spectroscopy the carbonate: phosphate ratio was found to correlate significantly and positively with fracture toughness. This is consistent with the results from FTIR and enforces the result that an increase in the number of carbonate substitutions leads to an increase in the fracture toughness of cancellous tissue, which is contrary to what one would typically expect. The negative correlation found between the hydroxy apatite: protein ratio shows that with a decrease in the relative amount of organic tissue in the bone the fracture toughness is reduced, which is expected according to Zioupos et al. (1999).

By correlating the pathology type with the spectra in PCA-LDA we were able to achieve a reasonable separation of the data. This separation was able to group the OA, OP and non-fracture groups. This shows that the use of PCA on Raman spectra is able to group fracture and non-fracture groups which could, with further work, prove to be applicable in a clinical setting and could contribute towards determination of a patient's fracture risk. Additionally PCA is able to consider the spectra irrespective of what data is being considered, and therefore presents the opportunity to combine the spectra and

diffractograms from Raman spectroscopy and XRD, which has previously shown differences between fracture and non-fracture groups (Dicken et al. 2016). This would perhaps improve the separation of fracture and non-fracture groups which with further research could help assess if a patient is osteoporotic or at a higher risk of osteoporosis.

5.5.5 **Multiple Regressions**

The results of Stepwise regression analysis suggest that different chemical characteristics of the tissue contribute to the resistance to fracture in different directions. They also strengthen the argument for the development of *in vivo* measurements of bone chemistry by XRD and Raman spectroscopy, as in conjunction with micro-architectural data an estimation of the fracture toughness of cancellous bone tissue can be achieved. As with previous work multiple Stepwise regression has been applied (Chapter 4) using the parameters that were found to individually correlate significantly with fracture toughness. These results showed that by taking the quantity (BV/TV) of bone as a base and considering multiple physicochemical parameters it is possible to produce highly correlated models to predict fracture toughness. This provides a potential basis for the development of *in vivo* models which could potentially be used with state of the art CT imaging and *in vivo* Raman spectroscopy and XRD to predict fracture toughness. The implementation of a combination of such results could be used in conjunction with DEXA to produce highly accurate prediction or replace the use of DEXA entirely. Whilst high for a human bone collection using multiple regressions on what is statistically a low sample number can be questioned as it falls outside the typical rule of ten. It has however been suggested that the rule is an unnecessary precaution as work by Austin & Steyerberg (2015) showed that linear regression models require only two subjects per variable to be accurate for the adequate estimation of adjusted regression coefficients and confidence intervals.

5.6 **Conclusion**

There were three principle aims of this study (i) to investigate the impact of bone chemistry and material properties at the sub-microscale on the fracture toughness of diseased cancellous bone tissue. The results showed that increases in the carbonate *v3* type A and carbonate *v2* correlated with a decrease in fracture toughness suggesting that

the crystals become thinner and more resolved with reduced fracture toughness. Additionally an increase in the mineral: organic ratio was seen to lead to a decrease in fracture toughness when assessed by Raman. (ii) To determine if the measured chemical parameters can be used in conjunction with micro-architecture to produce predictive models of Kc. The results showed by using BV/TV as a base and adding the mineral: organic ratio assessed by Raman spectroscopy can help improve the prediction of fracture toughness. Additionally in the A_L and A_C subgroups the addition of parameters assessed by XRD can further improve regression based predictive models. (iii) To determine if principal component analysis can be applied to Raman spectra in order to differentiate fracture from non-fracture groups. The results suggested a clear separation between the osteoarthritic and osteoporotic groups as well as separation between both diseased groups and the non-fractured control group.

5.7 **Acknowledgments**

The tests were carried out in the Biomechanics and Analytical laboratories of the Cranfield Forensic Institute of Cranfield University in Shrivenham, UK. Raman Spectroscopy was carried out on a bespoke system operated by Dr Benjamin Gardner at Institute of Physics and Engineering in Medicine, Exeter University, UK. Additionally we would like to acknowledge the support provided by the UK Department of Transport under the BOSCOS (Bone Scanning for Occupant Safety) project for which the human material was obtained in the Gloucester and Cheltenham NHS Trust hospitals under ethical consent (BOSCOS—Mr. Curwen CI REC ref. 01/179G).

5.8 **Reference**

Austin, P.C. & Steyerberg, E.W., 2015. The number of subjects per variable required in linear regression analyses. *Journal of Clinical Epidemiology*, 68(6), pp.627–636.

Baxter, J.D., Biltz, R.M. & Pellegrino, E.D., 1966. The physical state of bone carbonate. A comparative infra-red study in several mineralized tissues. *The Yale journal of biology and medicine*, 38(5), pp.456–70.

Beckett, S., 2009. 'Inter-Species Variation in Bone Mineral Cranfield Defence and Security Cranfield Defence and Security Inter-Species Variation in Bone Mineral'. PhD, Cranfield University, Shrivenham

van den Bergh, J.P.W. et al., 2010. Assessment of Individual Fracture Risk: FRAX and Beyond. *Current Osteoporosis Reports*, 8(3), pp.131–137.

Boivin, G. et al., 2008. The role of mineralization and organic matrix in the microhardness of bone tissue from controls and osteoporotic patients. *Bone*, 43(3), pp.532–538.

Boskey, A.L. et al., 2005. Comparison of mineral quality and quantity in iliac crest biopsies from high- and low-turnover osteoporosis: an FT-IR microspectroscopic investigation. *Osteoporosis International*, 16(12), pp.2031–2038.

Buckley, K. et al., 2015. Towards the in vivo prediction of fragility fractures with Raman spectroscopy. *Journal of Raman Spectroscopy*, 46(7), pp.610–618.

Camacho, N.. et al., 1999. Complementary information on bone ultrastructure from scanning small angle X-ray scattering and Fourier-transform infrared microspectroscopy. *Bone*, 25(3), pp.287–293.

Chadefaux, C. et al., 2009. Curve-fitting micro-atr-ftir studies of the amide i and ii bands of type i collagen in archaeological bone materials. *Oa Lib journal*, pp.129–137.

Chevalier, Y. et al., 2007. Validation of a voxel-based FE method for prediction of the uniaxial apparent modulus of human trabecular bone using macroscopic mechanical tests and nanoindentation. *Journal of biomechanics*, 40(15), pp.3333–40.

Collares, F.M. et al., 2014. Discrepancies in degree of conversion measurements by FTIR. *Brazilian Oral Research*, 28(1), pp.9–15.

Cook, R.B. et al., 2010. Fracture toughness and compressive properties of cancellous bone at the head of the femur and relationships to non-invasive skeletal assessment measurements. *Medical engineering & physics*, 32(9), pp.991–7.

Cook, R.B. & Zioupos, P., 2009. The fracture toughness of cancellous bone. *Journal of biomechanics*, 42(13), pp.2054–60

Currey, J.D., 2002. Bones: Structure and Mechanics, Princeton University Press.

Dall'Ara, E. et al., 2013. Tissue properties of the human vertebral body sub-structures evaluated by means of microindentation. *Journal of the mechanical behavior of biomedical materials*, 25, pp.23–32.

Dall 'ara, E. et al., 2007. The effect of tissue condition and applied load on Vickers hardness of human trabecular bone. *Journal of Biomechanics*, 40, pp.3267–3270.

Dicken, A.J. et al., 2016. Classification of fracture and non-fracture groups by analysis of

coherent X-ray scatter. *Scientific Reports*, 6, p.29011.

Donnelly, E. et al., 2006. Effects of surface roughness and maximum load on the mechanical properties of cancellous bone measured by nanoindentation. *Journal of biomedical materials research. Part A*, 77(2), pp.426–35.

FRAX, *Fracture Risk Assessment Tool*. Available at: https://www.shef.ac.uk/FRAX/tool.jsp [Accessed May 2, 2017].

Gadeleta, S.. et al., 2000. A physical, chemical, and mechanical study of lumbar vertebrae from normal, ovariectomized, and nandrolone decanoate-treated cynomolgus monkeys (macaca fascicularis). *Bone*, 27(4), pp.541–550

Gamsjaeger, S. et al., 2014. Vibrational spectroscopic imaging for the evaluation of matrix and mineral chemistry. *Current osteoporosis reports*, 12(4), pp.454–64.

Gibson, L.J., 1985. The mechanical behaviour of cancellous bone. *Journal of Biomechanics*, 18(5), pp.317–328.

Greenwood, C. et al., 2015. The micro-architecture of human cancellous bone from fracture neck of femur patients in relation to the structural integrity and fracture toughness of the tissue. *Bone*, 3, pp.67–75.

Greenwood, C. et al., 2016. Towards new material biomarkers for fracture risk. *Bone*, 93, pp.55–63.

Hengsberger, S., Kulik, A. & Zysset, P., 2002. Nanoindentation discriminates the elastic properties of individual human bone lamellae under dry and physiological conditions. *Bone*, 30(1), pp.178–184.

Huston, R.L. et al., 2013. Is osteoporosis systemic? *Advances in Bioscience and Biotechnology*, 4(4), pp.531–538.

International Osteoporosis Foundation, 2015. Facts and Statistics | International Osteoporosis Foundation. *https://www.iofbonehealth.org/facts-statistics [Accessed January 18, 2017]*.

Isaksson, H. et al., 2010. Precision of nanoindentation protocols for measurement of viscoelasticity in cortical and trabecular bone. Journal of Biomechanics, 43(12), pp.2410–2417.

Kanis, J.A. et al., 2008. FRAXTM and the assessment of fracture probability in men and women from the UK. Osteoporosis International, 19(4), pp.385–397.

Kanis, J.A. et al., 1997. Osteoporosis International Position Paper Guidelines for Diagnosis and Management of Osteoporosis. Osteoporos Int, 7, pp.390–406.

Martin, R. B., & Burr, D.B., 1989. Structure function, and adaptation of compact bone. American Journal of Physical Anthropology, 82(1), pp.116–117.

Meneghini, C. et al., 2003. Rietveld refinement on x-ray diffraction patterns of bioapatite in human fetal bones. Biophysical journal, 84(3), pp.2021–9.

Milovanovic, P. et al., 2014. Nano-structural, compositional and micro-architectural signs of cortical bone fragility at the superolateral femoral neck in elderly hip fracture patients vs. healthy aged controls. Experimental Gerontology, 55, pp.19–28.

Orkoula, M.G., Vardaki, M.Z. & Kontoyannis, C.G., 2012. Study of bone matrix changes induced by osteoporosis in rat tibia using Raman spectroscopy. Vibrational Spectroscopy,

63, pp.404–408.

Reilly, D.T., Burstein, A.H. & Frankel, V.H., 1974. The elastic modulus for bone. Journal of Biomechanics, 7(3), pp.271–275.

Rho, J.-Y., Kuhn-Spearing, L. & Zioupos, P., 1998. Mechanical properties and the hierarchical structure of bone. Medical Engineering & Physics, 20(2), pp.92–102.

Rho, J.-Y., Tsui, T.Y. & Pharr, G.M., 1997. Elastic properties of human cortical and trabecular lamellar bone measured by nanoindentation. Biomaterials, 18(20), pp.1325–1330.

Rho, J.Y. et al., 2002. Microstructural elasticity and regional heterogeneity in human femoral bone of various ages examined by nano-indentation. Journal of biomechanics, 35(2), pp.189–98.

Shea, J.E. & Miller, S.C., 2005. Skeletal function and structure: implications for tissue-targeted therapeutics. Advanced drug delivery reviews, 57(7), pp.945–57.

Shepherd, T.N. et al., 2011. Direct comparison of nanoindentation and macroscopic measurements of bone viscoelasticity. Journal of the mechanical behavior of biomedical materials, 4(8), pp.2055–62.

Siris, E.S. et al., 2004. Bone Mineral Density Thresholds for Pharmacological Intervention to Prevent Fractures. Archives of Internal Medicine, 164(10), p.1108.

Society, national osteoporosis, 2016. NOS. Available at: https://nos.org.uk/about-nos/media-centre/ [Accessed February 14, 2017].

Summers, G.D., 2001. Osteoporosis in men. Radiography, 7(2), pp.119–123.

Surovell, T.A. & Stiner, M.C., 2001. Standardizing Infra-red Measures of Bone Mineral Crystallinity: an Experimental Approach. Journal of Archaeological Science, 28, pp.633–642.

Turner, C.H. et al., 1999. The elastic properties of trabecular and cortical bone tissues are similar: results from two microscopic measurement techniques. Journal of biomechanics, 32(4), pp.437–41.

Weiner ', S. & Bar-Yosefa, O., 1990. States of Preservation of Bones from Prehistoric Sites in the Near East: A Survey. Journal of Archaeological Science, 17, pp.187–196.

Wolfram, U., Wilke, H.-J. & Zysset, P.K., 2010. Rehydration of vertebral trabecular bone: influences on its anisotropy, its stiffness and the indentation work with a view to age, gender and vertebral level. Bone, 46(2), pp.348–54.

Yan, J., Mecholsky, J.J. & Clifton, K.B., 2007. How tough is bone? Application of elastic-plastic fracture mechanics to bone. Bone, 40(2), pp.479–84.

Zioupos, P., Cook, R. & Coats, A.M., 2008. Bone quality issues and matrix properties in OP cancellous bone. Studies in health technology and informatics, 133, pp.238–45.

Zioupos, P., Currey, J.D. & Hamer, A.J., 1999. The role of collagen in the declining mechanical properties of aging human cortical bone. Journal of biomedical materials research, 45(2), pp.108–16.

Zuo, Q. et al., 2016. Characterization of nano-structural and nano-mechanical properties of osteoarthritic subchondral bone. BMC Musculoskeletal Disorders, 17.

Zysset, P.K. et al., 1999. Elastic modulus and hardness of cortical and trabecular bone lamellae measured by nanoindentation in the human femur. Journal of Biomechanics, 32(10), pp.1005–1012.

6 Thermal Decomposition Analysis to Assess the Mechanical Competency of Cancellous Bone

Adams GJ[1], Cook RB[2], Zioupos P[1]

1 Cranfield Forensic Institute, Cranfield University, Defence Academy of the UK, Shrivenham, UK

2 nCATS, School of Engineering Science, University of Southampton, Southampton, UK

6.1 Abstract

The important role of collagen and its impact on the mechanical competency of bone tissue is forever becoming clearer and the effect of altered or compromised collagenous tissue has been shown to have detrimental effects on the bone tissue. We have previously investigated the mechanical properties (fracture toughness, apparent & material density) of human cancellous bone from the femoral head, and found that a reduction in the apparent density of the tissue leads to a reduced fracture toughness. In the present study these same samples are investigated by assessing the thermal decomposition of the tissue considering the endo- and exo-thermic events pertaining to the collagen. The results showed that consideration of the onset of the exothermic peak correlated significantly with the fracture toughness of the tissue ($p=0.041$, $R^2=0.10$). The correlation was weak but it is suggested the impact is over shadowed by the morphology and micro-architecture of the tissue. The apparent lack of significant correlations in the endothermic peaks was most likely caused by requirements of the preparation process.

Keywords: *osteoporosis, fracture toughness (FT), Differential Scanning Calorimetry (DSC)*

6.2 **Introduction**

The study of human bone and its mechanical competency is important in the understanding of bone disease and in the development of biomaterials. Osteoporosis is a bone degeneration disease that affects an estimated 200 million women worldwide (International Osteoporosis Foundation 2015). The disease is typically characterised by a significant drop in bone mass beyond the loss of mass that typically occurs with aging (J. A.Kanis et al. 1997).

Bone is formed of two components, the organic and inorganic, and because of this composite nature there are multiple factors that affect the various mechanical properties of the tissue, such as stiffness and fracture toughness. The organic portion of bone can be further divided into collagenous and non-collagenous proteins, both of which play a vital role in the structure and strength of bone (Zioupos et al. 1999). The collagen in the bone matrix accounts for 85-90% of bone bound protein in the body (Knott & Bailey 1998). Multiple types of collagen are found in the bone but the majority of the collagen is type I, and there are also small amounts of types III, V and VI (Bätge et al. 1992; Bailey et al. 1992; Bailey & Knott 1999; Viguet-Carrin et al. 2006). Collagen is formed of three polypeptide chains which form a triple helix (Viguet-Carrin et al. 2006). Collagen forms in helical structures called fibrils, which are characterised by a 67nm periodicity and 40nm gaps or holes between the ends of the molecules, and each molecule overlaps by 27nm. (Weiner & Traub 1992; J.-Y Rho et al. 1998; Viguet-Carrin et al. 2006). The rest of the proteins are non-collagenous proteins (NCPs) and are mainly involved in the chemical and biological process involved in bone metabolism and formation (J.-Y Rho et al. 1998). The initial formation of the fibrils is governed by immature, bivalent cross-links located near the ends of new collagen fibres. Over time mature covalent cross-links form providing interfibrillar linkage of collagen molecules, and this provides support and strength to the fibrils structure (Knott & Bailey 1998). Different cross-links exist between the collagen fibrils. Pyridinium and Deoxy-Pyridinium are cross-links found in bone collagen, Deoxy-Pyridinium is only found in bone collagen. These bonds help to increase stiffness and enhance the dissipation of energy (Fantner et al. 2005). Changes in the collagen with age have been linked to deterioration in the mechanical properties displayed by bone tissue (Zioupos et al. 1999; Very et al. 1997). Whilst they only make up ~10% of the organic matrix in bone, the

NPCs provide ‘sacrificial’ bonds that help provide stiffness and increase energy dissipation (Fantner et al. 2005).

Heating the collagen causes a transformation of the triple helix to an amorphous random structure (Flory & Garrett 1958). During this thermal decomposition the collagen undergoes the so-called collagen shrinkage, whereby collagen shrinks as it is slowly heated. This shrinkage behaviour is dependent on the overall conditions of the cross-links in the collagen network (Zioupos et al. 1999). The derivative of the gradients of the heat flow curves in cortical bone has been shown to correlate significantly with age.

As well as the organic component of bone there is an inorganic structure, calcium hydroxyapatite (HA). This crystallographic structure is the mineral in bone tissue; it is very stiff and provides rigidity to bone. It is brittle on its own and has very low toughness. This mineral is primarily responsible for the stiffness that bone provides (Zioupos et al. 1999). Bone mineral can be described as a poorly crystalline, nano-crystalline hydroxyapatite which contains contaminants and substitutions in the crystal lattice. These include; HPO_4, Na, Mg, citrate, carbonate and K (J. D. Baxter et al. 1966; J.-Y Rho et al. 1998; Shea & Miller 2005). A general chemical formula of HA is $Ca_{10}(PO_4)_6(OH)_2$, however this is an ideal formula that is never actually found (Rey et al. 2006), due to substitutions within the crystal lattice which can dramatically affect the chemical composition of the mineral (Beckett 2009).

As a composite the interactions between the collagen matrix and collagen are highly important in determining the resultant strength of bone tissue. If there are abnormalities within the structure of the collagen matrix during the mineralisation process of the collagen matrix in young bone, for example in the cross-linking profile leading to an irregular structure, this would inhibit the deposition of mineral in the regular sheets resulting in compromised mechanical properties (Landis 1995). The role of the collagenous portion of bone in the resistance to fracture is highly important and impacted significantly by the quantity and quality of cross-links. This quantity and quality will be manifested in the thermal response of the tissue (Lozano et al. 2003; Miculescu et al. 2011). In the thermal decomposition of bone tissue there a two primary events between 50 and 530^{o}C, firstly an endothermic event (50-90^{o}C) which represents the dehydration of the collagen, followed by an exothermic peak (200-530^{o}C) which

represents the degradation and combustion of the collagen. The full combustion of the organic component of bone is completed by 650^{o}C (Lozano et al. 2003; Miculescu et al. 2011; Etok et al. 2007).

This study will report the thermal decomposition of cancellous bone assessed by differential scanning calorimetry using samples taken from the femoral head of individuals who had been deemed to be osteoporotic and had suffered a hip fracture. The thermal decomposition will be weighed against the fracture toughness of the tissue, which has been previously reported by (Cook & Zioupos 2009).

6.3 **Materials and Methods**

6.3.1 **Bone Specimens**

A sample set of femoral heads were collected from 37 osteoporotic (OP) patients who had received a total hip replacement surgery due to having suffered fragility fractures at the femoral neck or elective reasons. Specialist surgeons were able to remove the femoral heads intact during the surgery. Population characteristics are provided in Table 4-1. Following removal all samples were kept at -20^{o}C prior to sample preparation. Ethical approval for the collection and use of these specimens was provided by Gloucestershire NHS trust REC (acknowledgments).

Table 6-1Anthropometrical and demographic data of OP samples

	OP
Donors	37
Male/ Female	7 / 30
Number of specimens	60
Age range (yrs)	59 - 96
Age mean (yrs)	82.3 (SD=6.8)
Weight range (kg)	41.3-82.6
Weight mean (kg)	64.2 (SD=10.5)
Height range (m)	1.55-1.80
Height mean (m)	1.67 (SD=0.08)

6.3.2 **Specimen preparation**

Specimen preparation (including sectioning from the femoral head and cleaning) has previously been described in detail (Cook and Zioupos, 2009; Cook et al., 2010). Single Edge Notched Disc Specimen (SEND) samples were prepared to conform to an adjusted ASTM standard E399-90 in order to assess the necessary stress conditions to instigate crack growth from a man-made notch. Samples were divided into two subsets; with samples orientated along (A_L) the primary direction of the trabecular and those orientated across (A_C) the primary orientation of the trabecular structure. This was due the nature of cancellous bone being a cellular solid with a fibre like orientation. Where possible both A_L and A_C samples were taken from each specimen. All specimens were stored at −20 °C following a defatting process detailed in (Cook and Zioupos, 2009; Cook et al., 2010). The sectioning was performed by using a metallurgical saw (Struers® Accutom-2), and they were then sanded and polished by using progressively finer grades of carbide paper (400–2500 grit) to the dimensions required for material testing. Specimens were manufactured in the shape of discs, diameter 20mm and thickness 7.5mm, for mechanical material testing as SEND. Sample preparation was performed under constant water irrigation, to prevent the production of micro-cracks or other damage to the specimens.

Analysis by DSC required the samples to be powdered, and as such it was required that the sample be in a dry state. The samples were powdered using zirconium crucibles in a Mill MM 200. The particulates produced from the milling process were sieved to <106µm. The powdering process is carried out over short bursts to prevent any heating of samples to attempt to maintain the chemical and Nano-structural nature of the bone.

6.3.3 **Mechanical testing**

In a previous study the fracture toughness (K_C) of excised cancellous bone samples and their apparent density were determined *in vitro* (Cook & Zioupos 2009) and compared with patient QUS measurements in-vivo (Cook et al. 2010). 62 samples were taken from 37 osteoporotic and 13 osteoarthritic patients ranging from ages 59-96 years. The samples were taken from the centre of the femoral head and cut into disks

conforming to ASTM standard E399-90 to be used in determining the plane-strain fracture toughness.

6.3.4 **Differential Scanning Calorimetry**

The DSC analysis was carried out using a DSC 1 Mettler-Toledo. Temperature range used was 25-550^{o}C, heated at a rate of 10^{o}C/min. The powdered bone specimens were weighed and loaded into a flat base aluminium pan, and an empty reference pan was used. The DSC equipment was calibrated with aluminium standard 40ul. Both the endo- and exo-thermic curves were assessed. Consideration was made of the curve integral, the onset, endset and peak position. All data obtained was normalised for the mass of the sample where appropriate. Additionally the gradients of the peaks were taken as recommended by Zioupos et al. (1999) (Figure 6-2). This has been shown, in cortical bone, to correlate significantly with the mechanical competency of the tissue.

6.3.5 **Multiple Regressions**

Statistical analysis was carried out in two steps. Firstly the relationships between the thermal decomposition characteristics measured in this study and the previous reported K_C values were determined (Cook & Zioupos 2009). The Pearson's correlation values are reported throughout the study. In addition to investigating the correlations present within the dataset, multiple linear regression was also employed to further the statistical models developed in previous works that have considered the structural properties of osteoporotic and osteoarthritic bone and the impact of various micro-structural parameters on fracture toughness (Chapter 4).

6.4 **Results**

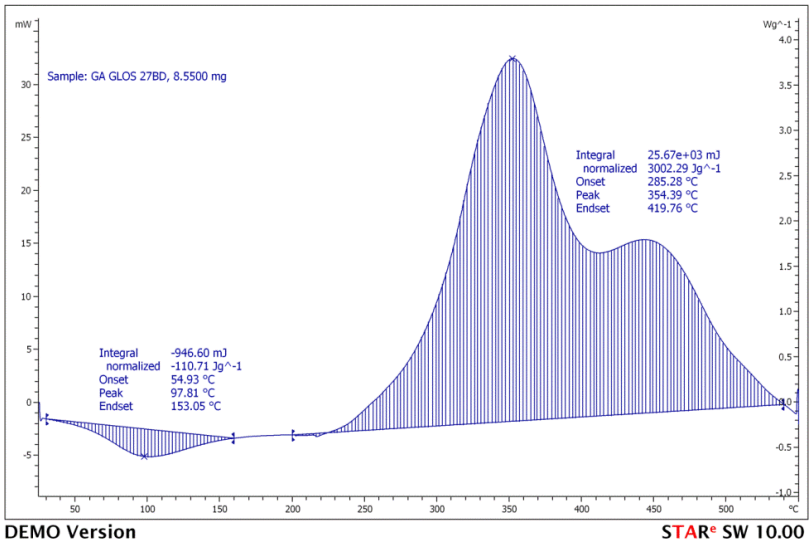

Figure 6-1 A typical output graph of difference in heat flow between the sample and the reference crucible over the entire temperature range

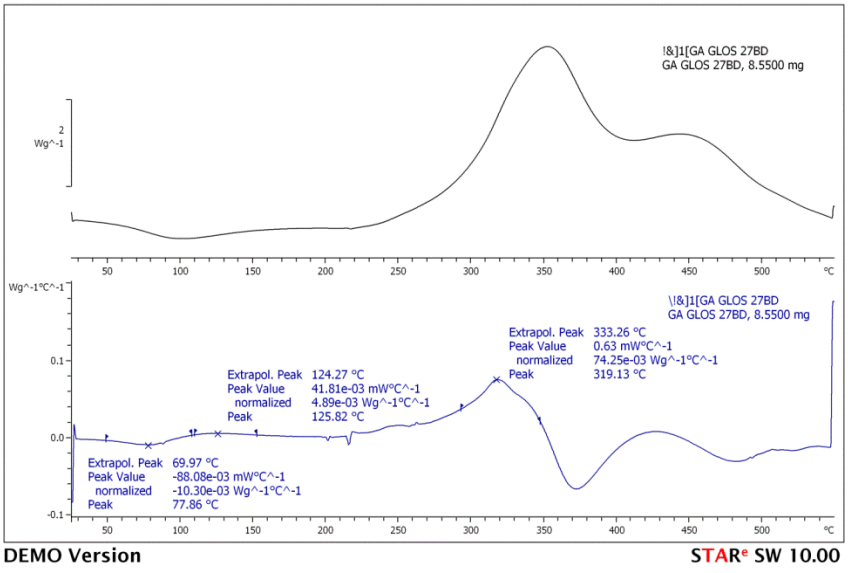

Figure 6-2 an example of how peak gradient values were obtained from the normalised heat flow plots

In DSC of bone there are three clear peaks (Figure 6-1); the first peak is endothermic and the subsequent two are exothermic. The average values for the normalised areas, onsets, peaks and endsets are shown in Table 6-2.

Table 6-2 Average values measured across the cohort with values for the Endothermic and Exothermic peaks

	Endothermic		Exothermic	
Parameter	Average Value	Standard Deviation	Average Value	Standard Deviation
Normalized integral (J/g)	-120.1	19.9	3126.3	273.2
Onset (^{o}C)	50.9	5.8	287.4	5.0
Endset (^{o}C)	141.7	15.0	420.7	14.3
Peak (^{o}C)	93.8	4.9	355.8	5.9

Table 6-2 shows the average values for the integral, onset, endset, and peaks values from the endothermic and exothermic peaks. The average exothermic value of the integral was notably lower than previous studies carried out on human skulls and radium (~8.4kJ/g) (Lozano et al. 2003).

6.4.1 **Endothermic**

The endothermic data is presented in Table 6-3. Across the entire cohort there was no correlation found between the peak statistics and the fracture toughness. It would be expected that the normalised integral might correlate positively with the fracture toughness. This is because it is expected that an increase in the quantity of collagen would lead to an increase in the resistance to fracture, which would correlate with the quantity of water in the tissue. The A_L and A_C loading configurations were also separated as this might have caused the correlation not to be apparent. The separation of the two groups showed higher R^2 values than with the groups combined, however none of the correlations were seen to be significant ($p<0.05$).

Table 6-3 The R2 (bold) and p-values for the correlations between the parameters measured in the endothermic peaks and the measured plane strain fracture toughness

	Both		A_L		A_C	
Parameter	R^2	p-value	R^2	p-value	R^2	p-value
Normalised Integral (J/g)	**0.001**	0.855	**0.094**	0.164	**0.034**	0.424
Onset (^oC)	**0.008**	0.560	**0.035**	0.407	**0.060**	0.285
Peak (^oC)	**0.016**	0.426	**0.024**	0.490	**0.067**	0.258
End set (^oC)	**0.001**	0.877	**0.052**	0.309	**0.090**	0.186

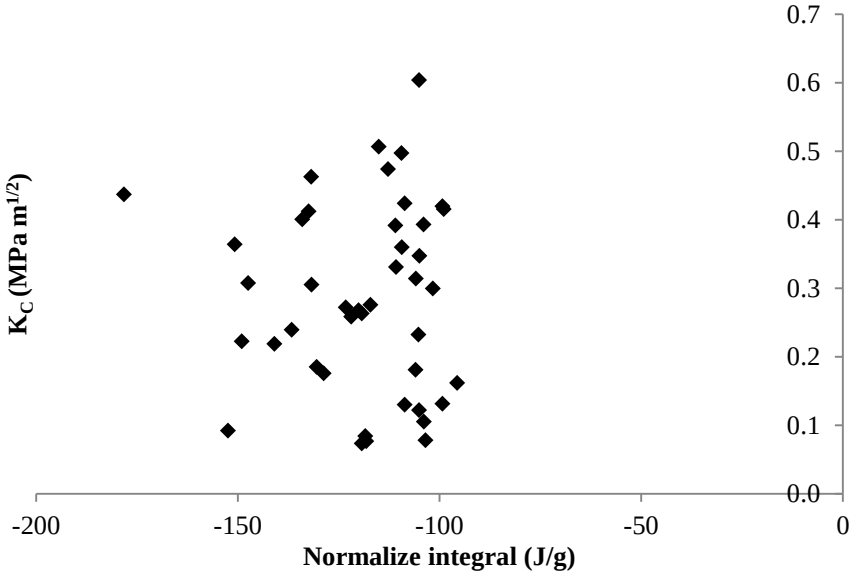

Figure 6-3 plot of the fracture toughness (Kc) vs the normalised integral for the Endothermic peak

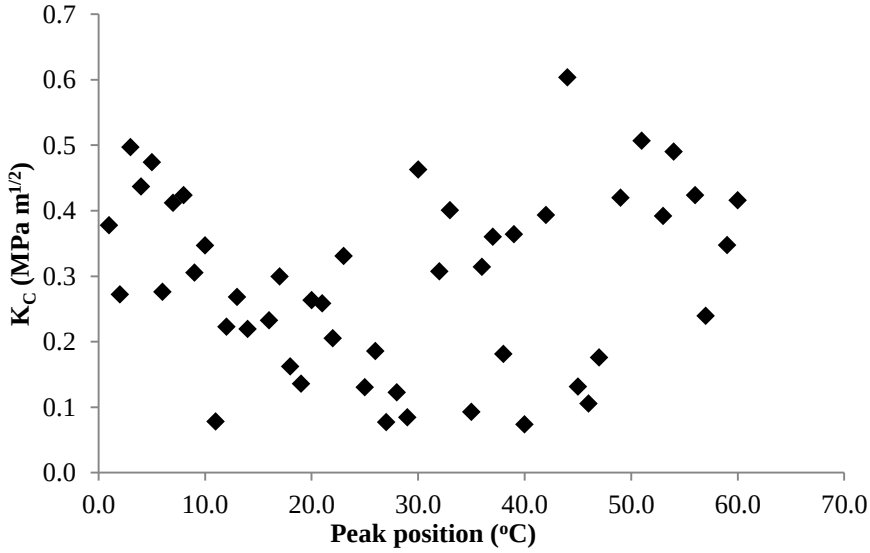

Figure 6-4 plot of fracture toughness (Kc) vs the peak position for the Endothermic peak

6.4.2 **Exothermic**

Table 6-4 The R2 (bold) and p-values for the correlations between the parameters measured in the exothermic peaks and the measured plane strain fracture toughness

	Both		A_L		A_C	
Parameter	R^2	p-value	R^2	p-value	R^2	p-value
Normalised Integral (J/g)	**0.100**	0.041	**0.052**	0.309	**0.090**	0.186
Onset (^oC)	**0.089**	0.052	**0.243**	0.020	**0.011**	0.657
Peak (^oC)	**0.098**	0.041	**0.079**	0.206	**0.076**	0.228
End set (^oC)	**0.033**	0.246	**0.032**	0.429	**0.015**	0.596

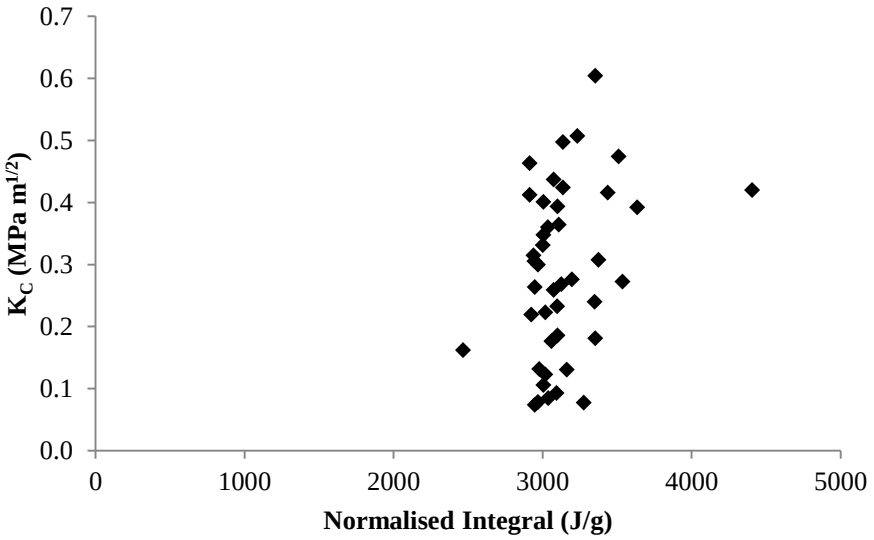

Figure 6-5 plot of fracture toughness (Kc) vs the normalised integral for the Exothermic peak

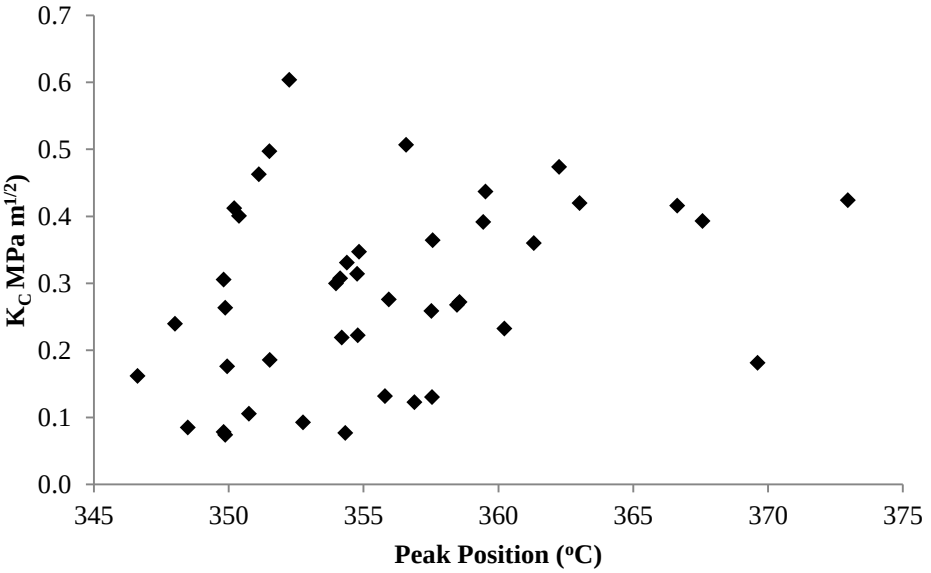

Figure 6-6 plot of fracture toughness (Kc) vs the peak position of the Exothermic peak

Table 6-5 The R2 (bold) and p-values for the correlations between the gradient derived peaks and the measured plane strain fracture toughness

	Both		A_L		A_C	
Parameter	R^2	p-value	R^2	p-value	R^2	p-value
1st Peak	**0.025**	0.304	**0.013**	0.612	**0.029**	0.462
2nd Peak	**0.001**	0.839	**0.000**	0.973	**0.006**	0.733
3rd Peak	**0.000**	0.899	**0.006**	0.734	**0.000**	0.926

Measurement of the exothermic peak showed that the normalised integral (p=0.041) (Figure 6-5) and the peak position (p=0.041) (Figure 6-6) correlated significantly with the fracture toughness, however the correlations were both seen to be weak, R^2=0.100 and R^2=0.098 respectively. This relationship is expected, as an increase in the quantity of collagen or number of cross-links in the organic matrix will increase the total energy available for the exothermic event. This relationship was only apparent when considering the entire cohort and did not persist in the A_C and A_L subgroups (Table 6-4). By separating the A_L and A_C subgroups one significant correlation was found between fracture toughness and the onset of the exothermic peak in the A_L subgroup only (R^2=0.243, p=0.020). By taking the gradient of the peaks as shown in Figure 6-2 and comparing the results with the fracture toughness (Cook & Zioupos 2009), no statistically significant correlations were found (Table 6-5). Measuring these peak gradients is however dependant on the collagen shrinkage and powdering the bone, due to the need for the cancellous tissue to be in a physiologically dry state.

6.4.3 **Multiple regressions**

The results of multiple Stepwise regressions are shown in Table 6-6. The results of multiple Stepwise regressions showed that only the addition of the exothermic onset position improved the prediction over the BV/TV alone. No other parameter was seen to improve the model significantly.

Table 6-6 multiple Stepwise regression steps using BV/TV as the base predictor with the addition of the Exothermic Onset position (Alpha to add 0.05)

	Step	
	1	2
Constant	-0.1517	2.0746
BV/TV	2.21	2.16
T-Value	7.79	8.24
P-Value	<0.001	<0.001
Exothermic Onset		-0.0077
T-Value		-2.74
P-Value		<0.001
S	0.0889	0.0823
R^2	60.89	67.33
R^2 (adjusted)	59.88	65.61

6.5 **Discussion**

Understanding the factors that affect the mechanical competency of human bone is important in the understanding and diagnosis of diseases. A number of studies have investigated the micro-structural characteristics of cancellous bone (Gibson 1985; Brown & Ferguson 1980; J.-Y Rho et al. 1993; J.-Y Rho et al. 1998; J.-Y Rho et al. 1997), however these studies fail to consider the ability of the bone to resist fracture which is a potentially more important consideration (Cook & Zioupos 2009; P Zioupos et al. 2008). The fracture properties of cancellous bone have previously been studied and it was shown that the fracture toughness is heavily correlated with the density of cancellous tissue. This measured density is a function of the quantity and quality of the cancellous tissue (Cook & Zioupos 2009). The work has been built on further by other studies (Greenwood et al. 2016, Chapter 4) where it was shown that the structural properties independent of the chemistry can account for the majority of cancellous bone toughness. Further work then showed that the chemical properties of the tissue can account for some of the resistance to fracture not accounted for by the micro-structure alone (Greenwood et al. 2016, Chapter 5). This however still does not fully explain the contributions to the measured fracture toughness. In a previous study (Zioupos et al. 1999) showed that the thermal decomposition in cortical bone tissue could be used to

inform the mechanical properties of the tissue, and was more successful and accurate than other chemical analytical techniques. It was therefore suggested that consideration of this thermal degradation of the tissue could help further inform on the factors affecting the fracture toughness.

Multiple studies have shown that osteoporosis leads to the deterioration of the mechanical properties and chemical components of bone tissue (Vanderschueren et al. 2000; Bono & Einhorn 2003; Boskey et al. 2005; Croucher et al. 1994; Boskey 1990; Saito & Marumo 2010; Cook et al. 2010; P Zioupos et al. 2008; Greenwood et al. 2015; Greenwood et al. 2016). This deterioration is in addition to typical age related changes that occur in the bone (Wall et al. 1979; Zioupos et al. 1999; P Zioupos et al. 2008). The organic portion of bone is generally considered to be primarily responsible for the ability of the bone to resist fracture (Zioupos et al. 1999). The organic portion of bone is formed from collagen and NCPs, and the collagen in bone acts as the matrix in the collagen: mineral composite. In the thermal decomposition of bone, collagen is first dehydrated then combusted. The dehydration event is represented in the first endothermic peak (Lozano et al. 2003). The combustion of the organic component is seen in the second peak of the DSC plot (Miculescu et al. 2011; Lozano et al. 2003). Whilst in this study temperatures were not high enough to allow investigation of the mineral, which requires temperature between 800-1200^{o}C (Miculescu et al. 2011), the interaction between the organic and mineral will impact upon the denaturation of the organic.

The samples required powdering before being analysed to ensure that any structural components of the tissue would not impact the heat flow curves. This however did require that the samples were dry. This will have impacted upon the first endothermic peak and may be responsible for the lack of correlation found between the peak and the fracture toughness. There is also the possibility that the milling process in powdering may have introduced heat during the process which may have impacted the results; however every effort was made to ensure that the milling container was not heated during the process. As previously mentioned the heat range used in this study was unable to quantify the thermal decomposition of the mineral portion of the tissue, so this has not been accounted for in the study. There is very little to no analysis of the thermal decomposition of human cancellous tissue with respect to its mechanical properties and

no comparison offered to the fracture toughness of the tissue. The results of this study have shown onsets, endsets and peak values in similar locations to those previously reported (Etok et al. 2007; Lozano et al. 2003). Another limitation of the powdering of cancellous bone is that it does not allow for the quantification of the shrinkage of the collagen with increase in heat which has been shown in cancellous bone to correlate with the age of the tissue (Zioupos et al. 1999). This could perhaps be possible if a single trabecular strut could be isolated.

6.6 **Conclusion**

The application of Differential Scanning Calorimetry to assess cancellous bone is limited by the need to homogenise the bone tissue by powdering, which requires the bone to be dry and limits the ability of DSC to measure changes in the endothermic region of the thermal decomposition of the tissue. With this limitation in mind there was no measureable correlation present in the endothermic event of the analysis with toughness. The exothermic peak on the other hand displayed weak, significant correlations with fracture toughness, most notably in the area of the peak suggesting that there is either a great amount of collagen in the tissue or a greater number of cross-links, which contribute to increased toughness. These correlations were however weak and provided no additional information, that is not obtainable through non-destructive means. With the powdering limitation in mind it is suggested that isolation of single trabeculae may prove to be more useful and will allow the measurement of the thermal shrinkage of the tissue. The results here have shown that for the assessment of cancellous bone, Differential Scanning Calorimetry is not able to provide any further information beyond that which is already provided by non-destructive techniques.

6.7 **References**

Bailey, A.J. et al., 1992. Post-translational modifications in the collagen of human osteoporotic femoral head. Biochemical and biophysical research communications, 185(3), pp.801–5.

Bailey, A.J. & Knott, L., 1999. Molecular changes in bone collagen in osteoporosis and osteoarthritis in the elderly. Experimental gerontology, 34(3), pp.337–51.

BÄTGE, B. et al., 1992. Compositional analysis of the collagenous bone matrix. A study on adult normal and osteopenic bone tissue. European Journal of Clinical Investigation, 22(12), pp.805–812.

Baxter, J.D., Biltz, R.M. & Pellegrino, E.D., 1966. The physical state of bone carbonate. A comparative infra-red study in several mineralized tissues. The Yale journal of biology and medicine, 38(5), pp.456–70.

Beckett, S., 2009. Inter-Species Variation in Bone Mineral Cranfield Defence and Security Cranfield Defence and Security Inter-Species Variation in Bone Mineral. Cranfield uniersity.

Bono, C.M. & Einhorn, T.A., 2003. Overview of osteoporosis: pathophysiology and determinants of bone strength. European Spine Journal, 12(2), pp.S90–S96.

Bono, C.M. & Einhorn, T.A., 2003. Overview of osteoporosis: pathophysiology and determinants of bone strength. European spine journal : official publication of the European Spine Society, the European Spinal Deformity Society, and the European Section of the Cervical Spine Research Society, 12 Suppl 2, pp.S90-6.

Boskey, A.L., 1990. Bone mineral and matrix. Are they altered in osteoporosis? Orthopedic Clinics of North America, 21(1), pp.19–29.

Boskey, A.L. et al., 2005. Comparison of mineral quality and quantity in iliac crest biopsies from high- and low-turnover osteoporosis: an FT-IR microspectroscopic investigation. Osteoporosis International, 16(12), pp.2031–2038.

Brown, T.D. & Ferguson, a B., 1980. Mechanical property distributions in the cancellous bone of the human proximal femur. Acta orthopaedica Scandinavica, 51(3), pp.429–37.

Cook, R.B. et al., 2010. Fracture toughness and compressive properties of cancellous bone at the head of the femur and relationships to non-invasive skeletal assessment measurements. Medical engineering & physics, 32(9), pp.991–7.

Cook, R.B. & Zioupos, P., 2009. The fracture toughness of cancellous bone. Journal of biomechanics, 42(13), pp.2054–60.

Croucher, P.I., Garrahan, N.J. & Compston, J.E., 1994. Structural mechanisms of trabecular bone loss in primary osteoporosis: specific disease mechanism or early ageing? Bone and Mineral, 25(2), pp.111–121.

Etok, S.E. et al., 2007. Structural and chemical changes of thermally treated bone apatite. Journal of Materials Science, 42(23), pp.9807–9816.

Fantner, G.E. et al., 2005. Sacrificial bonds and hidden length dissipate energy as mineralized fibrils separate during bone fracture. Nature materials, 4(8), pp.612–6.

Flory, P.J. & Garrett, R.R., 1958. Phase Transitions in Collagen and Gelatin Systems 1. Journal

of the American Chemical Society, 80(18), pp.4836–4845.

Gibson, L.J., 1985. The mechanical behaviour of cancellous bone. Journal of Biomechanics, 18(5), pp.317–328.

Greenwood, C. et al., 2015. The micro-architecture of human cancellous bone from fracture neck of femur patients in relation to the structural integrity and fracture toughness of the tissue. BONR, 3, pp.67–75.

Greenwood, C. et al., 2016. Towards new material biomarkers for fracture risk. Bone, 93, pp.55–63.

International Osteoporosis Foundation, 2015. Facts and Statistics | International Osteoporosis Foundation. Available at: https://www.iofbonehealth.org/facts-statistics [Accessed January 18, 2017].

Kanis, J.A. et al., 1997. Osteoporosis International Position Paper Guidelines for Diagnosis and Management of Osteoporosis. *Osteoporosis International* , 7, pp.390–406.

Knott, L. et al., 1995. Biochemical changes in the collagenous matrix of osteoporotic avian bone. *The Biochemical journal*, 310 (Pt 3, pp.1045–51.

Knott, L. & Bailey, A.J., 1998. Collagen cross-links in mineralizing tissues: a review of their chemistry, function, and clinical relevance. Bone, 22(3), pp.181–7.

Landis, W.J., 1995. The strength of a calcified tissue depends in part on the molecular structure and organization of its constituent mineral crystals in their organic matrix. *Bone*, 16(5), pp.533–44

Lozano, L.F. et al., 2003. Thermal analysis study of human bone. *Journal of Materials Science*, 38(23), pp.4777–4782.

Miculescu, F. et al., 2011. Complex Analysis on Heat Treated Human Compact Bones. *University Politehnica of Bucharest, Scientific Bulletin, Seria B, Chemisty and Materials Science*, 73(4).

Rey, C. et al., 2006. Physico-chemical properties of nanocrystalline apatites: Implications for biominerals and biomaterials. *Materials Science and Engineering: C, 27(2) pp.198-205*

Rho, J.-Y., Kuhn-Spearing, L. & Zioupos, P., 1998. Mechanical properties and the hierarchical structure of bone. *Medical Engineering & Physics*, 20(2), pp.92–102.

Rho, J.-Y., Tsui, T.Y. & Pharr, G.M., 1997. Elastic properties of human cortical and trabecular lamellar bone measured by nanoindentation. *Biomaterials*, 18(20), pp.1325–1330.

Rho, J.Y., Ashman, R.B. & Turner, C.H., 1993. Young's modulus of trabecular and cortical bone material: Ultrasonic and microtensile measurements. *Journal of Biomechanics*, 26(2), pp.111–119.

Saito, M. & Marumo, K., 2010. Collagen cross-links as a determinant of bone quality: a possible explanation for bone fragility in aging, osteoporosis, and diabetes mellitus. *Osteoporosis international* 21(2), pp.195–214.

Shea, J.E. & Miller, S.C., 2005. Skeletal function and structure: implications for tissue-targeted therapeutics. *Advanced drug delivery reviews*, 57(7), pp.945–57.

Vanderschueren, D., Boonen, S. & Bouillon, R., 2000. Osteoporosis and osteoporotic fractures in men: a clinical perspective. *Baillière's best practice & research. Clinical endocrinology & metabolism*, 14(2), pp.299–315.

Very, J.M. et al., 1997. Effect of aging on the amide group of bone matrix, measured by FTIR spectrophotometry, in adult subjects deceased as a result of violent death. *Calcified tissue international*, 60(3), pp.271–5.

Viguet-Carrin, S., Garnero, P. & Delmas, P.D., 2006. The role of collagen in bone strength. *Osteoporosis international*, 17(3), pp.319–36.

Wall, J.C., Chatterji, S.K. & Jeffery, J.W., 1979. Age-related changes in the density and tensile strength of human femoral cortical bone. *Calcified Tissue International*, 27(1), pp.105–108.

Weiner, S. & Traub, W., 1992. Bone structure: from angstroms to microns. *the Federation of American Societies for Experimental Biology Journal*, 6(3), pp.879–85.

Zioupos, P., Cook, R. & Coats, A.M., 2008. Bone quality issues and matrix properties in OP cancellous bone. *Studies in health technology and informatics*, 133, pp.238–45.

Zioupos, P., Currey, J.D. & Hamer, A.J., 1999. The role of collagen in the declining mechanical properties of aging human cortical bone. *Journal of biomedical materials research*, 45(2), pp.108–16.

7 Micro-CT Values versus Nano-Indentation for the Prediction of Micro Material Properties of Cortical Bone

Adams GJ[1], Cook RB[2], Zioupos P[1]
1 Biomechanics Labs, Cranfield forensic Institute, DA of the UK, Shrivenham SN6 8LA, UK
2 nCATS, School of Engineering Science, University of Southampton, Southampton, UK

7.1 Abstract

When investigating bone diseases, fractures and treatments, determination of the mechanical properties of bone is of great clinical and biological importance. With advancements in state of the art medical imaging and Finite Element (FE) modelling we are approaching patient specific FE based fracture risk analysis. Before this can be achieved, fundamental relationships between voxel based imaging, computed tomography (CT), and material properties of bone must be established. Assessment of the material properties of bone by nano-indentation and μCT to be used in FE simulations has previously been performed using the average material modulus. This can be taken a step further by determining the material properties of each voxel based in relation to its density. Five samples were taken from six different animals covering a range of mineral contents: Mesoplodon densirostris rostrum, tympanic bulla of a whale, bovine femur, elephant tusk dentine and deer antler. Nano-indentations were performed using a CSM-Nano Hardness Tester. The density of the samples was determined using a QRM-MicroCT-HA calibration phantom. Large variations were found between the density and hardness of the samples, which cover most naturally occurring physiological ranges of bone density. They also show that there is a large intra-sample variability suggesting voxel-hardness measurements will provide a more accurate correlation between density and hardness. Analysis of a voxel by voxel hardness rather than average sample hardness could prove to be useful in development of FE models. Development of such FE models could lead to the more frequent use of patient specific analysis and yield more accurate fracture risk prediction. Although human tissue was not part of this analysis, human bone sits nicely in the middle of this very broad range of mineralisation states and therefore it is also covered by this approach.

Keywords: *computed tomography (CT), Nano-indentation, material model*

7.2 **Introduction**

Bone is a natural composite formed of hard and brittle hydroxyapatite reinforced with collagen fibres (Currey 2002). The quality, quantity and interactions of these two components fundamentally determine the mechanical characteristics of bone at the material level (Saito & Marumo 2010; Seeman & Delmas 2006; Greenwood et al. 2016; P Zioupos et al. 2008). At the micro tissue level bone is formed of collagen fibrils reinforced with plates of hydroxyapatite intrafibrillarly. At this level the bone tissue is by weight ~65% mineral, 20-25% collagen (mainly type I), 10% water and <1% non-collagenous proteins (Currey 2002). Small variations in both the concentration of these different components and the chemical continuance lead to differences in the material density of the bone tissue. These differences in structure may explain some of the variations experienced between bones in the human body but also differences between locations on the same bone and in bone diseases. This makes the chemical and structural nature of bone of great interest when treating patients suffering from bone diseases that cause bones to be structurally compromised, such as osteoporosis. Osteoporosis is the most common metabolic bone disorder, and affects 1 in 3 women and 1 in 5 men around the world according to the international Osteoporosis Foundation (International Osteoporosis Foundation 2015). The disease is characterised by low bone mass at the organic level and a deterioration of bone tissue. This compromising of the bone at the structural and tissue level leads to an increase in fracture risk.

At the micro-structural level bone can be separated into two parts; the dense cortical bone and the cellular cancellous bone that is formed of trabecular struts. There are conflicting reports on the material properties of these two tissue types with results from Zysset et al. (1999) suggesting that cancellous bone has a lower modulus than cortical regions, however they do recognise potential reasons for this measured disparity. Work by Dall'ara et al. (2013) showed an overlap in indentation modulus within the cortical and cancellous structures of a vertebral body. This work also addressed the reasons suggested for the differences reported by Zysset et al. (1999). The hardness of bone tissue has been shown to be highly dependent on the degree of mineralisation of the tissue (Boivin et al. 2008). Using the evidence available it is likely that the two forms of bone micro-structure are not fundamentally different and

differences in modulus are most likely due to changes in the degree of mineralisation which will manifest itself in the measured material density (Zioupos et al. 2008). The material density has been shown to be lower in the intermediate cancellous regions of bone, most likely due to higher turnover rates which may be the cause of previously reported differences (Zysset et al. 1999; Zioupos et al. 2008).

Over the last decade or so there have been significant steps made towards developing patient specific Finite Element (FE) models to predict the likelihood of fracture under certain conditions (Niebur et al. 2000; Chevalier et al. 2007; Zysset et al. 2013;Vilayphiou et al. 2015). With advancements in state of the art medical imaging and FE modelling we have been getting ever closer to this goal. Before this can be achieved fundamental relationships between voxel based imaging, μ-Computed Tomography (μ-CT), and material properties of bone must be established. Assessment of the material properties of bone by Nano-indentation and μCT to be used in FE simulations has previously been performed using the average material modulus (Chevalier et al. 2007). This can be taken a step further by determining the material properties of each voxel based in relation to its density. The study described herein reports the density-indentation relationships across a very wide range of bone densities and suggests possible relationships that may be employed in FE simulations to more accurately simulate the stiffness of bone tissue.

7.3 **Materials and Methods**

Cortical bone samples were taken from seven different species covering a wide range of mineral contents; Mesoplodon densirostris rostrum, tympanic bulla of a whale, Dugong, elephant tusk dentine, Bovine femur and Red deer antler.

7.3.1 **Specimen preparation**

Nano-indentation required the samples to be mounted in resin so that the indentation surface could be ground and polished flat and fully supported during indentations. The back portion of the SEND samples was removed using a diamond cutter and mounted in epoxy resin, and the samples were also mounted in epoxy resin. The resin was left to cure for 48 hours before being ground to a flat surface then polished using 0.3μm polishing solution.

7.3.2 **Imaging-μCT**

All samples were imaged using a cone beam μCT scanner, XTEK CT H 225 at 50 kV, 65 μA with a 500ms exposure time. The resultant voxel size was ~16 μm. All image data was manually reconstructed using CT Pro 3D. With CT Pro the beam hardening and noise reduction filters were applied to provide an optimal image, and this image setting was then standardised across the data set to ensure the data collected was comparable.

7.3.3 **Image Analysis**

Image analysis was carried out using VG Studio Max 2.2. Regions of interest (ROI) were taken from the centre of each sample ~9 mm^3 to exclude any external surfaces from the scan. A surface determination was performed using the grey level of an internal void as the background and the largest void-less section of bone, as per the manufacturer's recommendations. After the surface determination an automatic morphometric report was exported which contained; BV/TV, specific surface, mean trabecular thickness, mean trabecular number, and mean trabecular spacing.

From the histogram the mean, mode, minimum and maximum grey level were recorded to be used in calculation of the material density. A QRM-MicroCT-HA calibration phantom was scanned and reconstructed under the same conditions in order to determine D_{mat}. Determination of material density is more favourable than deriving Hounsfield units (HU) in this context as HU provides a relative density based on the attenuation coefficients of the material that cannot be measured by traditional densitometry. However density as a mass per unit volume can easily be compared with physical densitometry techniques.

7.3.4 **Density Calibration**

A QRM HA calibration phantom was used to determine the material density; this uses hydroxyapatite of different known concentrations. The phantom was imaged under the same conditions then manually reconstructed to the same beam hardening and noise reduction settings. The individual densities of hydroxyapatite are isolated and the average grey values are used to produce a calibration curve.

7.3.5 **Nano-Indentation**

Nano-indentations were performed on both the SEND and cortical samples. In the case of the SEND samples 40-80 indentations were carried out per sample with half the indentations being carried out transversely on the trabeculae and half in the longitudinal on the trabeculae. The cortical samples were indented at the previously determined locations measured in the results from μ-CT, with 20 indentations per 100x100μm site. All indentations were carried out using a CSM-Nano Hardness tester. Testing was load controlled to 10mN with a linear loading rate and unloading rate of 30s and a 30 second pause.

7.4 **Results**

Table 7-1 Average values for all the samples used. Including the density in g/cm^3 and HU calculated from CT images, mineral content and hardness and modulus

Sample	**ρ_{Mean} (g/cm^3)**	**Min content w/w (%)**	**Hardness Vickers**	**Modulus (GPa)**
Rostrum	2.6±0.3	91.9	300.1±31.9	69.5±5.4
Bulla	2.3±0.3	83.2	131.9±21.0	44.8±5.5
Dugong	2.1±0.2	60.9	66.4±7.7	24.4±2.7
Bovine	2.0±0.2	67.1	70.9±6.7	27.8±1.4
Dentine	1.9±0.3	47.8	57.9±7.2	16.9±1.6
Antler	1.6±0.2	44.3	54.3±9.0	9.2±1.9

Table 7-1 shows the results of the average values for the cohort from all the measurements taken in this study with their associated errors. As expected the higher mineral content corresponded with a higher modulus and hardness. Unfortunately however the mineral content was not measured for this sample. Figure 7-1 shows two of the samples used in this study; (a) dentine and (b) dugong. The image shows that there is a difference in grey value between the samples and that there is also a visually noticeable intra-sample variability in the grey.

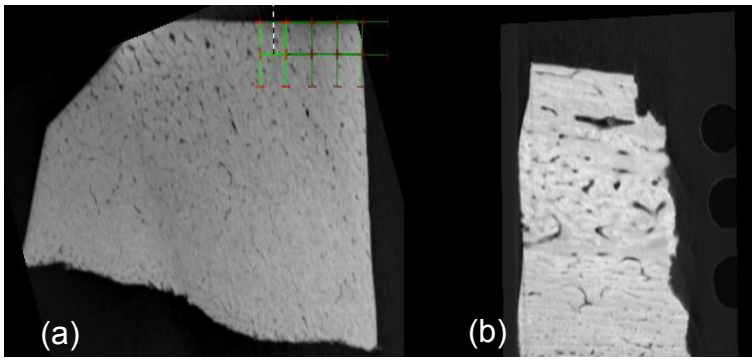

Figure 7-1 2D images taken from (a) dentine and (b) Dugong showing the differences in grey scale

Figure 7-2 shows the results of plotting density data calculated from the µCT versus the mechanical properties measured from nano-indentation. The equations describing the respective slopes are given below:

$$(\boldsymbol{a})\boldsymbol{E} = \mathbf{1.5932}\boldsymbol{e}^{\mathbf{1.8956}\boldsymbol{\rho}} \qquad \text{Equation 7-1}$$

$$(\boldsymbol{b})\boldsymbol{E} = \mathbf{0.3842}\boldsymbol{e}^{\mathbf{2.0292}\boldsymbol{\rho}} \qquad \text{Equation 7-2}$$

$$(\boldsymbol{c})\boldsymbol{E} = \mathbf{258.22}\boldsymbol{\rho}^{\mathbf{2}} - \mathbf{905.51}\boldsymbol{\rho} + \mathbf{841.66} \qquad \text{Equation 7-3}$$

$$(\boldsymbol{d})\boldsymbol{E} = \mathbf{0.9799}\boldsymbol{e}^{\mathbf{1.5061}\boldsymbol{\rho}} \qquad \text{Equation 7-4}$$

These results show a clear increase in both the hardness and modulus with material density. This relationship is consistently non-linear and shows a rapid increase in the modulus and hardness above densities of ~2.2g/cm^3. The site specific plots (Figure 7-2 (c) & (d)) show an extrapolation within the average plots in (a) and (b) but do not provide any large changes to the equations of the curves. They do however demonstrate that intra-sample densities versus modulus relationships exist. The relationship between the mineral content and material density was seen to increase linearly (Figure 7-3), however there were outliers. The region that was ashed was not present in the scan which may be the source of this disparity as it is typically expected that increases in material density would be accompanied by increases in mineral content.

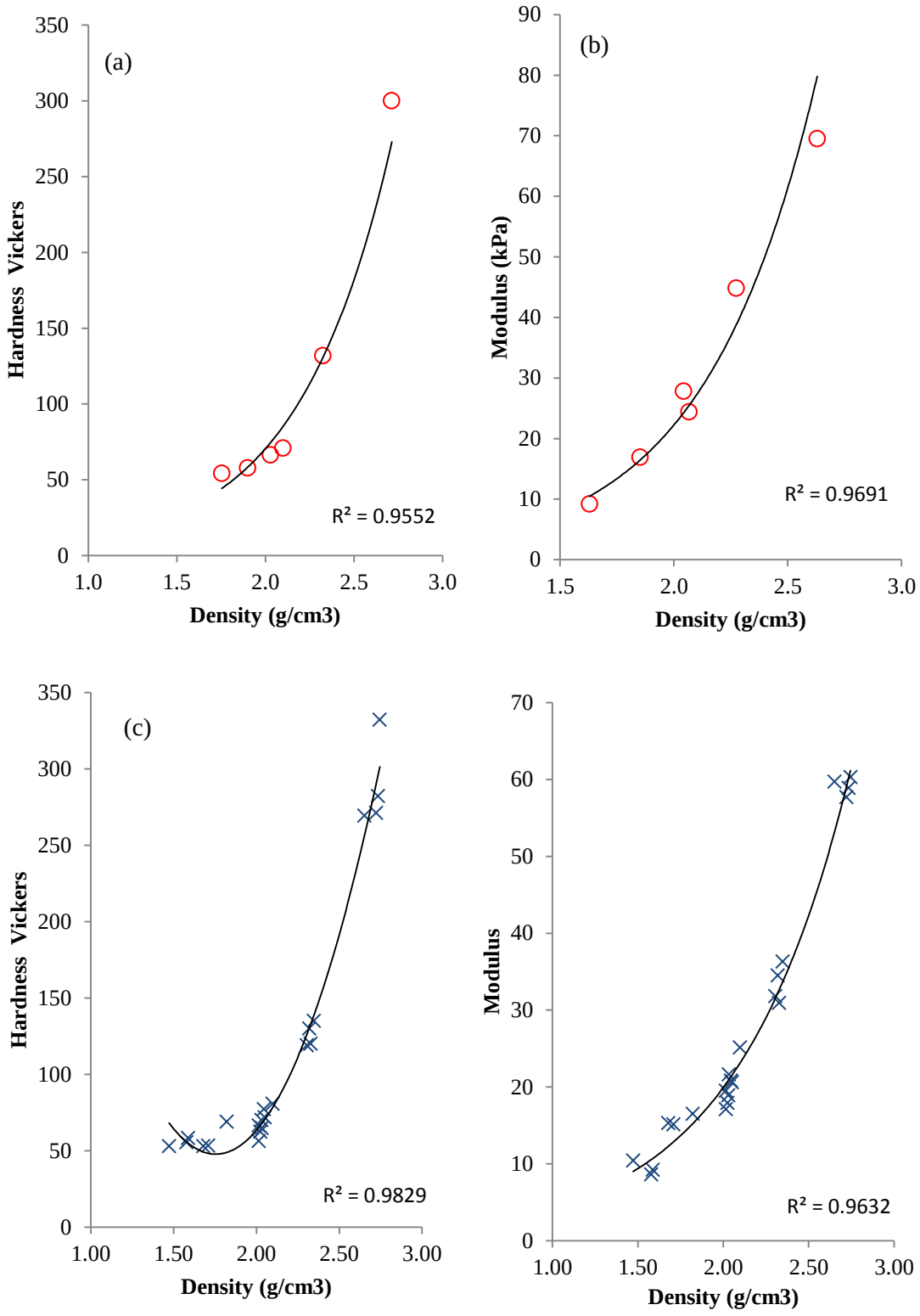

Figure 7-2 Density calculated from the average µ-CT images vs (a) the Vickers hardness over the whole cohort, (b) the modulus measured by indentations over the whole cohort. Density from individual 50x50µm regions over the tissue vs (c) the Vickers hardness over the whole cohort, (d) the modulus over whole cohort

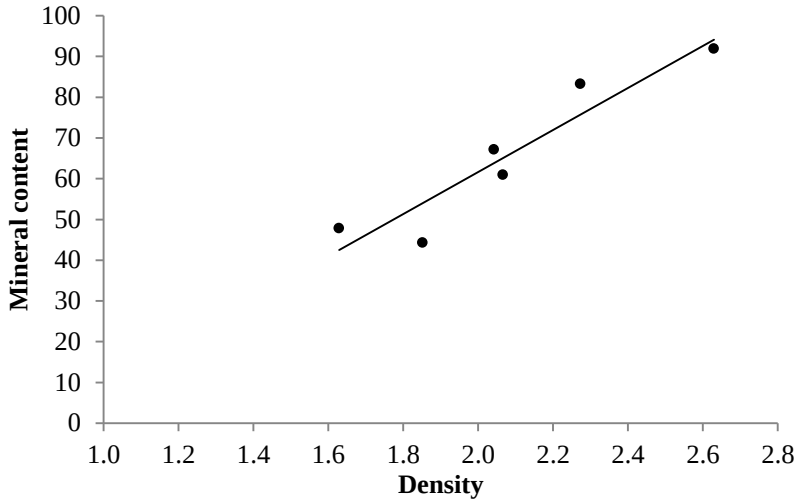

Figure 7-3 mineral content from ashing vs material density measured by µCT

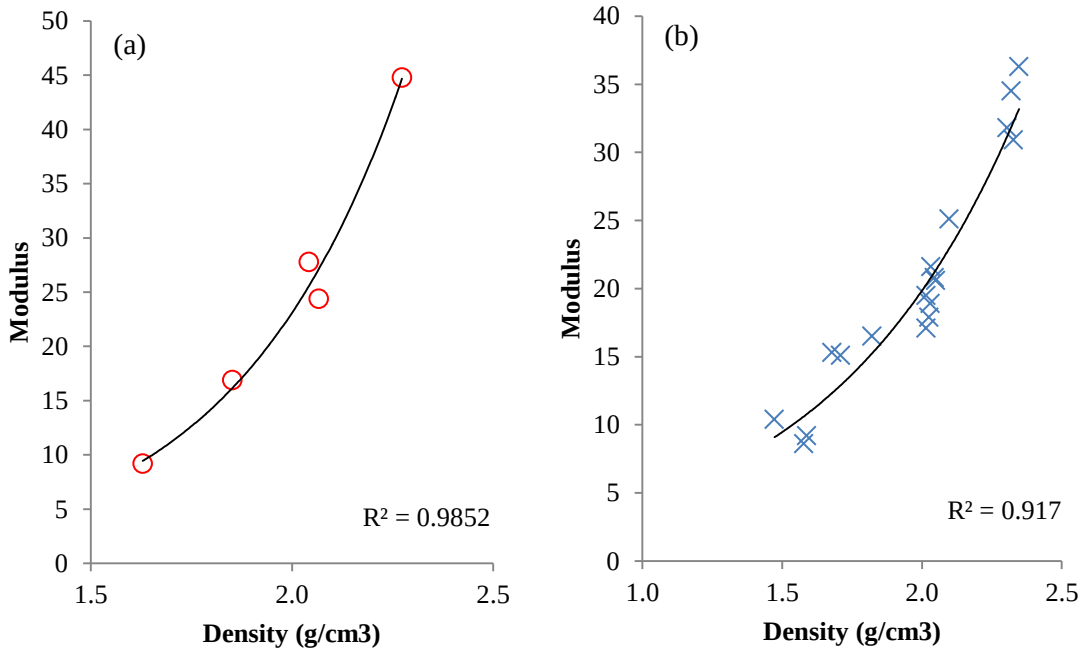

Figure 7-4 density vs modulus for dentine, antler, bovine, dugong and bulla (a) the average values of modulus and density, (b) the site matched modulus and density

Figure 7-4 shows the plot for density versus modulus excluding the high mineral Rostrum in order to extract an equation for the line that may be more applicable to human bone, as human bone tissue density has been shown to sit in approximately 1.6-2.2 g/cm^3. The equation describing this line is given in Equation 7-5 and Equation 7-6. These equations have been selected using Microsoft Excel (2010) auto fitting software by selecting the curve with the 'best fit' determined by the highest R^2 value.

$$(\boldsymbol{a})\boldsymbol{E} = \mathbf{0.1855}\boldsymbol{e}^{\mathbf{2.4123}\boldsymbol{\rho}}$$ Equation 7-5

$$(\boldsymbol{b})\boldsymbol{E} = \mathbf{1.027}\boldsymbol{e}^{\mathbf{1.4806}\boldsymbol{\rho}}$$ Equation 7-6

7.5 **Discussion**

The aim of this study was to determine the relationship between μCT and the material properties of various bone tissues covering a broad physiological range, and to try to account for intra- as well as inter-sample variability with a view to later implement these established relationships in FE simulations. The material density correlates positively with the mineral content which has been shown to correlate significantly with the modulus of bone tissue (Boivin et al. 2008), and this has been further reinforced by the plot shown in Figure 7-3. The deviations in this plot are most likely due to small intra-sample variations in between the section of samples that were ashed and the sections that were mounted and imaged by μCT. The relationships for the density modulus were consistently exponents, however with varying coefficients depending on whether the average sample values were taken or the individual indentation sites were used, shown by Figure 7-2. Additionally, focusing on the region that is of most interest for application of human samples again causes changes in the coefficient values (Figure 7-4).

This study does not include the use of human bone tissue, which should fit in the region of 1.6-2.2 g/cm^3, however the authors cannot be certain that this curve would still apply. The study also fails to account for the anisotropy that existed within bone at the micro-level which has previously been reported (Zysset et al. 1999; Dall'ara et al. 2013). This anisotropy is not detectable through density measurements so implementation of anisotropy would require a model that considered direction and assumes the direction of the tissue at specific points. As such a homogeneous model, while limited, is the most feasible. Of course the exclusion of cancellous samples limits the potential application of these results, although multiple studies would suggest that any disparities between cortical and cancellous bone indentation modulus would be due to the material density rather than micro-structural features (Zysset et al. 1999; Dall 'ara

et al. 2007; Boivin et al. 2008; Schileo et al. 2008). Caution should also be taken when looking at the individual site data as there is no way to verify whether or not the translation between the mappings on the nano-indenter microscope and the µCT images are accurate. Verification of this would require carrying out indentations in-situ of the scanner which is not currently possible.

Whilst this study the nano-scale has been observed by indentations the comparison has been with the bulk material properties in the order of 100µm x 100µm. this is in contrast to existing modelling approaches that have focused on the material properties at the scale of nano-meters to determine the impact of different collagen/HA compositions or layering and the impact on modulus at the nano-scale (Ji 2012; Bar-On 2013). A study by Nobakhti (2013) has also tried considered the impacts of cement lines on the mechanical properties of the tissue within a functional unit of bone. These studies have focused largely on the biological and nano-mechanical properties to explain the differences in bones higher structural properties whereas in this study we have focused on attempting to determine the density-modulus relationship on the smallest scale measurable by common µCBCT. The approach presented here is expected in the shorter term to lead to a more functional understanding of the density modulus relationship in bone measured by methods comparable to state of the art medical CT imaging.

7.6 **Conclusion**

The results presented here show that the mineral content of bone tissue increases with the material density of the tissue. The density and modulus have a non-linear relationship and follow an exponential curve, and by taking the equation of the line that describes the curve it may be possible to predict the modulus at specific sites in bone tissue from densities measured by µCT images. This may in turn allow for an accurate conversion of grey value to modulus in µFA simulations based on µCT images for investigation of the mechanical competency of samples. This could ultimately lead to the development of patient specific µFE models to significantly improve the prediction of patients fracture risk. Although human tissue was not part of this analysis, human bone sits nicely in the middle of this very broad range of mineralisation states and therefore it is also covered by this approach. Here we present a novel way to assess the material properties of human bone tissue and suggest a model that can be used in µ-FE

models to input material properties. This sample specific assessment of the base material property has the potential to greatly improve the accuracy of μ-FE analysis and represents another step toward patient specific μ-FE models.

7.7 **References**

Bar-On B, Wager H. D. 2013 Structural motifs and elastic properties of hierarchical biological tissues – A review. *Journal of Structural Biology.* 183(2) pp.149-64

Boivin, G. et al., 2008. The role of mineralization and organic matrix in the microhardness of bone tissue from controls and osteoporotic patients. *Bone*, 43(3), pp.532–538.

Chevalier, Y. et al., 2007. Validation of a voxel-based FE method for prediction of the uniaxial apparent modulus of human trabecular bone using macroscopic mechanical tests and nanoindentation. *Journal of biomechanics*, 40(15), pp.3333–40.

Currey, J.D., 2002. Bones: Structure and Mechanics, Princeton University Press.

Dall'Ara, E. et al., 2013. Tissue properties of the human vertebral body sub-structures evaluated by means of microindentation. *Journal of the mechanical behavior of biomedical materials*, 25, pp.23–32

Dall 'ara, E. et al., 2007. The effect of tissue condition and applied load on Vickers hardness of human trabecular bone. *Journal of Biomechanics*, 40, pp.3267–3270.

Greenwood, C. et al., 2016. Towards new material biomarkers for fracture risk. *Bone*, 93, pp.55–63.

International Osteoporosis Foundation, 2015. Facts and Statistics | International Osteoporosis Foundation. https://www.iofbonehealth.org/facts-statistics [Accessed January 18, 2017].

Ji J, Bar-On B, Wagner H. D. 2012.Mechanics of electrospun collagen and hydroxyapatite/collagen nanofibers. *Journal of the Mechanical Behavior of Biomedical Materials.* 13 pp.185-93

Niebur, G.L. et al., 2000. High-resolution finite element models with tissue strength asymmetry accurately predict failure of trabecular bone. *Journal of Biomechanics*, 33(12), pp.1575–1583.

Nobakhti S., Limbert G., Thurner P.J. 2013. Cement lines and interlamellar areas in compact bone as strain amplifiers - contributors to elasticity, fracture toughness and mechanotransduction. Journal of the Mechanical Behavior of Biomedical Materials. 29, pp.235-51

Saito, M. & Marumo, K., 2010. Collagen cross-links as a determinant of bone quality: a possible explanation for bone fragility in aging, osteoporosis, and diabetes mellitus. *Osteoporosis international*. 21(2), pp.195–214.

Schileo, E. et al., 2008. An accurate estimation of bone density improves the accuracy of subject-specific finite element models. *Journal of Biomechanics*, 41(11), pp.2483–2491.

Seeman, E. & Delmas, P.D., 2006. Bone Quality — The Material and Structural Basis of Bone Strength and Fragility. *New England Journal of Medicine*, 354(21), pp.2250–2261.

Vilayphiou, N. et al., 2015. Age-related changes in bone strength from HR-pQCT derived microarchitectural parameters with an emphasis on the role of cortical porosity. *Bone*. 83 pp.233-240

Yan, Y.-B. et al., 2011. Relationship between architectural parameters and sample volume of human cancellous bone in micro-CT scanning. *Medical engineering & physics*, 33(6), pp.764–9.

Zioupos, P., Cook, R. & Coats, A.M., 2008. Bone quality issues and matrix properties in OP cancellous bone. *Studies in health technology and informatics*, 133, pp.238–45

Zioupos, P., Cook, R.B. & Hutchinson, J.R., 2008. Some basic relationships between density values in cancellous and cortical bone. *Journal of Biomechanics*, 41(9), pp.1961–1968.

Zysset, P.K. et al., 1999. Elastic modulus and hardness of cortical and trabecular bone lamellae measured by nanoindentation in the human femur. *Journal of Biomechanics*, 32(10), pp.1005–1012.

Zysset, P.K. et al., 2013. Finite element analysis for prediction of bone strength. *BoneKEy Reports*, 2.

8 Grey Scale Based Material Models and Element Softening to Predict the Fracture Toughness using micro-Finite Element Models of Cancellous Bone

G. J. Adams [1],M. Gibson[1],R. B. Cook[2],P. Zioupos[1]

1 Cranfield Forensic Institute, Cranfield University, Defence Academy of the UK, Shrivenham, UK

2 nCATS, School of Engineering Science, University of Southampton, Southampton, UK

8.1 Abstract

The accurate assessment of the mechanical properties of cancellous bone tissue is extremely valuable for the understanding of bone disease and an individual's fracture risk. The implementation of Finite Element (FE) simulations has the potential to provide many insights into understanding how and why bone fails in certain scenarios. To achieve this understanding the base material properties of the tissue must be established for use in these models, as well as understanding the points at which the material will fail. In the present study we have used µ-CT image data alongside a grey value based modulus prediction model to produce µFE models. These models have then been further progressed to include a fracture like event using an element-by-element softening protocol. With the addition of this protocol, the grey value based material model has been able to produce some valuable results that suggest with further development these combined methods may be able to simulate the initiation and growth of fracture across cancellous bone tissue. The accurate simulation of cancellous tissue has the potential to provide insights into how bone fails in the body and with the continually increasing computational power available may be able to provide simulation and assessment of an individual's fracture risk *in vivo.*

Keywords: *Cancellous bone; modulus; Nanoindentation; Micro-CT; Finite element modelling, fracture toughness*

8.2 **Introduction**

With an aging population the rates of osteoporosis are on the rise, with an estimated 200 million women worldwide suffering from the condition (International Osteoporosis Foundation 2015). Osteoporosis is defined as having a bone mass 2.5 standard deviations below the young adult reference mean (Summers 2001). This reduced bone mass results in an increased risk of fragility fracture which, in the UK alone, is currently estimated to cost £3,496 million each year and is expected to increase to £5,465 million by 2025 (International Osteoporosis Foundation 2015). Given the severity and prevalence of the disease there is a need to understand the underlying factors that cause this bone loss and the material quality changes that result in the reduced competency of the tissue (P Zioupos et al. 2008).

The current protocol in the determination of an individual's facture risk is carried out using the FRAX tool, which was developed by Sheffield University (J. A. Kanis et al. 2008). The FRAX tool uses an assessment of the patient's bone mineral density (BMD) which is obtained using the dual energy X-ray absorptiometry (DEXA), and combines this with information on the patient's lifestyle to predict the individual's 10 year fracture risk (Kanis et al. 2008). The assessment of BMD using DEXA produces information on the total quantity and quality of the bone tissue, whilst failing to consider the individual cancellous architecture as well as the tissue quality. Consideration and understanding of the fracture toughness of cancellous bone tissue can help contribute towards understanding the fundamental mechanisms that results in a higher fracture risk (Cook & Zioupos 2009). Work by Cook and Zioupos (2009) took initial steps towards determining the fracture toughness of cancellous bone tissue in individuals previously determined to have suffered a fracture at the neck of the femur. The study showed that determination of BMD by means of quantitative ultrasound correlated with the density and fracture toughness of the cancellous tissue determined using ASTM fracture toughness testing (Cook R. B. 2006; Cook & Zioupos 2009). Recent research has taken steps towards understanding the micro-structural and physicochemical changes that occur during osteoporosis (Cook & Zioupos 2009; Greenwood et al. 2015; Dicken et al. 2016; Greenwood et al. 2016; Berli et al. 2017). The quantity of bone (BV/TV) has been shown to be the largest contributor to bone fracture toughness (Greenwood et al. 2015, Chatper 4). Additionally the inclusion of

other micro-structural parameters such as trabecular thickness and number when used in statistical models alongside BV/TV can help produce models that can contribute to predicting fracture toughness (Chapter 4). Additionally the consideration of the physicochemical properties of the cancellous bone tissue show different biomarkers between fracture and non-fracture groups (Greenwood et al. 2016). The addition of some of these physicochemical biomarkers has also been shown to improve statistical models to predict the fracture toughness of the tissue (Chapter 5). The use of all of these analytical and statistical tools however have not been able to fully explain the variations seen in fracture toughness and not able to fully predict the fracture toughness of cancellous bone tissue; this is perhaps due to the variation of structure within the individual fracture toughness samples and is unable to account for localised defects within the sample. The use of micro-finite element analysis may be able to account for these localised structural variations and present the potential to exceed the predictive capability of statistical models using structural and physicochemical parameters. Additionally it may provide insights into the location and nature of cancellous fractures.

8.3 **Materials and Methods**

8.3.1 **Bone samples**

A sample set of femoral heads were collected from 37 osteoporotic (OP) and 8 osteoarthritic (OA) patients who received total hip replacement surgery due to having suffered fragility fractures at the femoral neck or elective reasons. During the surgery specialist surgeons were able to remove the femoral heads intact. Population characteristics are provided in Table 4-1. Following removal all samples were kept at -20^{o}C prior to sample preparation. Ethical approval for the collection and use of these specimens was provided by Gloucestershire NHS trust REC (acknowledgments). In addition to the cancellous samples, material was sequestered from 6 different animals covering a range of mineral contents: Mesoplodon densirostris rostrum, tympanic bulla of a whale, bovine femur, elephant tusk dentine and deer antler. These samples have been characterised in a previous study (Chapter 7).

Table 8-1 Age and sex data for the osteoporotic samples

	OP
Donors	5
Male/ Female	2 / 3
Number of specimens	5
Age range (yrs)	59-84
Age mean (yrs)	76 (SD=10)

8.3.2 **Sample Preparation**

Specimen preparation (including sectioning from the femoral head and cleaning) has previously described in detail (Cook and Zioupos, 2009; Cook et al., 2010). Single Edge Notched Disc Specimen (SEND) samples were prepared to conform to an adjusted ASTM standard E399-90 in order to assess the necessary stress conditions to instigate crack growth from a man-made notch. Samples were divided into two subsets; with samples cut orientated along (A_L) the primary direction of the trabecular and those orientated across (A_C) the primary orientation of the trabecular structure. This was done because cancellous bone is a cellular solid with a fibre like orientation. Where possible A_L and A_C samples were taken from each specimen. All specimens were stored at −20 °C following a defatting process detailed in (Cook and Zioupos, 2009; Cook et al., 2010). The sectioning was performed by using a metallurgical saw (Struers® Accutom-2), they were then sanded and polished by using progressively finer grades of carbide paper (400–2500 grit) to the dimensions required for material testing. Specimens were manufactured in the shape of discs, diameter 20mm and thickness 7.5mm, for mechanical material testing as SEND. Sample preparation was performed under constant water irrigation, to prevent the production of micro-cracks or other damage to the specimens.

8.3.3 **Mechanical testing**

In a previous study the fracture toughness (K_C) of excised cancellous bone samples and their apparent density were determined *in vitro* (Cook & Zioupos 2009) and compared with patient QUS measurements in-vivo (Cook et al. 2010). 62 samples were taken from 37 osteoporotic and 13 osteoarthritic patients ranging from ages 59-96 years. The samples were taken from the centre of the femoral head and cut into disks conforming to ASTM standard E399-90 to be used in determining the plane-strain fracture toughness.

8.3.4 **Micro-computed tomography**

Both sample sets were imaged using µ-CT. Each sample was imaged using a Nikon CT H225 (X-Tek Systems Ltd, Tring, Hertfordshire, UK) cone beam µ-CT (CBCT) scanner. Samples were imaged at 50kV and 65µA with a 1000ms exposure. The resultant voxel size of the scan was ~24µm. All scans were manually reconstructed using CT Pro 3D. During reconstruction conditions were optimised to reduce beam hardening, the noise and beam hardening corrections were standardised across all the samples to ensure the results were comparable. Image analysis and visualisation was carried out using VG Studio Max 2.2 (Volume Graphics GmbH, Heidelberg, Germany). Firstly the samples' structural properties were determined, including; trabecular thickness (TbTh), spacing (TbSp) and number (TbN), surface area (BS), material volume (BV) and total volume (TV). The density of both samples sets was also determined using a QRM MicroCT-HA (QRM GmbH, 91,096 Möhrendorf, Germany) calibration phantom. This uses hydroxyapatite of different known concentrations to produce a calibration curve of grey scale vs density. Using this calibration the material density of the samples can be determined, which is often referred to as tissue mineral density. For the cortical samples surface grey values were mapped at predetermined locations in 100x100µm squares with 3 voxel depth.

8.3.5 **Nano-Indentation**

Nano-indentation required the samples to be mounted in resin so the indentation surface could be ground and polished flat and fully supported during indentations. The back portion of the SEND samples was removed using a diamond cutter and mounted in

epoxy resin, the human and animal cortical bone samples were also mounted in epoxy resin. The resin was left to cure for 48 hours before being ground to a flat surface then polished using 0.3µm polishing solution.

Nano indentations were performed on both the SEND and cortical samples. In the case of the SEND samples 40-80 indentations were carried out per sample with half the indentations being carried out transversely on the trabeculae and half in the longitudinal on the trabeculae within the sample. The cortical samples were indented at the previously determined locations measured in the results from µ-CT, with 20 indentations per 100x100µm site. All indentations were carried out using a CSM-Nano Hardness tester. Testing was load controlled to 10mN with a linear loading rate and unloading time of 30s and a 30 second pause.

8.3.6 **Material models**

A material model was developed using nano-indentations on the cortical sample set. A material model was developed using the average indentation modulus of each sample alongside the average density of the samples. Full details of the material model are given in Chapter 7.

$$E = \mathbf{1.027}e^{\mathbf{1.4806}\rho} \qquad \text{Equation 8-1}$$

Where $\boldsymbol{\rho}$ is the material density calculated from grey values measured in µ-CT imaging (Chapter 7).

8.3.7 **Finite Element Analysis**

Following µ-CT imaging the image data was imported into Simpleware ScanIP. Using ScanIP the samples were aligned upright with the Z-Axis, a manual threshold was applied using the upper and lower limits identified in VG Studio Max to create a mask. The sample was cropped so only one side of the disc was visible, to remove the upper half of the disc, from which a sample had been extracted for other analytical techniques to be carried out post-test (Figure 8-1). The voxel data was then down sampled to 64µm^3 to reduce the complexity of the model and the subsequent analysis time without having a significant impact on the result of the simulations (Shanker et al.

2016). The resultant meshes were comprised of approximately 6 million elements made up of all tetrahedral elements that were optimised for the model geometry; during the meshing process smoothing was applied to the surface elements to represent the sample structure as closely as possible. Within ScanIP a material modulus placeholder was set so that material properties could be later defined in Ansys and node sets were defined for the constrained Zmin boundary and the hole where the grips had been located during testing; these node sets contained only the surface nodes at the respective locations. A flow diagram of testing through to modelling is given in Figure 8-1.

Two different material models were used; the first being the measured modulus from nano-indentation in which the average modulus from the results of nano-indentation on each sample were used, which has previously been shown to be useful for μ-FE modelling (Chevalier et al. 2007). For the second material model the modulus was calculated using the average grey value for each sample which was converted into material density then applied to Equation 7-6. In both cases a single modulus was used for each sample, the yield strain, post yield modulus and Poisson's ratio were taken to be 0.77% of the initial modulus, 0.55% of initial modulus, and 0.3 respectively.

The simulations were subsequently carried out using Ansys Mechanical APDL. The disc was constrained by a zero displacement in all directions at the face of the cropped surface which corresponded to the crack location from the initial mechanical testing, a displacement equal to that which was measured during testing was applied to the hole in the sample where the grip was located during testing (Figure 8-1).

Due to limitations of computational time, each material model was initially employed using only bilinear kinematic hardening with a reduced data collection rate of 10% (Appendix). Following this pre testing the model that most closely matched the initial loading stiffness recorded by Cook & Zioupos (2009) was progressed to include an element softening or "deletion" protocol. The purpose of this is to attempt to simulate the inclusion of non-biased strain-dependent fracture site prediction. The softening was applied in a loop that periodically identified elements that had exceeded a user specified failure strain of 1%. The input code used to apply the displacement and implement the element softening can be found in the appendix.

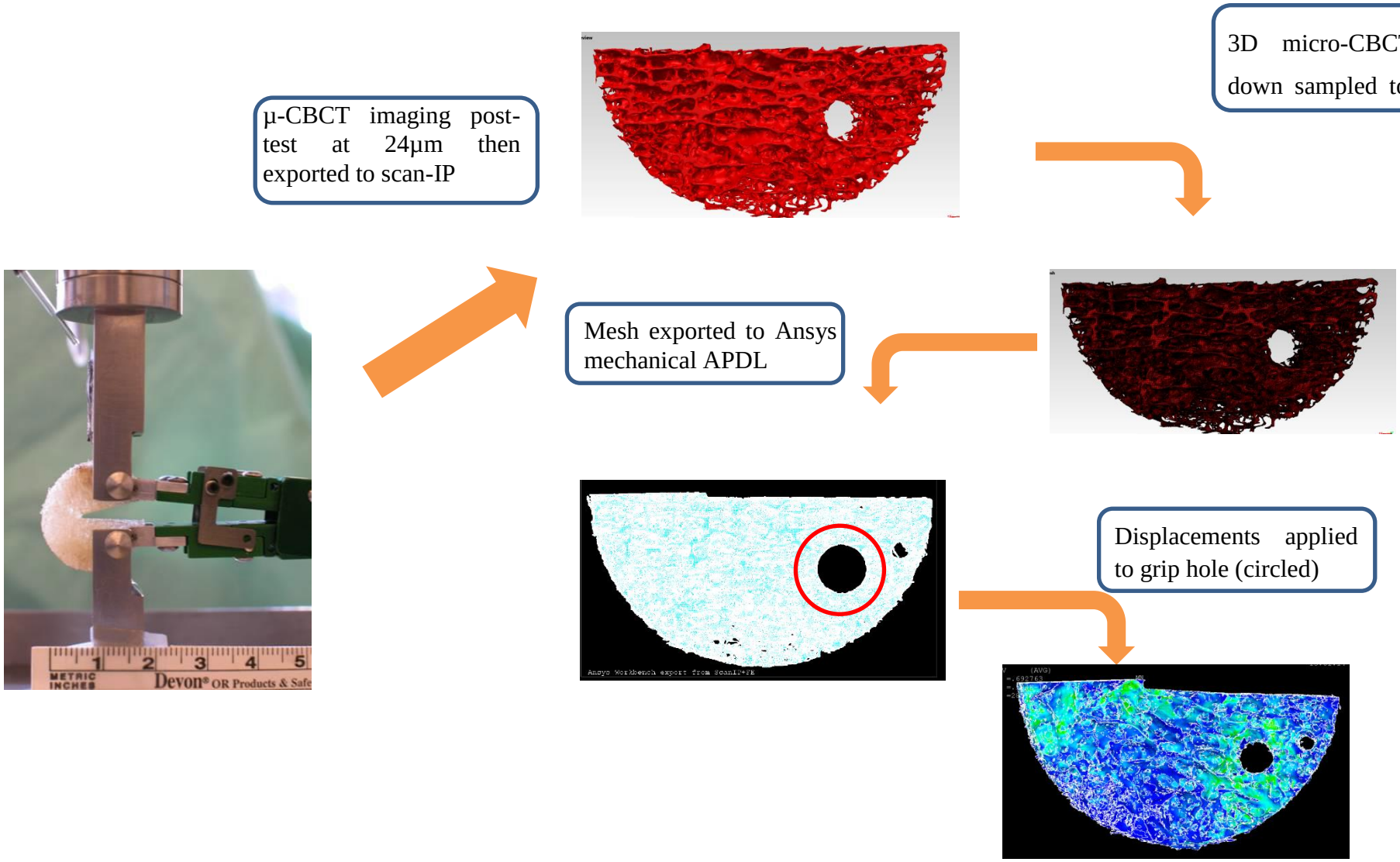

Figure 8-1 Diagram of work flow from mechanical testing (taken from Cook & Zioupos (2009) with permission) to µ-CT image results in Scan IP (top) down sampled in scan-IP then meshed to a tetrahedral/hexahedral optimised mesh, exported to Ansys Mechanical APDL to µ-FE modelling results displaying the local von Mises stresses

8.4 **Results**

Table 8-2 Sample statistics for each sample showing the BT/TV, two different modulus values to be use in micro-FE models and measured plane strain fracture toughness taken from Cook and Zioupos (2009)

Sample	BV/TV	Material modulus (GPa)		Kc (MPa $m^{1/2}$)
		Indentation	Density prediction	
1	0.36	15.07±1.54	17.46±2.44	0.27
2	0.32	16.06±1.14	17.47±2.27	0.44
3	0.22	14.02±1.42	16.90±2.37	0.35
4	0.25	16.45±1.25	17.63±2.47	0.47
5	0.14	13.92±1.38	12.41±1.86	0.07

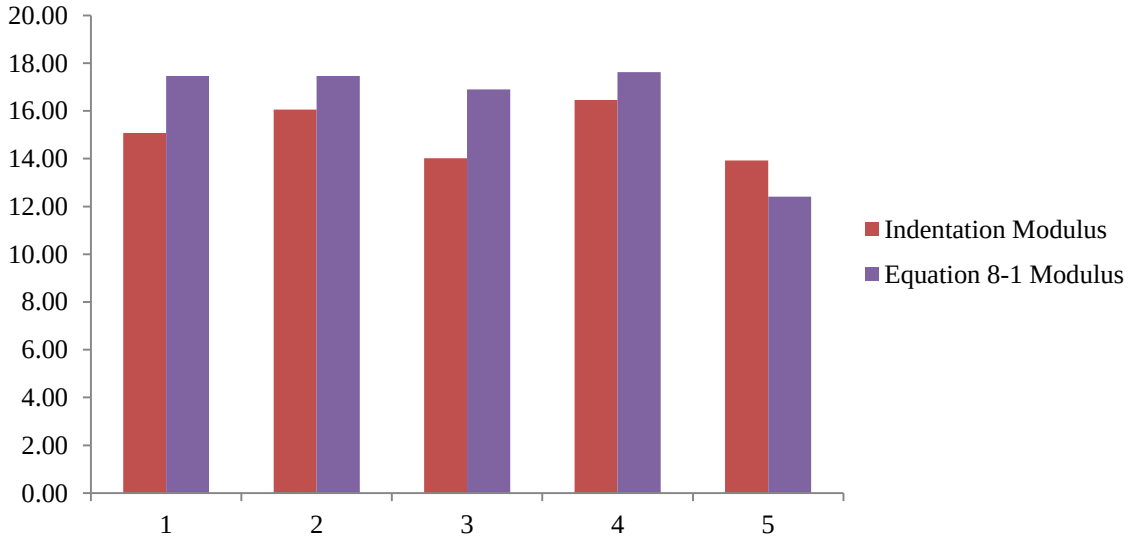

Figure 8-2 Comparison of the material models and the indentation modulus collected for each sample

Comparisons of the material level modulus used in the models for each sample are given in Figure 8-2. They show that the moduli from both nano-indentation and the density based prediction ranged from 12.41-17.63 GPa which is within the typical ranges reported for human bone (Reilly et al. 1974; Zioupos & Currey 1998; Zysset et al. 1999; Hengsberger et al. 2003). This suggests that the material models are to some reasonable degree representative of human bone tissue. Initial testing using these two

modulus values carried out with bilinear kinematic hardening showed that the initial stiffnesses were representative of the initial loading found in the fracture toughness test by Cook & Zioupos (2008).

The material modulus calculated using Equation 8-1 was deemed to be closer to the measured stiffnesses than those using the indentation modulus (Figure 8-3) with the exception of samples 2 and 3 which will be discussed later. Therefore the modulus calculated from Equation 8-1 was progressed to the second stage of simulation involving the element softening protocol.

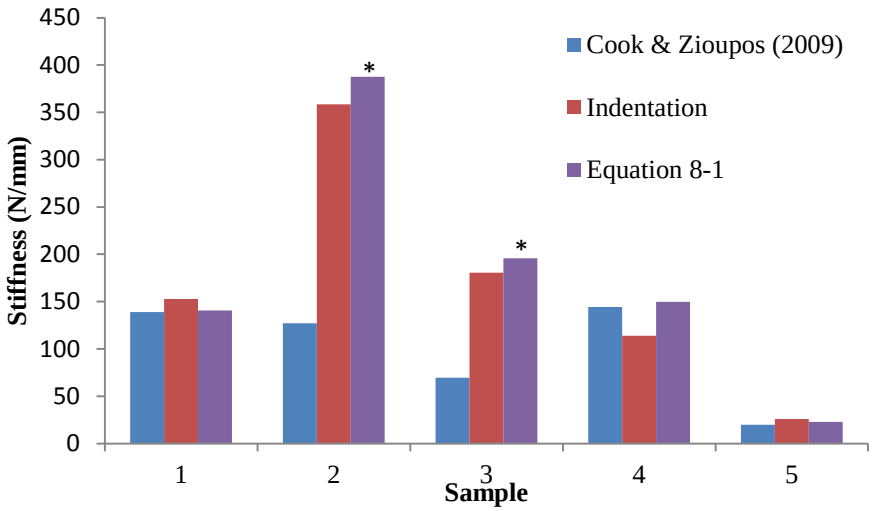

Figure 8-3 comparison of the measured stiffness's for both material models with the measured stiffness from Cook & Zioupos (2009). * samples are not considered in determining which models should be progressed to the element softening stage

After the addition of the element softening protocol the initial stiffness of the model was not seen to change, which is expected because the model is still in a linear phase. The element softening was able to add an event to the force displacement curve that was representative of a material failure (Figure 8-4).

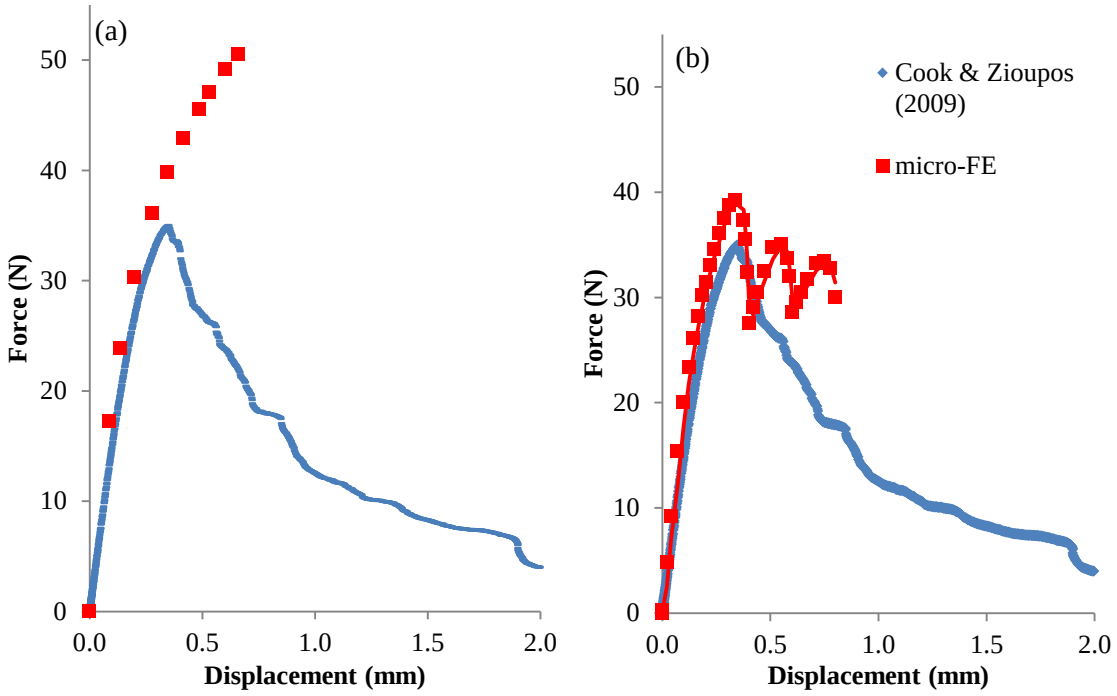

Figure 8-4 Force displacement curves for sample 1 comparing load data from Cook & Zioupos (2009) with (a) initial model including only bilinear kinematic hardening, and (b) with the addition of the element softening loop

The apparent 'bouncing' seen in Figure 8-5 following the initial fracture point is due to the element softening only occurring at the end of each load step, as such the force continues to climb between each load step before the next series of failed elements are softened.

Table 8-3 Comparison of peak load and displacements at peak load for measured and simulated samples

	Peak load (N)		Displacement at peak load (mm)	
Sample	Cook and Zioupos (2009)	µ-FE	Cook and Zioupos (2009)	µ-FE
1	35.53	39.26	0.35	0.34
2	40.54	66.51	0.43	0.38
3	29.07	60.32	0.83	0.61
4	42.61	37.03	0.48	0.34
5	6.91	6.86	1.23	0.59

The comparison of the µ-FE simulations using element softening with the measured mechanical data is given in Table 8-3. The comparison of the sample sets were not found to significantly correlate in either the peak load or the displacement at peak load, p=0.21 and p=0.13 respectively. Some of the sample did however closely align, as previously mentioned the limitations in sampling may have been responsible for the lack of correlation which will be discussed later.

8.5 **Discussion**

There is a need for the development of accurate micro-finite element analysis models to help further the understanding of bone fractures, specifically in regions of cancellous bone tissue. In order to accurately carry out such simulations two things are required; an accurate representation of the cancellous tissue structure and material models that can accurately represent the linear and non-linear mechanical characteristics of the tissue. The first of these can be achieved through µ-CT imaging which has been shown to produce suitable models that enable simulations that were not previously possible (Niebur et al. 2000; Chevalier et al. 2007). The second is arguably more challenging and has yet to be fully defined, in the present study we have presented possible methods for the definition of the initial materials modulus as well as the addition of a non-linear response of the tissue to load that ultimately tries to represent fracture through the process of element softening.

The largest limitation of this study is the order in which the stages of the study have been performed. The mechanical loading was the first step to be carried out, followed by the removal of some bone tissue in order to carry out ashing for mineral content determination. Following this the µ-CT imaging was carried out – because of the previous removal of tissue, modelling of the whole sample was not possible. Therefore the samples were segmented in half in order to exclude the compromised portion of the sample from the simulation. This segmentation could potentially result in a misrepresentation of the sample stiffness as the samples were not homogenous. In addition to only half the sample being included in the FE analysis the segmentation point may have been misplaced relative to the fracture location, although every effort was made to ensure the segmentation was in a suitable position. In the case of samples 2 and 3 it is suggested that the combination of the fact that only half of the sample was

included in the simulation, and that the segmentation may have excluded the regions of the tissue that originally failed, that the results were not reliable. Therefore samples 2 and 3 were not considered in determining which models should be progressed to the element softening stage. This study also suffers the limitation addressed by Sabet (2015) of fails to make a multiscale approach which will be required to further understand diseases such as osteoporosis.

These results show that the use of grey scale based material models combined with the present element softening protocol may be implemented in micro-finite element models in order to predict the fracture of cancellous bone tissue. As highlighted, the present research is subject to a potential sampling issue; however with further work the models can be fully validated. This element softening approach to the understanding of fracture can be implemented in multiple instances outside of cancellous bone as a method to produce micro-finite element models with a non-user defined fracture location. Additionally this work has identified the need for the production of accurate information on the failure characteristics of individual trabeculae, not just cancellous tissue as a whole, as this can greatly help inform models that are attempting to produce simulation of the fracture characteristics of cancellous tissue starting at the very base principles.

8.6 **Conclusion**

This study has investigated the use of µ-FE simulations to determine if it is possible to predict the fracture toughness of cancellous bone tissue using µ-CT image data alongside modulus predictive materials models. The results presented here have shown firstly that the use of grey scale based modulus predictive models, using grey values measured by µ-CT, can predict the material modulus to be similar to that measured by nano-indentation. Additionally the results suggest that the use of such models may be more suitable than nano-indentation data as it enables an assessment of the entire sample's modulus and not just a small number of selected sites that nano-indentation offers. Secondly this study has shown that by implementing a strain based element softening loop it is possible to simulate some representation of fracture at the material level in cancellous bone. With further development and validation it is

suggested that such models may be implementable in a clinical setting in order to inform on an individual's fracture risk.

8.7 **References**

Berli, M. et al., 2017. Localized tissue mineralization regulated by bone remodelling: A computational approach R. K. Roeder, ed. *PLOS ONE*, 12(3), p.e0173228.

Chevalier, Y. et al., 2007. Validation of a voxel-based FE method for prediction of the uniaxial apparent modulus of human trabecular bone using macroscopic mechanical tests and nanoindentation. *Journal of biomechanics*, 40(15), pp.3333–40.

Cook, R.B. & Zioupos, P., 2009. The fracture toughness of cancellous bone. *Journal of biomechanics*, 42(13), pp.2054–60.

Cook, R.B. 2005. 'Non-invasively assessed skeletal bone status and its relationship to the biomechanical properties and condition of cancellous bone'. PhD, Cranfield University, Shrivenham

Dicken, A.J. et al., 2016. Classification of fracture and non-fracture groups by analysis of coherent X-ray scatter. *Scientific Reports*, 6, p.29011.

Greenwood, C. et al., 2015. The micro-architecture of human cancellous bone from fracture neck of femur patients in relation to the structural integrity and fracture toughness of the tissue. *Bone*, 3, pp.67–75.

Greenwood, C. et al., 2016. Towards new material biomarkers for fracture risk. *Bone*, 93, pp.55–63.

Hengsberger, S. et al., 2003. How is the indentation modulus of bone tissue related to its macroscopic elastic response? A validation study. *Journal of Biomechanics*, 36(10), pp.1503–1509

International Osteoporosis Foundation, 2015 Facts and Statistics | International Osteoporosis Foundation. Available at: *https://www.iofbonehealth.org/facts-statistics* [Accessed January 18, 2017].

Kanis, J.A. et al., 2008. FRAXTM and the assessment of fracture probability in men and women from the UK. *Osteoporosis International*, 19(4), pp.385–397.

Reilly, D.T., Burstein, A.H. & Frankel, V.H., 1974. The elastic modulus for bone. *Journal of Biomechanics*, 7(3), pp.271–275.

Sabet F.A, Najafi A.R, Hamed E., Jasiuk I. 2015. Modelling of bone fracture and strength at different length scales: a review. *Interface Focus*

Shanker, T. et al., 2016. In Finite Element Optimisation Techniques Applied to Human Vertebral Cancellous Bone. *Human Response to Vibration 2016| UK Conference*

Summers, G.D., 2001. Osteoporosis in men. *Radiography*, 7(2), pp.119–123.

Zioupos, P., Cook, R. & Coats, A.M., 2008. Bone quality issues and matrix properties in OP cancellous bone. *Studies in health technology and informatics*, 133, pp.238–45.

Zioupos, P. & Currey, J.., 1998. Changes in the Stiffness, Strength, and Toughness of Human Cortical Bone With Age. *Bone*, 22(1), pp.57–66.

Zysset, P.K. et al., 1999. Elastic modulus and hardness of cortical and trabecular bone lamellae measured by nanoindentation in the human femur. *Journal of Biomechanics*, 32(10), pp.1005–1012.

.

9 Overall Discussion

The overall aim of the research was to assess the structural and chemical properties of human osteoporotic and osteoarthritic bone to determine what, if any, measurable parameters contributed to the measured plane strain fracture toughness of the tissue. Additionally consideration was made of the suitability of μCBCT to assess bone micro-structure and investigation was carried out into the variations that occur in micro-structure over the full range of bone porosities. The following is a discussion of the outcomes and potential limitations of the research.

9.1.1 **Bone structure assessment**

Firstly the relationship between the density of bone at the material level and the local porosity was investigated. This revealed that there is a non-linear relationship across the full range with the highest densities found to exist at the highest and lowest porosities, whilst the lowest material density was found to exist in the intermediate porosities of bone tissue. These findings were consistent with those previous findings by Zioupos et al. (2008) in which a 'boomerang' type relationship was demonstrated. These findings were however controversial and it was suggested that the apparent relationship being observed was a limitation of the measuring techniques used (Schileo et al. 2008; Schileo et al. 2009). The use of μCBCT is however not subject to these same limitations which suggests that the relationship exists as a physical phenomenon in mammalian bone tissue, although the extent of the relationship was determined to be less than that which was previously reported (Zioupos et al. 2008). The use of μCBCT however is not without limitation and the suitability of the technique to measure the material density has been brought into question (Cassetta et al. 2014; Kim 2014). Other studies have however found the measurements taken from μ-CBCT to be suitable, commonly by applying a conversion to the data (Laib & Rüegsegger 1999; Mah et al. 2010; Berteau et al. 2012; Palacio-Mancheno et al. 2014). This has also been displayed here, with agreement being found between the physical measurements and μCBCT data at the apparent density level.

The assessment of the structural properties of mammalian bone tissue across its porosities can be a useful tool in the assessment and determination of the remodelling

nature of bone tissue. The remodelling rates of bone have long been considered to be affected by the area of the available surfaces on the bone tissue (Currey 2002). As such, determination of the area of these available surfaces in the given quantity of bone tissue can help inform on the remodelling rates of the tissue (Zioupos et al. 2009). The study presented here has shown the measured porosity-surface distribution that exists within a large selection of mammalian tissue was determined to be consistent with previous reported works (Martin 1984; Fyhrie et al. 1995; Buenzli et al. 2012), although the positions and values of the maxima are different. The results of porosity-surface distribution can be used to inform remodelling models in order to predict the potential locations and rates of bone loss (Berli et al. 2017). Further development and validation of such works can contribute to the understanding of bone loss and disease.

In these studies the tissue used was taken from the right femur of an adult Asian elephant (3432 kg, 24 year old). The sheer size of femur has enabled the collection of a vast number of samples from a single 'patient' which has enabled the exclusion of inter-patient variations of the relationships, and effects that have been observed are solely due to the intra-sample variations, which in turn has reduced the noise in the data collected. This ability to collect such a large number of samples whilst simultaneously eliminating inter-patient variability is why the elephant femur was selected over the multiple human femurs that would have been required to achieve the same size cohort. However the samples being collected from an elephant, whilst still mammalian, have limited applicability to the human patients, and as such validation of these relationships with a human or multiple human samples is required to validate the study and provide data that may be more clinically applicable. The elephant samples collected were stored wet and frozen which may have affected the measurements, however it is more suitable than not freezing them as the freezing prevents the degradation of the tissue.

9.1.2 **Parameters affecting fracture toughness**

In assessing the parameters that impact the fracture toughness of osteoporotic and osteoarthritic cancellous bone it has been determined that there are significant relationships between the architecture and fracture toughness, which are considerably different depending on the loading orientation. This dependence on loading orientation was determined by implementation of multiple regressions, the results of which showed

that in loading across the primary orientation of the cancellous architecture multiple structural properties independently contributed significantly to the resistance to fracture; whilst in the A_L loading configuration, no parameter added to fracture prediction beyond the porosity alone. One potential limitation of these findings is the dependence on statistical models and while the samples size available for this research has been extremely high (for human cancellous bone samples with measurement of plane strain fracture toughness) from a statistical perspective the sample numbers have been low (n=82). In the application of multiple regression analysis the 'rule of 10' has not been adhered to, although it has been demonstrated that the rule is over cautious and lower ratios of predictors to samples are suitable and accurate for a statistically valid model to be developed (Austin & Steyerberg 2015). This use of multiple regressions based on the micro-architecture of cancellous bone to predict its fracture toughness has provided a basis to introduce the inclusion of micro-architecture alongside the currently used DEXA standard in order to improve the assessment of a patient's fracture risk (Kanis et al. 1997; Kanis et al. 2008).

The use of porosity with the addition of physicochemical analysis has been shown to further explain differences in fracture toughness alongside the structural properties, highlighting that there are both quality changes at the micro-structural and physicochemical level. Physicochemical analysis has also been employed alongside porosity in multiple regression analysis; this produced results counter to those where purely structural data was used and a larger number of parameters were found to contribute to the resistance to fracture in the A_L loading configuration than in the across configuration. This suggests that at the micro-level cancellous bone is being orientated in order to resist fracture across the primary orientation whilst simultaneously employing physicochemical adaptations in order to resist fracture. A limitation is that this research has looked at the properties of the tissue in relation to its plane strain fracture toughness, which is a direct measure of how the tissue behaves at the sub-organ material level. This measurement does not consider the structure and scale of the tissue at the organ level and no research has been conducted to determine how this measure of fracture toughness impacts upon the fracture risk of an individual.

The analysis of Raman spectra by principal component analysis (PCA) was able to distinguish between fracture and non-fracture groups. This is not limited in the same way as the other analysis as it is purely a consideration of those having suffered a fracture and subsequently being determined to be osteoporotic or osteoarthritic versus those who were at the time of death not suffering from any apparent bone condition. The use of PCA furthers previous work that has shown that the application of PCA to diffractograms produced by XRD can separate fracture and non-fracture groups (Dicken et al. 2016). This apparent success of PCA in both instances sets out the opportunity to combine both Raman spectra and XRD diffractograms which could potentially increase the separation of fracture and non-fracture groups. The PCA carried out here has, however, been limited by the location from which the cancellous samples were obtained, as the fracture samples were taken from the femoral head and the non-fracture samples were taken from the greater trochanter. This is a limitation as the use of the trochanter tissue introduces an additional variability between the sample groups beyond the apparent bone conditions.

In this research investigations have also been carried out into the assessment of the thermal decomposition of the cancellous tissue in relation to its fracture toughness. The results of the investigation showed that the thermal decomposition was not able to provide any additional insight into the factors affecting the fracture toughness of the tissue beyond that provided by analytical techniques such as FTIR, Raman spectroscopy and XRD. This may be due to the sample preparation required for DSC whereby the dehydration of the collagen in cortical bone tissue may have masked the effects that the cross-links and material toughness of bone tissue may have exhibited as shown in the past (Zioupos et al. 1999). The thermal decomposition was investigated in this case as the previous work by Zioupos et al. (1999) showed significant differences with age, given that serval parameters had displayed correlations it was expected that these would be compounded in the thermal decomposition. From the results however this was found not be to true.

When considering the chemical and material properties of the tissue, the micro-architecture must always be considered; this is demonstrated by considering just the

quantity of cancellous bone tissue parameters that do not appear individually to have high correlations can significantly add to potential predictive models.

9.1.3 **Simulations of stiffness and fracture toughness**

The models developed here explored the effects of material properties that can be used in the simulation of cancellous bone fracture and have attempted to provide a holistic approach to μFEA of bone tissue. The material model was based on the indentations of a wide array of bone tissues over almost the full range of mineralization levels available in nature. The tissue used was cortical bone which whilst similar to cancellous it is certainly not identical, the assumption has been made that the density-modulus relationship observed in the wide range of cortical bone is transferable to cancellous bone as well. Additionally the model was not able to account for the anisotropy at the material level that has been previously reported (Goldstein 1987; J.-Y Rho et al. 1998; J.-Y Rho et al. 1997). Despite these limitations the comparisons of the initial stiffness, *in vivo* vs *in silico,* of the samples was encouraging and warrants further development and validation of the present model.

Following the first basic FEA model on a simple single material modulus the addition of a fracture like event was attempted by means of element softening. This method used a strain based criterion to 'fail' elements in order to allow the model to represent fracture. The results for some samples were encouraging, however possibly due to the limitations of the sampling the implementation of fracture was ultimately unsuccessful. Such softening protocols however present a promising opportunity to simulate fracture. The combination of these two models, with further work and validation, may prove to be integral in the understanding of bone fracture toughness.

9.2 **Conclusions**

The current protocol in the assessment and determination of bone degeneration and deterioration diseases such as osteoporosis (OP) relies on assessing a patient's areal bone mineral density (BMD_a) by means of dual-energy X-ray absorptiometry (DEXA). This assessment by DEXA gives a measurement of the quantity of bone over a specified area, typically taken at the hip. The results of this analysis are used in the Fracture Risk Assessment tool (FRAX), which uses the patient's lifestyle and physical characteristics

to determine their risk of fracture. This is the current gold standard in the determination of whether a patient is osteoporotic or at an increased risk of fracture. Over the last couple of decades research into OP has suggested many different physiological characteristics that may be able to be used to further the current protocol in the determination of the OP condition. Most of these studies have however tried to determine different markers that could be used to set a single parameter that may be slightly different in typical OP samples from a population. Such an approach has a great potential for error or misdiagnosis for those that sit on the border between healthy and OP, normally referred to as osteopenia. This on/off approach taken by many fails to consider the actual fracture toughness of the tissue and the impact these structural and physicochemical characteristics have on fracture toughness. Understanding and quantifying this may be able to lead to better diagnosis by assessing the fracture toughness of the patient's hip *in vivo*. Additionally it may provide information that could be used to combat the onset of osteoporosis and lead to a better diagnosis and understanding of the risk faced by patients that have been determined to suffer with osteopenia.

Therefore the research carried out has aimed to help further the understanding of bone fracture by investigating the structural and physicochemical properties of cancellous bone tissue and assess what impact, if any, these qualities have on the fracture toughness of the tissue. The research aimed to do this by achieving four objectives that were previously outlined:

Objective 1

Comparisons have been made between physical laboratory measurements of bone density and porosity and the corresponding measurements that could be obtained from µ-CBCT. This comparison showed some discrepancy between the physical measurements and the data obtained from µ-CBCT and showed that in the intermediate porosities of bone (~50%) the physical measurements were notably lower. This difference however exists mostly due to the limitations of the Archimedes technique which is limited by the full penetration of water and existence of un-mineralised tissue, specifically that with a density of less than $1 g/cm^3$. Even with this difference the results showed that the material density of bone displays a "boomerang" relationship with

respect to its apparent density. This relationship has previously been disputed and could provide a strong basis for bone remodelling models which can contribute significantly to understanding of bone disease. The μ-CBCT of course has its limitations, which were explored in chapter 3, with regards to the placement of the threshold for repeatable accurate determination of the morphology. This showed that imaging the bone samples fully submerged in water or in air produced statistically comparable data across the entire range of physiological bone porosity. This result provided a basis to ensure that it was possible to produce reliable data to fulfil the other objectives of the research to achieve the overall aim of the study.

Objective 2

Following the work of chapters 2 & 3 it was determined that the present protocol for the assessment of the morphology and density across the available porosities was suitable. Therefore the next step was to assess the morphology and density of OP and osteoarthritic (OA) cancellous bone from the femoral neck by μ-CBCT from patients that had suffered a hip fracture. This showed, in agreement with DEXA, that the quantity of bone has the largest impact on the ability of bone to resist fracture. However the quantity of bone was not able to fully account for the measured fracture toughness and additional parameters were found to contribute significantly to the fracture resistance of the tissue. The fracture toughness samples were separated into two groups within the cohort; those loaded across the primary orientation of the trabecular and those loaded along the primary orientation of the trabecular. This revealed, in agreement with the generally accepted adaptive nature of bone remodelling, that the bone will remodel in such a way to resist fracture in the direction in which it is primarily loaded. As such the degree of anisotropy and average trabecular thickness will contribute to the resistance of fracture, whilst when loaded perpendicular to the primary direction other structural parameters do not contribute to the resistance to fracture.

Objective 3

The assessment of the physicochemical properties of the OP and OA cancellous bone tissue showed that multiple parameters assessed by different analytical means

significantly correlated with the toughness of the tissue. Measured by FTIR, increases in carbonate *v3* (type A) and carbonate *v2* correlated significantly with a decrease in fracture toughness which suggests that the HA crystals become more resolved, resulting in a reduced toughness. Assessment by Raman Spectroscopy showed that increases in the mineral: organic ratio correlated with a decreased fracture toughness showing that an increase in the brittle component of the tissue reduces the toughness. Additionally correlations were found between the $CL_{00\ell}$ and fracture toughness as well as correlations between the measured LP and fracture toughness. These all show that there are significant chemical changes that occur within the bone tissue that lead to changes in the fracture toughness, in both the quantity of the individual components of the tissue and in the quality of those components.

Furthermore the results of PCA that was applied to the Raman spectroscopy data also revealed that there are marker differences between osteoporotic, osteoarthritic and undiseased bone tissue. This ability to distinguish between these groups presents an opportunity to identify those most at risk of suffering a fragility fracture.

Objective 4

Using the morphological and chemical data obtained, multiple regressions were employed to determine the relative contribution of the individual parameters to the bone fracture toughness in order to attempt to predict the fracture. The use of purely the morphological data was used to produce three different models, all of which used the BV/TV as the base as the quantity of the bone was the biggest contributor and also the most representative of DEXA. The first of these considered the entire cohort indiscriminately of the loading direction; this produced a model that used BV/TV with the addition of the trabecular number, trabecular spacing and BS/TV. This model showed an adjusted R^2=74.08. The A_C group showed that the addition of the degree of anisotropy and trabecular thickness contributed to the fracture, producing a modelling with an adjusted R^2=77.14. In the A_L group no other parameters contributed beyond BV/TV alone. This highlighted two things: firstly that bone remodels in such a way to resist fracture in a specific direction and secondly that the morphological structure of the tissue can account for a large proportion of the tissue's fracture toughness. However it does not entirely explain the differences in fracture toughness suggesting that the

chemistry of the tissue is playing a significant role. The results of the chemical assessment were therefore added to the models which showed that the assessment of the mineral:organic ratio by Raman Spectroscopy and assessment of the coherence length in the <002> and the lattice parameter in the 'a' axis assessed by pXRD could help improve the predictive power of the models in the A_C group to produce an adjusted R^2=89.54. In the A_L group the inclusion of the lattice parameter in the 'c' axis could be added to the BV/TV to produce a model with an adjusted R^2=85.46. This suggested that within the individual trabeculae the organisation at the chemical level contributes to the resistance to fracture.

In order to carry out finite element analysis a micro-scale material model was developed to translate from grey scale values to modulus and aimed to produce predictive FE models. Elastic-plastic models were initially carried out to compare material models with indentation based models, which produced similar results that both followed the initial stiffness of the laboratory measurements. After it had been determined that the model provided a reasonable prediction of the material properties for use in µ-FE, the implementation of simulated fracture was attempted by utilising automated stop/restarts to identify elements that fulfilled a predetermined failure criterion (strain>1%). In elements that had exceeded 1% strain the modulus was reduced significantly to reduce their contribution to the stiffness of the model. The peak force and displacement at peak force were compared with the laboratory measurements. The results of this showed that the prediction of fracture using µFEA may in fact be possible, however due to the previously discussed limitations of this research it was not successful.

The fulfilment of these objectives has enabled the fulfilment of the overall research aim by determining the structural characteristics and chemical characteristics that contribute to bone's resistance to fracture.

10 Future work

Throughout the course of this research further areas for study have been identified and are listed below:

- Determine if the relationships that have been observed here still hold true when the morphology and density of the bone tissue is assessed using state of the art clinical CT scanners. Additionally measuring the morphology in a µ-CBCT at progressively lower resolutions could be carried out in order to determine the resolutions that would need to be achieved for accurate *in vivo* assessment.
- Implementation and application of the surface-volume relationships shown in chapter 3 should be used in remodelling models to predict areas vulnerable to excessive remodelling. Some such work by Berli et al. (2017) has already begun to look into developing these remodelling models.
- Carry out investigations into how material fracture toughness impacts fracture risk by obtaining a suitable cohort of non-fractured samples to carry out investigations that mirror those carried out on the cohort presented here.
- Determine if the lower resolution assessment of bone morphology is able to produce similar models to predict fracture toughness using multiple regression analysis. Such assessment would ensure the method is suitable to be implemented in a clinical setting for fracture risk predictions.
- Carry out *in vivo* Raman and FTIR measurements to determine if they are comparable to the *ex vivo* studies that have been presented.
- Repeat the PCA analysis using samples from the same location on age and sex matched individuals to verify the results seen here. Additionally PCA analysis should be carried out *in vivo* which could provide a clear predictor for fracture risk.
- PCA should be carried out on a continuous XRD and Raman data stream to determine if the separation between fracture and non-fracture groups can be significantly increased compared to the two assessments individually.
- An element coarsening procedure should be applied to determine the coarsest mesh suitable to help reduce computation times.

- Application of the finite element softening procedure presented here on a cohort of cancellous and cortical samples that isn't subject to the post test limitation that this cohort has been subject to.
- Following the two previous verifications the method should be applied to the proximal femur and compared with *ex vivo* side fall mechanical testing. This would validate the use of the element softening procedure and modulus prediction equations for patient fracture risk prediction.

Should some or all of these recommended plans for future work be carried out and deemed to be successful it would be expected that one or more of the results could be implemented either alongside or as a replacement for DEXA to help improve predictions of patient fracture risk. This could allow for earlier preventative measures to be taken to ultimately prevent fragility fractures in those suffering from osteoporosis to help improve life expectancy and quality of life.

10.1 **References**

Austin, P.C. & Steyerberg, E.W., 2015. The number of subjects per variable required in linear regression analyses. *Journal of Clinical Epidemiology*, 68(6), pp.627–636.

Berli, M. et al., 2017. Localized tissue mineralization regulated by bone remodelling: A computational approach R. K. Roeder, ed. *PLOS ONE*, 12(3), p.e0173228.

Berteau, J.-P. et al., 2012. Computed tomography, histological and ultrasonic measurements of adolescent scoliotic rib hump geometrical and material properties. *Journal of biomechanics*, 45(14), pp.2467–71

Buenzli, P.R. et al., 2012. Endocortical bone loss in osteoporosis: The role of bone surface availability. *International Journal for Numerical Methods in Biomedical Engineering*, 29(12) pp.1-13.

Cassetta, M. et al., 2014. How Accurate Is CBCT in Measuring Bone Density? A Comparative CBCT-CT In Vitro Study. *Clinical Implant Dentistry and Related Research*, 16(4), pp.471–478.

Currey, J.D., 2002. Bones: Structure and Mechanics, Princeton University Press.

Dicken, A.J. et al., 2016. Classification of fracture and non-fracture groups by analysis of coherent X-ray scatter. *Scientific Reports*, 6, p.29011.

Fyhrie, D.P. et al., 1995. Human vertebral cancellous bone surface distribution. *Bone*, 17(3), pp.287–291.

Kanis, J.A. et al., 2008. FRAXTM and the assessment of fracture probability in men and women from the UK. *Osteoporosis International*, 19(4), pp.385–397.

Kanis, J.A. et al., 1997. Osteoporosis International Position Paper Guidelines for Diagnosis and Management of Osteoporosis. *Osteoporosis International* , 7, pp.390–406.

Kim, D.-G., 2014. Can dental cone beam computed tomography assess bone mineral density? *Journal of bone metabolism*, 21(2), pp.117–26.

Laib, A. & Rüegsegger, P., 1999. Calibration of trabecular bone structure measurements of in vivo three-dimensional peripheral quantitative computed tomography with 28-µm-resolution microcomputed tomography. *Bone*, 24(1), pp.35–39.

Mah, P., Reeves, T.E. & McDavid, W.D., 2010. Deriving Hounsfield units using grey levels in cone beam computed tomography. *Dento maxillo facial radiology*, 39(6), pp.323–35.

Martin, R.B., 1984. Porosity and specific surface of bone. *Critical reviews in biomedical engineering*, 10(3), pp.179–222.

Palacio-Mancheno, P.E. et al., 2014. 3D assessment of cortical bone porosity and tissue mineral density using high-resolution ??cT: Effects of resolution and threshold method. *Journal of Bone and Mineral Research*, 29, pp.142–150.

Schileo, E. et al., 2008. An accurate estimation of bone density improves the accuracy of subject-specific finite element models. *Journal of Biomechanics*, 41(11), pp.2483–2491.

Schileo, E., Taddei, F. & Baleani, M., 2009. Letter to the Editor referring to the article "Some basic relationship between density values in cancellous bone and cortical bone" published on Journal of Biomechanics (volume 41, Issue 9, Pages 1961-8). *Journal of biomechanics*, 42(6), p.793.

Zioupos, P., Cook, R.B. & Hutchinson, J.R., 2009. More thoughts on the relationship between apparent and material densities in bone. *Journal of Biomechanics*.

Zioupos, P., Cook, R.B. & Hutchinson, J.R., 2008. Some basic relationships between density values in cancellous and cortical bone. *Journal of Biomechanics*, 41(9), pp.1961–1968.

Zioupos, P., Currey, J.D. & Hamer, A.J., 1999. The role of collagen in the declining mechanical properties of aging human cortical bone. *Journal of biomedical materials research*, 45(2), pp.108–16.

11 Appendices

Pseudo Code for the application of material changes:

Begin environment

Initialise simulation environment

Define parameters and results arrays

Enter Pre-Processor

Read in mesh

Define bilinear kinematic material model (Figure 10-1)

Assign values for E_1 and E_2

Exit Pre-Processor

Enter Solution processor

Constrain cut surface of sample

Apply Displacement

For 0 < Displacement < Limit

Apply Displacement

Solve current model

For each element:

If $\varepsilon^{Total}_{vM} > \varepsilon_f$

Modify E to E_3

End If

End For

Resolve model

End For

Exit Solution Processor

Enter Post-Processor

For 0 < Displacement < Limit

Sum nodal reaction loads at loading point

Copy summed reaction load to results array

End For

Write results array to output .csv

Exit Post-Processor

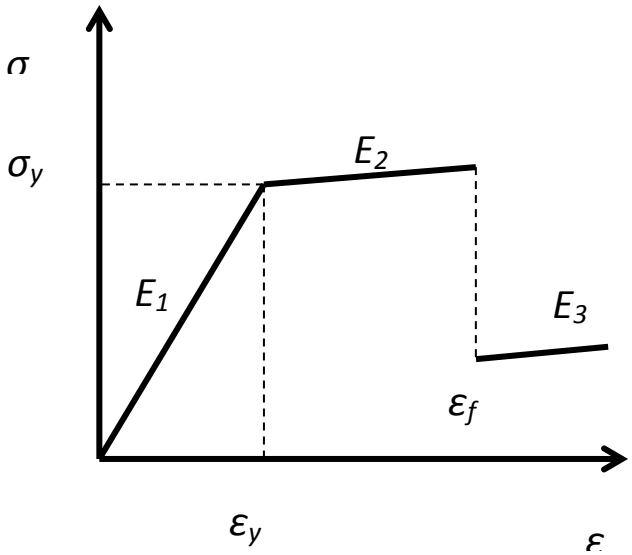

Figure 10-1 graphical representation of the material model of stress versus strain, E_1 is the initial modulus, E_2 is the second stage of the bilinear kinematic hardening, and E_3 is the modulus post failure. σ_y and ε_y are the yield stress and strain respectively. ε_f is the failure strain.